DAHLGREN DIVISION
NAVAL SURFACE WARFARE CENTER
Dahlgren, Virginia 22448-5100

NSWCDD/TR-98/61

PERFORMANCE EVALUATION OF PRECISE ABSOLUTE NAVIGATION (PAN) SOLUTIONS OVER FOUR TEST COURSES

BY BRUCE R. HERMANN

THEATER WARFARE SYSTEMS DEPARTMENT

JANUARY 1999

REPORT DOCUMENTATION PAGE

Form Approved
OMB No. 0704-0188

1. AGENCY USE ONLY (Leave blank)	2. REPORT DATE	3. REPORT TYPE AND DATES COVERED
	January 1999	Final

4. TITLE AND SUBTITLE

Performance Evaluation of Precise Absolute Navigation (PAN) Solutions Over Four Test Courses

5. FUNDING NUMBERS

6. AUTHOR(s)

Bruce R. Hermann

7. PERFORMING ORGANIZATION NAME(S) AND ADDRESS(ES)

Commander
Naval Surface Warfare Center
Dahlgren Division (Code T12)
17320 Dahlgren Road
Dahlgren, VA 22448-5100

8. PERFORMING ORGANIZATION REPORT NUMBER

NSWCDD/TR-98/61

9. SPONSORING/MONITORING AGENCY NAME(S) AND ADDRESS(ES)

10. SPONSORING/MONITORING AGENCY REPORT NUMBER

11. SUPPLEMENTARY NOTES

12a. DISTRIBUTION/AVAILABILITY STATEMENT

Approved for public release; distribution is unlimited.

12b. DISTRIBUTION CODE

13. ABSTRACT (Maximum 200 words)

This report describes a method where the Global Positioning System (GPS) Precise Positioning Service (PPS) solutions recorded in the field can be reprocessed at a later time with the precise ephemerides without requiring that the observations be saved. The reprocessing with the precise ephemerides improves the quality of the navigation solutions compared with the solutions obtained when the real-time broadcast ephemerides are used.

This report continues the investigation of the Precise Absolute Navigation (PAN) technique by exploring its accuracy under highway conditions. Ellipsoid height solutions from survey vehicles traveling at highway speeds have the potential to map terrain heights in a fast, efficient manner. The absolute terrain heights, determined from GPS ellipsoid height solutions, can be used to calibrate remote sensing devices, such as Synthetic Aperture Radar (SAR) images. The performance of PAN is compared with PPS solutions, range-corrected Standard Position Service (SPS) solutions, and relative solutions using smoothed pseudorange. The relative merits of each are discussed.

14. SUBJECT TERMS			15. NUMBER OF PAGES
Global Positioning System (GPS)	Precise Positioning Service (PPS)		69
Precise Absolute Navigation (PAN)	Synthetic Aperture Radar (SAR)		16. PRICE CODE
Standard Position Service (SPS)	ephemerides	ellipsoid height solutions	

17. SECURITY CLASSIFICATION OF REPORTS	18. SECURITY CLASSIFICATION OF THIS PAGE	19. SECURITY CLASSIFICATION OF ABSTRACT	20. LIMITATION OF ABSTRACT
UNCLASSIFIED	UNCLASSIFIED	UNCLASSIFIED	SAR

FOREWORD

A mission of the National Imagery and Mapping Agency (NIMA) requires that geodetic quality absolute positions be determined autonomously and/or in areas far removed from other sites. The use of Differential Global Positioning systems (DGPS) techniques or relative positioning is sometimes precluded. Keyed GPS receivers can output Precise Positioning Service (PPS) navigation solutions. Because they are computed in real time, PPS solutions necessarily use the broadcast ephemerides and, consequently, are subject to ephemeris and satellite-clock prediction errors. The PPS solutions can be recorded, but the broadcast ephemerides and the observations, when corrected for Selective Availability (SA), cannot. This report demonstrates, through simulations, that field-recorded PPS solutions can be reprocessed with the more accurate precise ephemerides. Reprocessing with the precise ephemerides offers improved navigation solutions, but does not require that the SA-corrected pseudorange or phase observations be saved. The method is called Precise Absolute Navigation (PAN). This report continues the evaluation of the PAN algorithm, which has been described in previous documentation.

Support for this development was provided by NIMA under the direction of Mr. Stephen Malys (NIMA/TRB) and Mr. Ken Croisant (NIMA/TRB, ESMD).

The author wishes to thank Dr. Randall Smith (NIMA/TR) for suggesting this technique as one of interest to NIMA for particular applications. The author also wishes to thank the following individuals at NIMA in St. Louis for assisting in the development of PAN: Mr. Gus Jones, Mr. Brian Tallman (GIMGH), and Mr. Brian Deem, for providing data and suggestions; and Ms. Lisa McCormick for processing data sets through the Data Correction Facility (DCF).

This report has been reviewed by Mr. Everett Swift, Program Manager for NIMA-related projects; Dr. Jeffery Blanton, Head, Space Systems Applications Branch; and Mr. James Sloop, Head, Space and Weapons Systems Analysis Division.

Approved by:

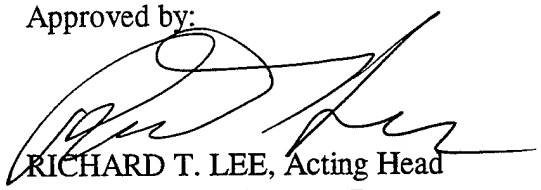

RICHARD T. LEE, Acting Head
Theater Warfare Systems Department

CONTENTS

ILLUSTRATIONS

ILLUSTRATIONS (Continued)

TABLES

1.0 INTRODUCTION

The purpose of the Precise Absolute Navigation (PAN) development is to improve, by postprocessing, the accuracy of a set of Precise Positioning Service (PPS) navigation solutions from keyed receivers. Real-time, stand-alone navigation solutions necessarily use the broadcast ephemerides as the source of the satellite position and satellite clock estimates. However, in certain cases, the particular mission could benefit from more accurate navigation solutions. If the mission is not time critical, it may be acceptable to wait until the postfit ephemerides are available and, thus, improve the PPS navigation solutions with these precise ephemerides. In this case, significantly better results can be expected.

With precise ephemerides, static absolute position solutions can achieve submeter repeatability [1], [2]. Meter-level navigation solutions have been demonstrated by postprocessing L_1 observations with postfit precise ephemerides, clock estimates, and an ionospheric model [3]. Applications where precise absolute navigations would be of interest include cases where auxiliary data for differential or relative solutions are not available, or where the track of a moving vehicle or ship is desired at remote locations far from other sites.

In the operational environment, the PPS navigation solutions will be obtained from a keyed receiver. A keyed receiver will be able to correct for the effects of Selective Availability (SA) and AntiSpoofing (AS) that are intentionally introduced to degrade the accuracy of the system. AS encrypts, and SA corrupts the Global Positioning System (GPS) signals—making the precise signal and the full accuracy of the broadcast ephemerides accessible to authorized users only. These keyed receivers can display the navigation solution in real time, but the field-corrected satellite ephemerides and the SA-corrected pseudorange and phase observations are classified and therefore are not available to the user. The PPS position solutions are unclassified and can be recorded in the field, along with the GPS time and the particular satellites contributing to the solution. In order to improve the PPS solutions at a later time with the postfit precise ephemerides, the following information is required:

- the GPS epoch
- the satellites contributing to the PPS solution at that epoch
- the PPS solution
- the broadcast ephemerides used to form the PPS solutions
- the precise ephemerides

Section 2 begins by comparing PAN solutions with three relative positioning methods using three data sets that explore various problems that could be experienced with real-world conditions. Wherever possible, On-The-Fly kinematic relative positioning is used as truth for these evaluations. The accuracy of kinematic positioning has been shown to be in the centimeter level. This has been

documented elsewhere, as seen in References [4], [5], and [6]. Section 3 continues with an analysis of a four-day data set collected by the National Imagery and Mapping Agency (NIMA) over a road course between St. Louis, Missouri, and Toledo, Ohio, in July 1997. No reference sites dedicated to this experiment were set out, but some data from the National Oceanographic and Atmospheric Administration (NOAA) Continuously Operating Reference Sites (CORS) and the Naval Surface Warfare Center, Dahlgren Division (NSWCDD), Dahlgren, Virginia, were used to obtain relative positioning solutions.

2.0 PAN RESULTS COMPARED WITH OTHER METHODS

This section investigates how well the absolute terrain heights along selected ground tracks can be determined. Previous work has shown that in the case of airborne vehicles, PAN is capable of ±1-m determination of ellipsoid heights. PPS navigation solutions, as well as relative methods, are also possible candidates for the proposed task.

Depending upon the accuracy required for the terrain heights, any of five different positioning methods could be used. PPS navigation solutions and PAN navigation solutions derived from the PPS are the two methods that do not require a reference site. Three relative positioning methods that require at least one static reference site are range-corrected Standard Position Service (SPS), relative positioning with one or two frequency pseudoranges, and kinematic relative positioning. The advantage of the relative methods is that all data can be handled unclassified and collected without a keyed receiver.

To perform an evaluation, two existing data sets were identified as test cases, and a third data set was collected locally near Naval Surface Warfare Center, Dahlgren, Virginia (NSWCDL). The two existing data sets include aircraft data collected by the Applied Research Laboratory at the University of Texas at Austin (ARL/UT) in 1995, which has been used in previous evaluations of PAN, and the data set that was collected at Holloman Air Force Base (AFB) by NSWCDD, NIMA, and several other organizations in November 1996. The static sites that collected data simultaneously with Holloman include the Naval Postgraduate School (NPS) Monterey, ARL/UT at Austin, NSWCDD at Dahlgren, and four locations in Canada.

The third data set was collected by placing an antenna on a vehicle roof and traveling along Route 301 near Dahlgren. Two 40-km, round-trip circuits of this course were made to evaluate repeatability of the solutions.

2.1 Piper Aircraft Data from ARL/UT

The Piper aircraft data was collected by ARL/UT on day 237 of 1995. It is a well-behaved data set with observations collected at 5-s intervals. For this analysis, 603 epochs were used to perform the comparison. The On-The-Fly kinematic relative positioning technique was used as the truth. The time span of the analysis was limited by the kinematic integer ambiguity resolution restrictions caused by the distance between the aircraft and the reference site, as illustrated in Figure 1. The aircraft flew over the reference site MSI en route to its loiter area. This allowed the integers to be established.

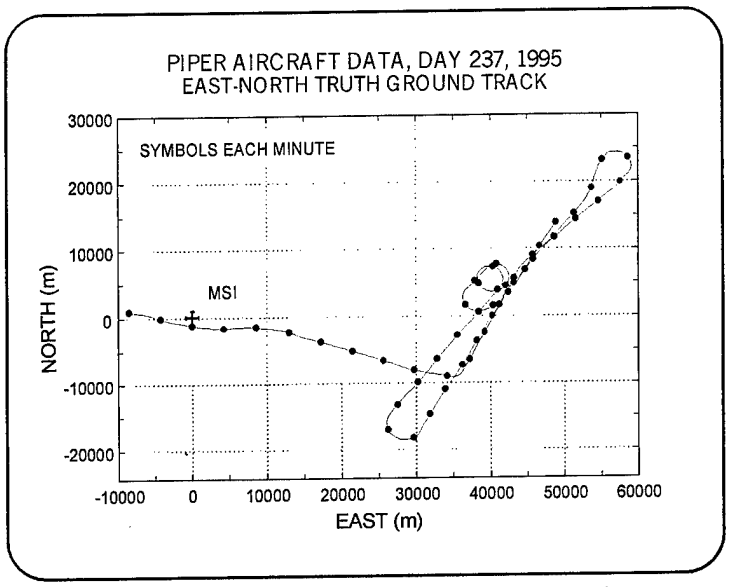

Figure 1—Piper Aircraft Ground Track

However, the aircraft distance was mostly greater than 30 km from MSI and, as a consequence, if satellite signals dropped out or were lost, the integers could not be reestablished. The east-north ground track of the Piper aircraft is shown in Figure 1 with respect to MSI, and the ellipsoid height is shown in Figure 2. The height plot indicates that the altitude was continually changing on the order of 10 to 20 m, probably due to turbulence. This effect can simulate the height variations of terrain and so is a good test case for that reason. The geometric dilution of precision (GDOP) and the number of satellites in view at the aircraft are plotted in Figure 3.

Position differences were computed among the four alternative processing methods and the On-The-Fly kinematic solutions, which were taken as truth. The four methods were:

(1) Relative positioning using smoothed pseudoranges

(2) Simulated PPS navigation solutions

(3) PAN-improved PPS solutions using the precise ephemerides

(4) Range-corrected SPS navigation solutions.

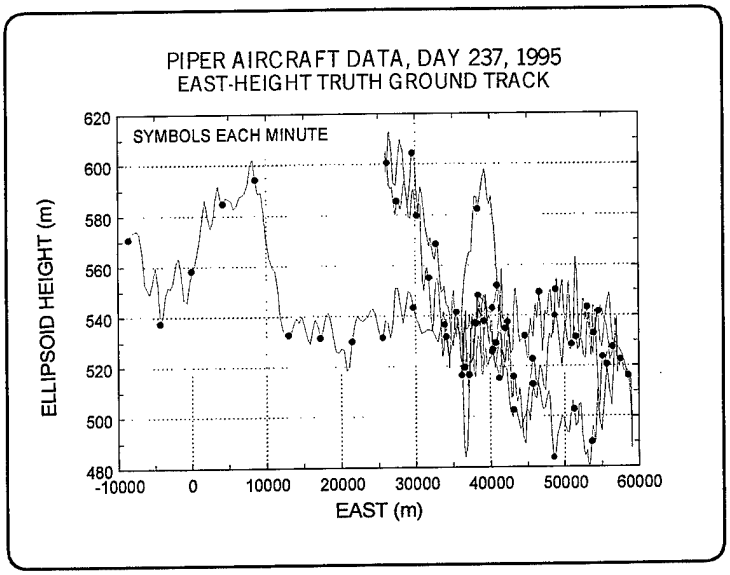

Figure 2—Piper Aircraft Ellipsoid Height

Cases (1), (4), and (5) (Truth) require the use of a reference site. The other two do not need a reference. However, PPS needs SA-corrected data (a keyed receiver); PAN needs the PPS solutions, a list of the satellites used at each epoch, a copy of the broadcast ephemerides used by the receiver to compute the PPS solutions, and a precise ephemeris.

The differences in the east, north, and vertical directions are plotted in Figures 4 (PPS), 5 (PAN), 6 (range-corrected SPS), and 7 (smoothed pseudorange relative positioning). Notice that Figures 4 and 6 have a maximum vertical scale of ±15 m, while the other two have a scale of ±5 m. Based on the standard deviations, the smallest deviations from the truth come from the smoothed pseudorange solutions, followed by PAN, range-corrected SPS, and PPS. Dr. Benjamin Remondi's

smoothed relative pseudorange solutions are a good choice if keyed receivers are to be avoided. In this case, the reference site can be thousands of kilometers distant. This long-distance capability will be demonstrated in Section 2.4.

This data set illustrates that under normal conditions where satellite tracking is steady and GDOP is good, the solutions from all techniques are acceptable. In particular, the PAN algorithm did a good job of improving the PPS solutions. Comparison of the standard deviations listed in Figures 4 and 5 shows a reduction in each component by almost a factor of four.

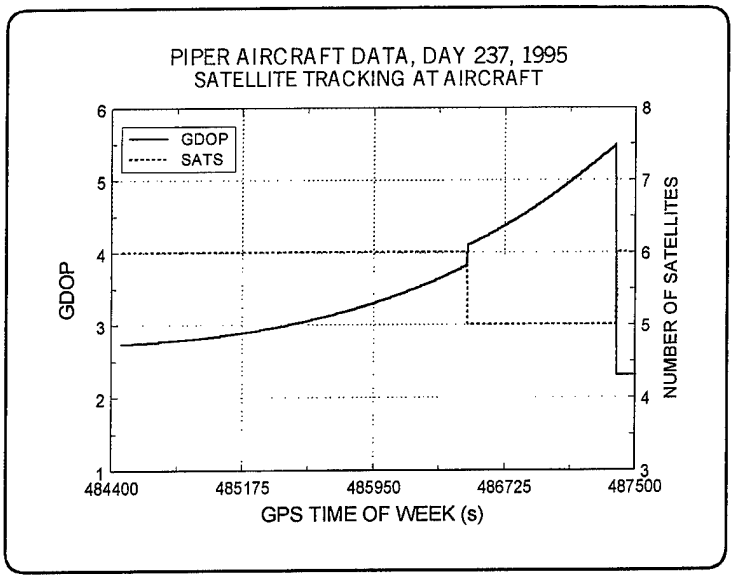

Figure 3—Piper Aircraft GDOP and the Number of Satellites Being Tracked

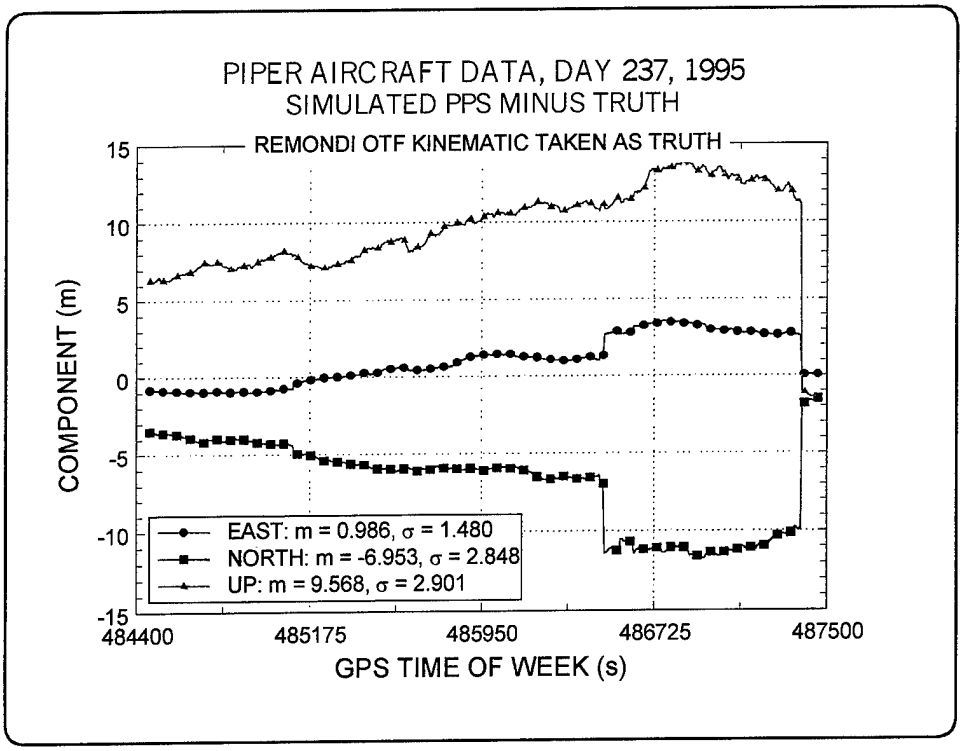

Figure 4—PPS Solutions Minus Truth for the Piper Aircraft

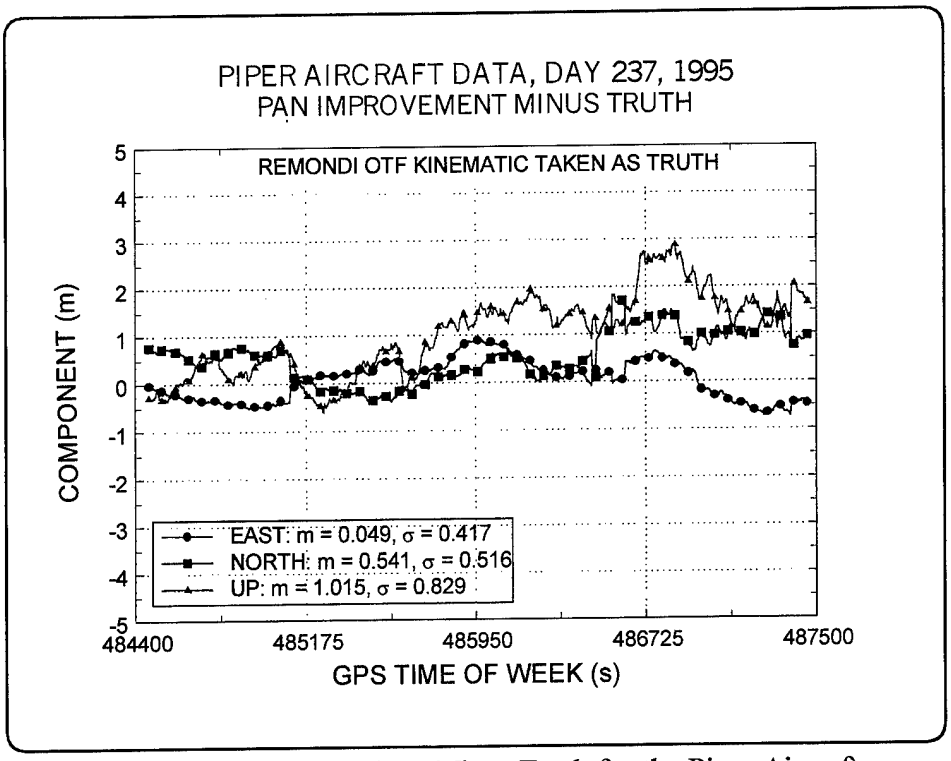

Figure 5—PAN Solutions Minus Truth for the Piper Aircraft

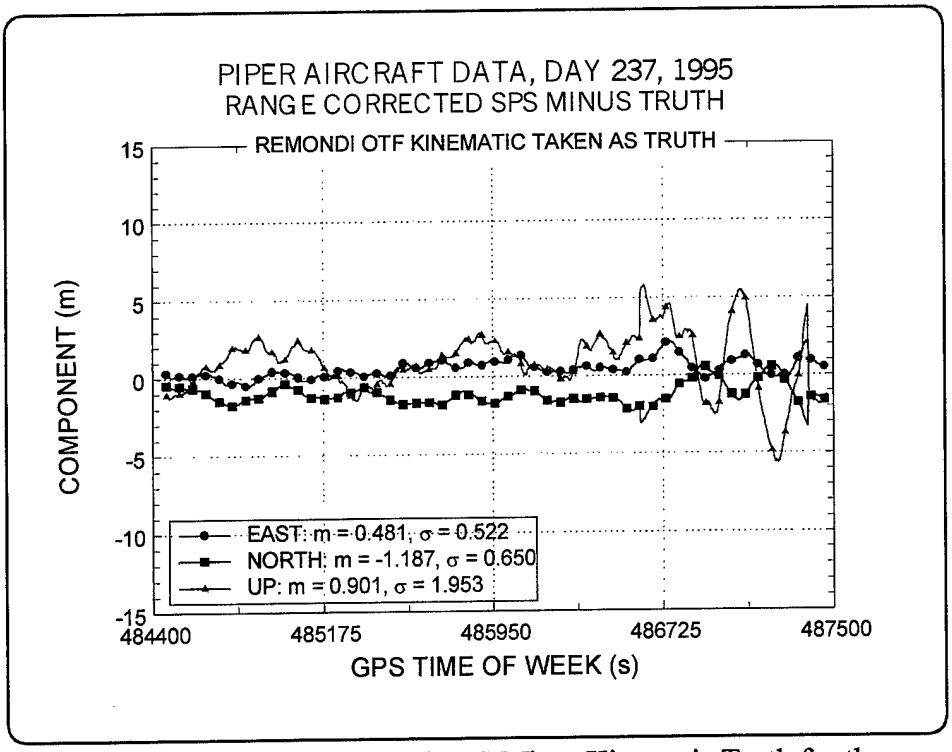

Figure 6—Range-Corrected SPS Minus Kinematic Truth for the Piper Aircraft

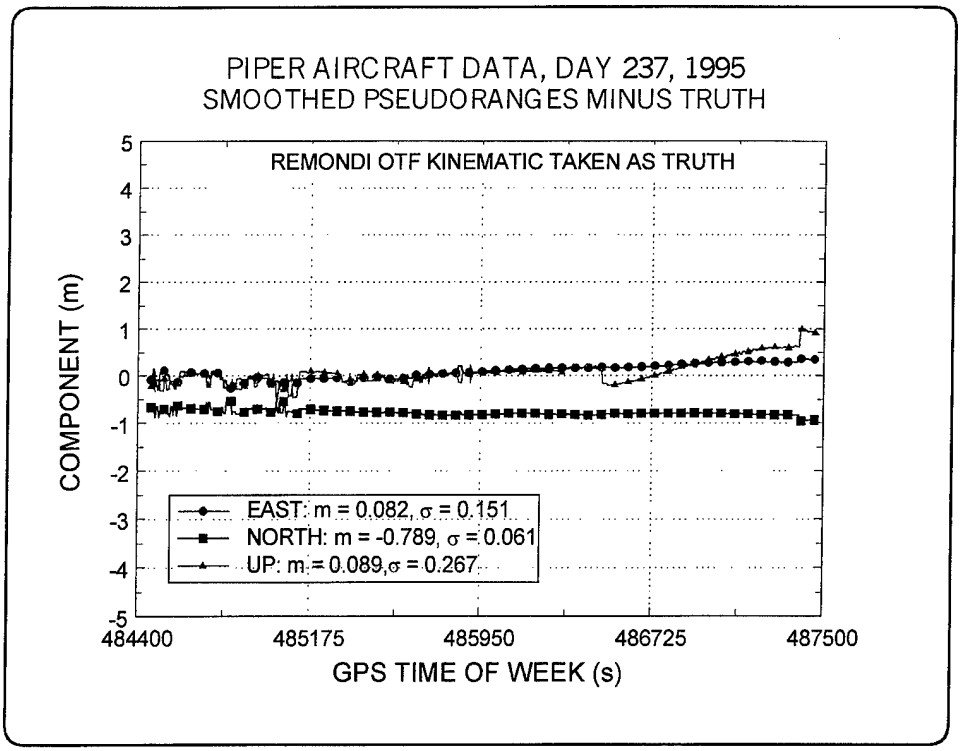

Figure 7—Smoothed Pseudorange Relative Positioning Minus Kinematic Truth for the Piper Aircraft

2.2 Dahlgren/Port Royal Route 301 Circuits

A map of the Dahlgren region is shown in Figure 8. A vehicle with an Ashtech Z-XII receiver and a GPS antenna on its roof collected 1-s data on 1 April 1997. A reference site was operating simultaneously at NSWCDL. The route the vehicle took begins at NSWCDL and continues to Route 301 and northeast to the Potomac River. At the Potomac, the vehicle reversed course and traveled south along Route 301 to Port Royal. At the crossroads, the vehicle turned around and headed back north to the Potomac. This route was repeated a second time.

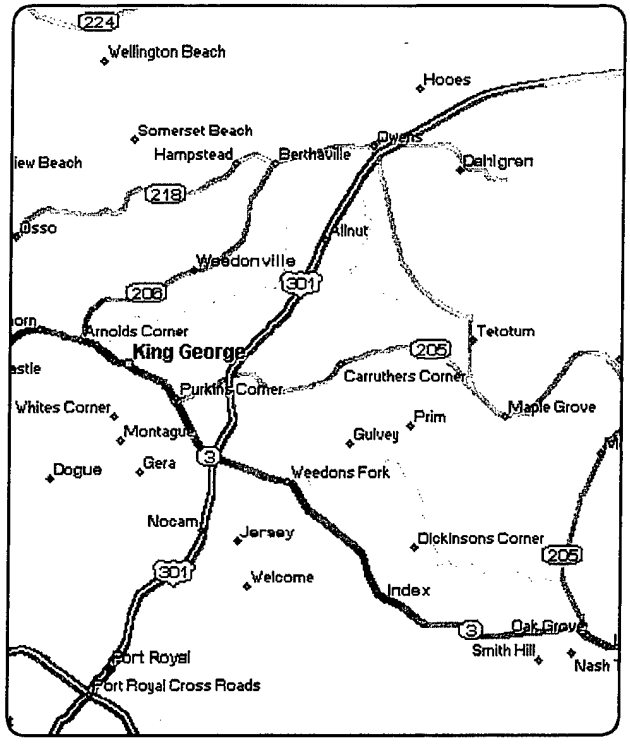

Figure 8—Map of Dahlgren and Port Royal Area

In contrast to the aircraft data, the Route 301 data was far from benign; it is now questionable whether it was suitable for evaluating the merits of the various processing schemes. There were many satellite dropouts due to blockages

by passing vehicles and roadside trees and terrain. The blockages resulted in repeated losses of lock of satellites by the Ashtech Z-XII receiver. This caused havoc with the processing programs, which previously had not been stressed to this degree. The lesson learned is that data collected along a highway route may be extremely difficult to process unless a concerted effort is expended to build adequate protection into the existing software. Getting meaningful operational results from this type of data may require considerable hand editing, given the current maturity of the software.

The GDOP and the number of satellites tracked during the two circuits of the course are plotted in Figure 9. Compare this figure with its counterpart for the aircraft solutions in Figure 3. The repeated loss and reacquisition of satellites, as shown by the dashed line with × symbols in the figure, were mainly due to obstructions by trees along the roadside. Several of the satellites available during this time were at low elevation angles, and at certain places the trees significantly obscured the sky. The GDOP, indicated by the solid line, is dependent upon the number of satellites available at any time and fluctuates as the number in view changes. This causes the accuracy of the solutions to change from epoch to epoch as the satellites come in and out of view. During the first half of the data span, the number of satellites in view rarely surpassed five, but there were fewer dropouts than later in the span. During the second half of the span, the number of satellites visible in the sky was greater, but the number of dropouts was more frequent. Eventually, the On-The-Fly kinematic truth could not obtain correct integers for the new satellites and stopped producing solutions. Figure 10 shows the gaps in the truth during the second circuit. This figure shows the changing distance between the vehicle antenna and the static reference site located on the roof of Building 1200 at NSWCDL.

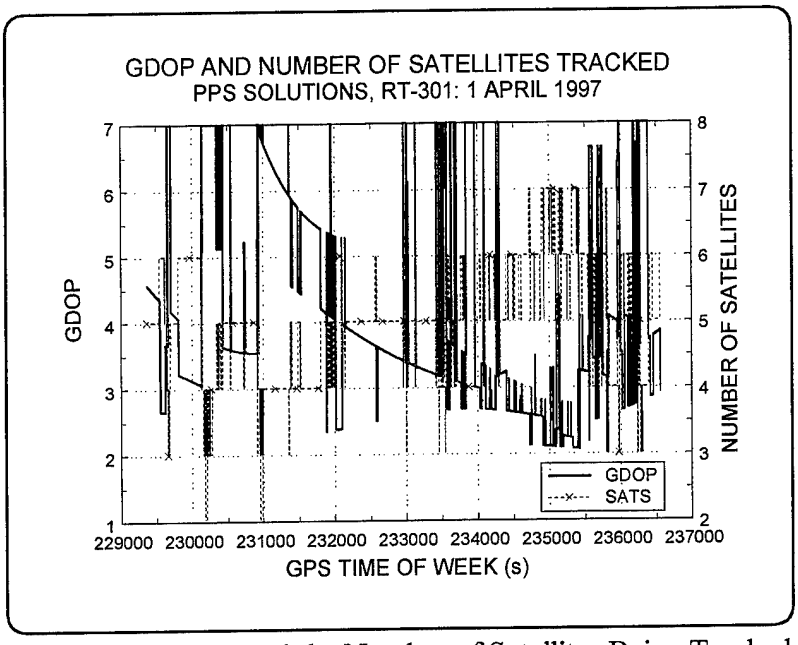

Figure 9—GDOP and the Number of Satellites Being Tracked by the Receiver

Since the interest here is in the accuracy of the determination of ellipsoid height, Figure 11 shows the height solutions obtained from each of the five positioning techniques plotted on the same graph. The plot covers the entire time period of observations. The kinematic solutions, which are considered the most accurate when they exist, are shown as the filled circles. At the beginning of the observations (at about 229,500 s), the integer ambiguities have not been established, and the kinematic ellipsoid heights are at zero (no solutions). After a few hundred seconds, the kinematic solutions begin and continue uninterrupted until about 235,200 s. There are then two periods of dropouts as indicated in Figure 10. The other four positioning techniques produce solutions as long

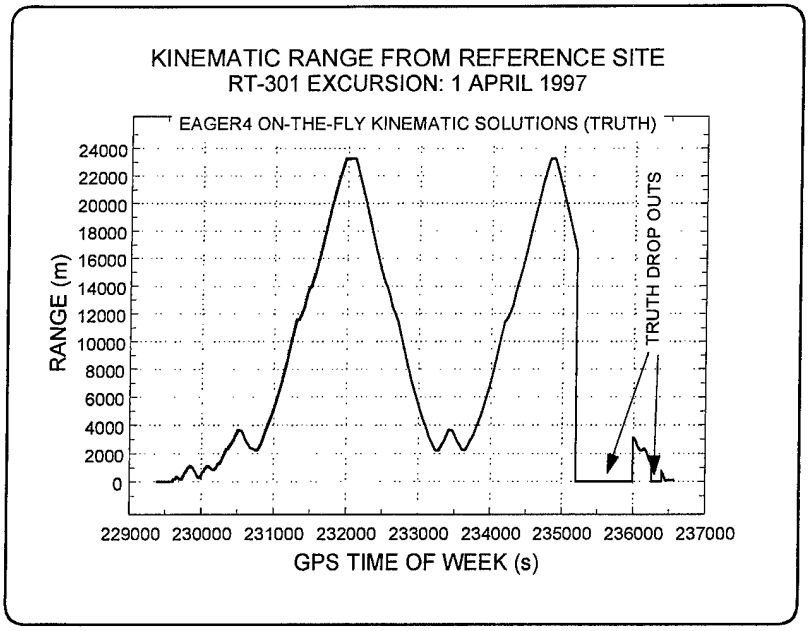

Figure 10—The Range of the Vehicle from the Reference Site Showing the Periods of Dropouts

as there are enough unblocked satellites in view. In a very general sense, all the solutions agree to within about 10 m. When there are bad solutions, such as near 233,600 s, they are obviously bad.

Repeatability can be demonstrated by viewing a short segment of the route on both of the two circuits. On Route 301, the vehicle covered the same ground in the same lane each time around, so the heights are reproducible. The only differences were in the geometry of the satellites, the speed of the vehicle, and stops due to traffic signals. Figure 12 shows a segment of the southbound course, which can be identified in Figure 11 by comparing the time of week. Figure 13 shows the same segment on the second lap. Particular features due to variations in the road height can be identified on both plots. Qualitatively, the repeatability for the kinematic solutions looks good to within 1- m peak difference. This gives some credibility for using the kinematic as truth under these conditions. Presumably, the error is as large as it is because of the constant changing of the satellites in view. It would be interesting to investigate in detail the behavior of the pseudorange and phase observations at the vehicle, but this would take a considerable amount of time to do. With a better editing algorithm available, it may be possible to eliminate many of the spikes seen in the solutions. They are probably due to the existence of questionable observations making their way into the solutions.

Differences among the four techniques and the kinematic truth are shown in Figures 14 through 17. All are plotted as east, north, and vertical components on a ±10-m scale. The solution spikes are due to bad observations as described above. The simulated PPS and the PAN solutions are similar in character, with the PAN solutions being slightly less noisy as determined by the standard deviations. In this data set, the ephemerides are not the major source of error. The PAN algorithm uses the PPS solutions as the starting point and exchanges the broadcast ephemerides for the precise. Any errors in the PPS solutions not due to the ephemerides are carried unchanged over into the PAN solutions. The gap in all plots between 235,200 and 236,000 s is where the truth is lacking.

2.3 Positioning the NIMA Vehicle at Holloman AFB

During the evening of 7 November and the early morning hours of 8 November 1996, two NIMA vehicles carried Ashtech receivers to various known sites at Holloman AFB in New Mexico. A NIMA reference site was also operating, but, due to a software problem, the data from this receiver was not saved. However, during about 2 of the 12 hours of NIMA operation, NSWCDD operated

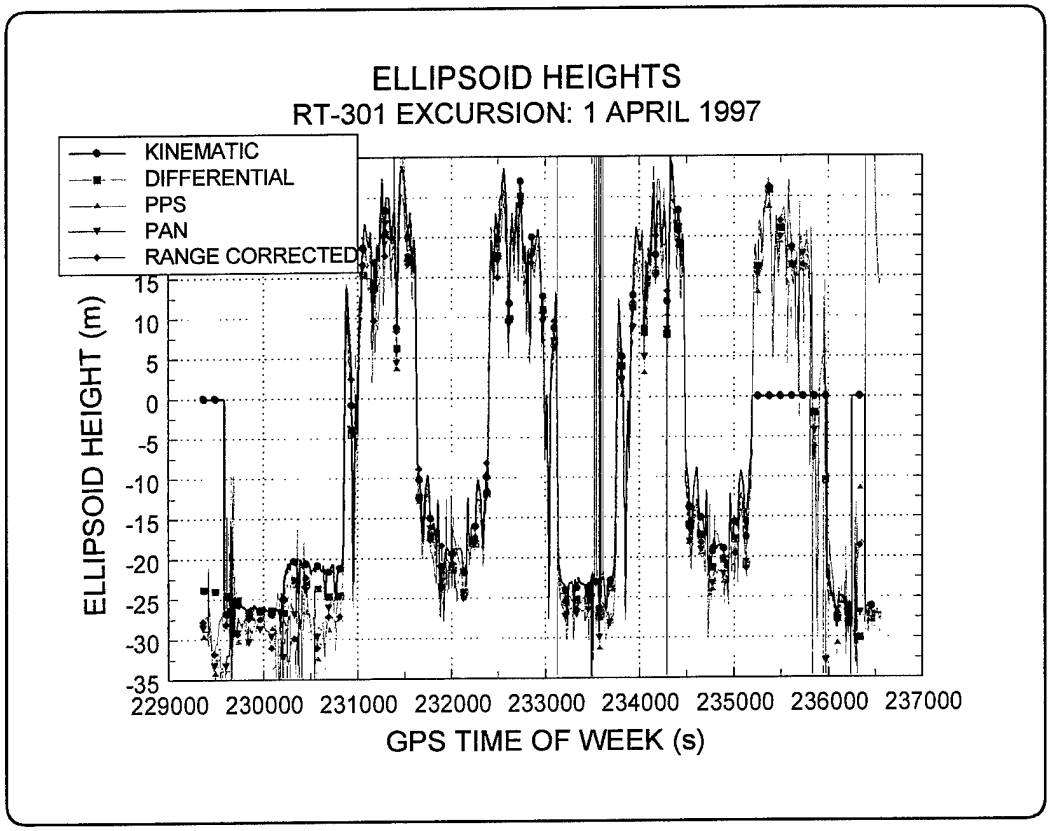

Figure 11—Ellipsoid Height Solutions

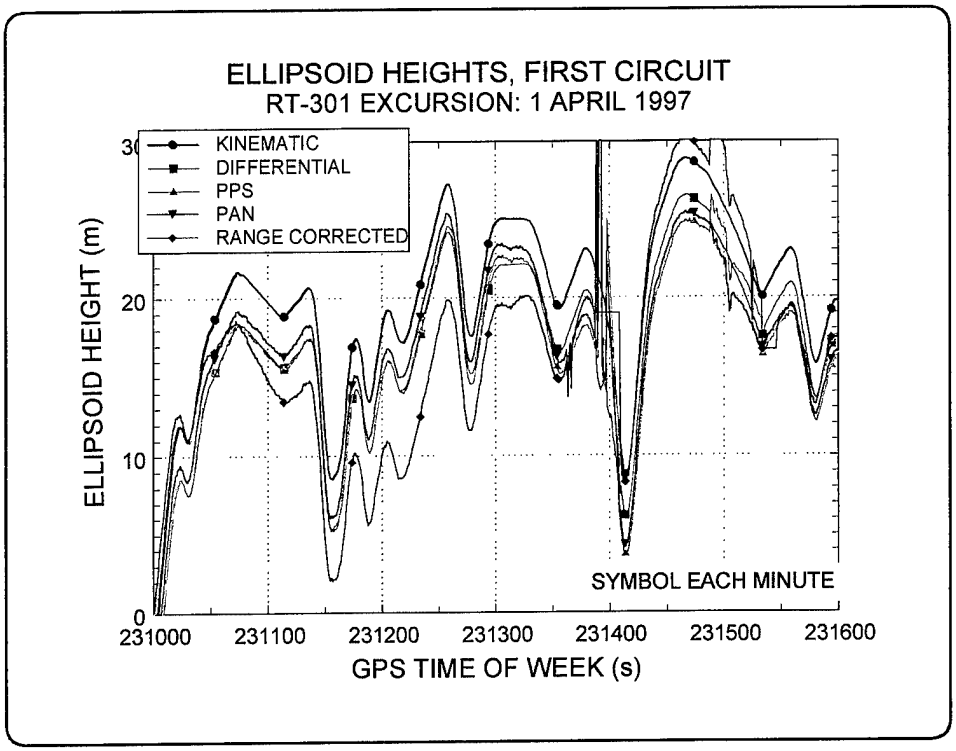

Figure 12—Ellipsoid Heights for a Southbound Segment on Lap 1

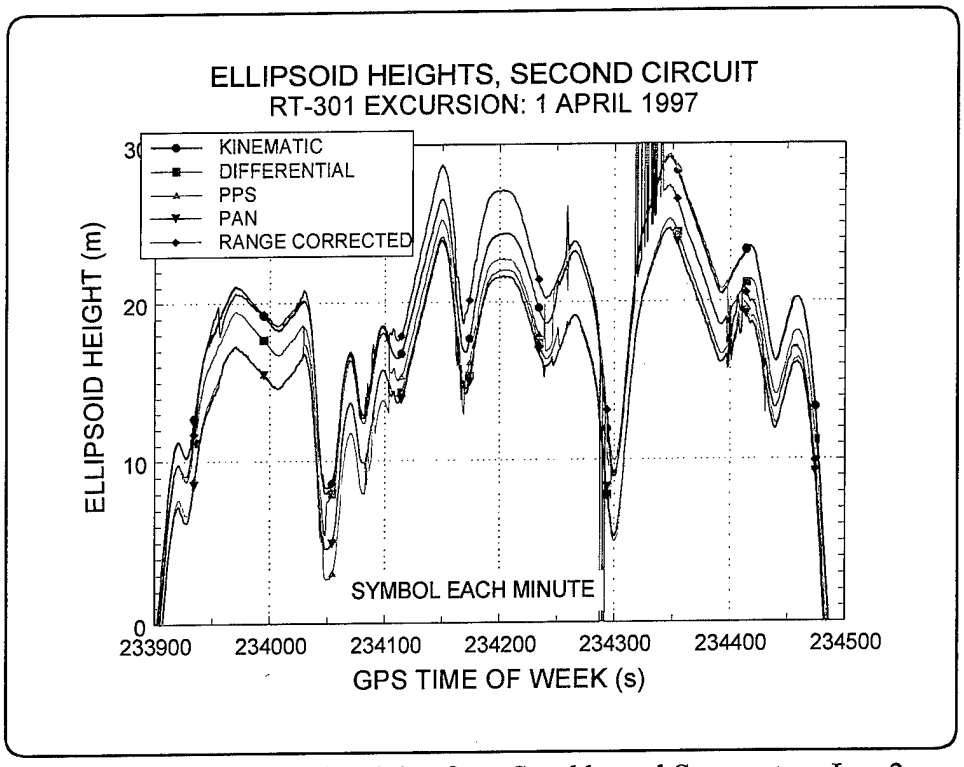

Figure 13—Ellipsoid Heights for a Southbound Segment on Lap 2

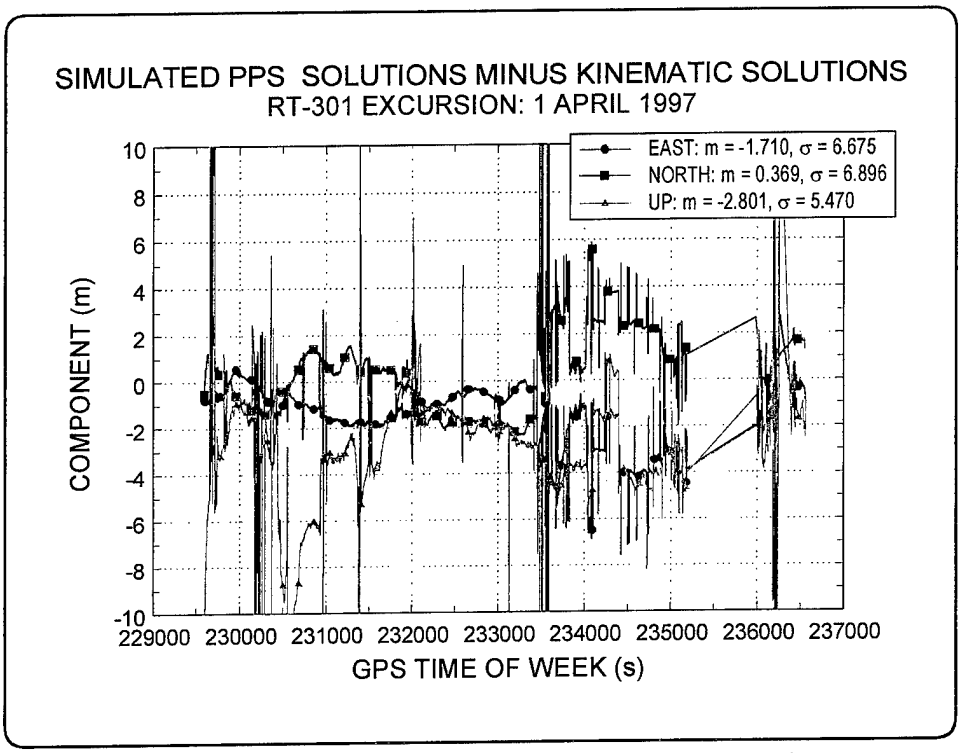

Figure 14—PPS Solutions Minus Kinematic Truth

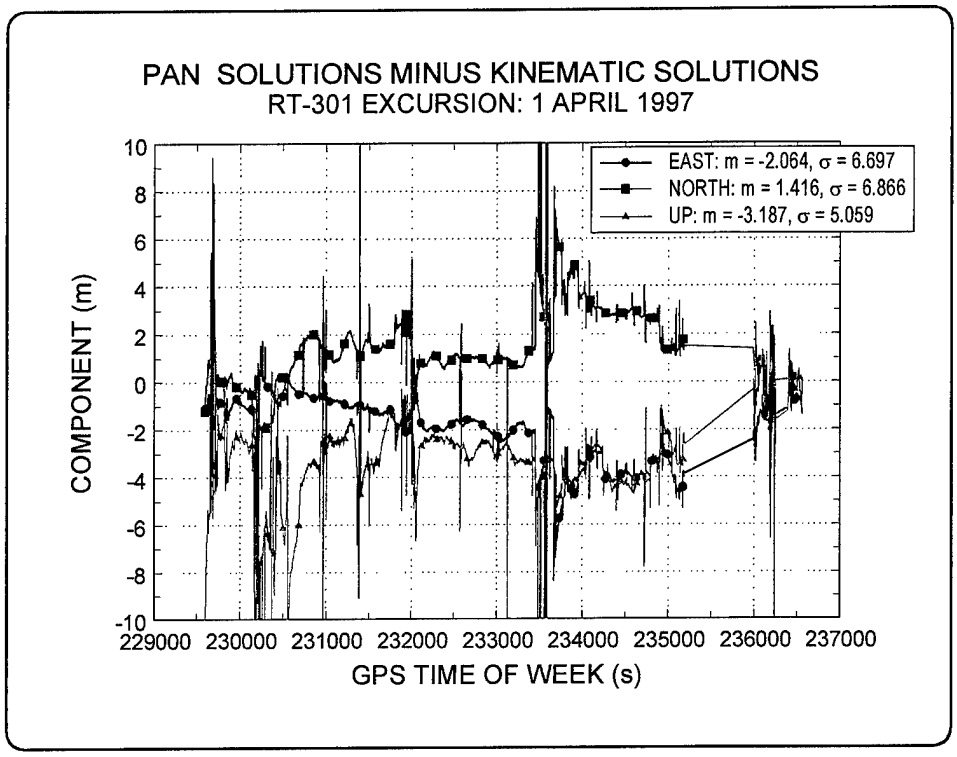

Figure 15—PAN Solutions Minus Kinematic Truth

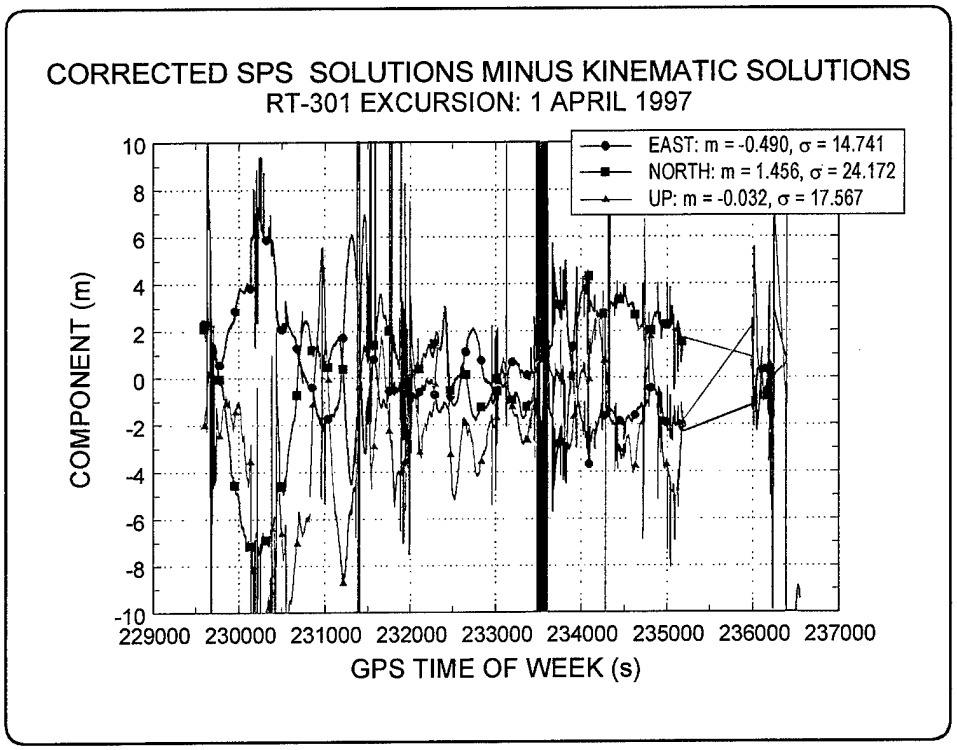

Figure 16—Range-Corrected SPS Minus Kinematic Truth

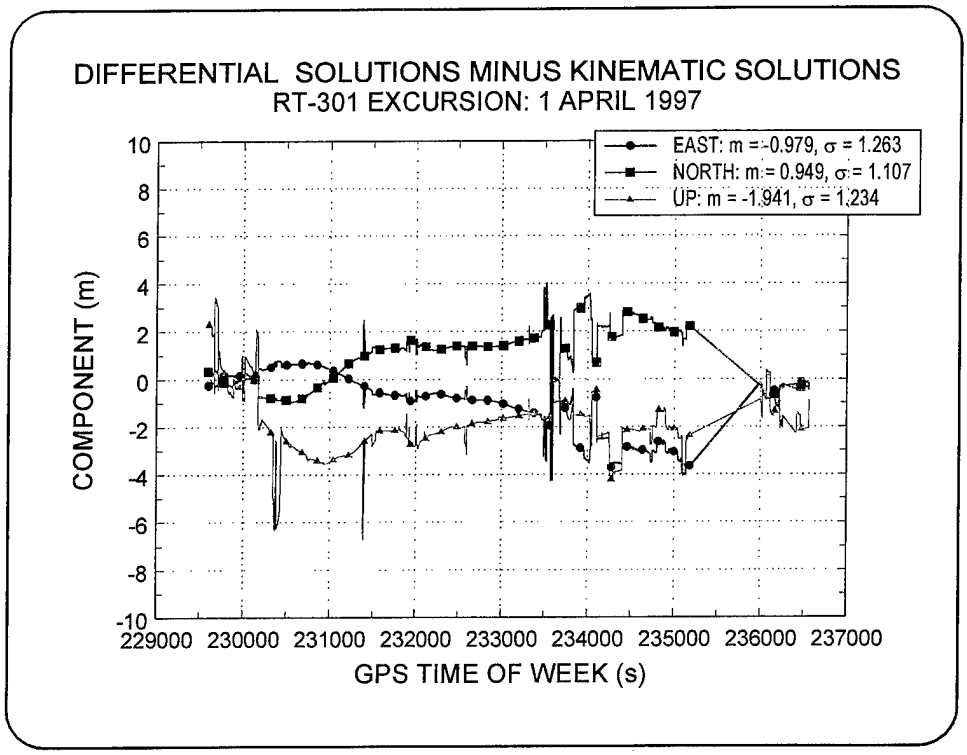

Figure 17—Smoothed Pseudorange Relative Positioning Minus Kinematic Truth

a receiver at site F901 not far from the NIMA vehicle route. This 2-hr segment was used here to evaluate the ellipsoid height accuracy at a closed course and at previously surveyed markers.

A plot showing the route of the NIMA vehicle that was on the course during the 2-hr period is shown in Figure 18. The route begins at the upper left, and progresses east and south toward the lower right, stopping at each of the sites indicated. Near site ST11, the vehicle turned around and headed north again. The 2-hr period ended just north of ST63. The NSWCDD reference site F901 is shown as a ✠ symbol at the origin near the lower right corner of the plot. The GDOP and the number of satellites in view is shown in Figure 19. At this time of day and at this location, the number of satellites tracked at F901 were never fewer than seven, and the

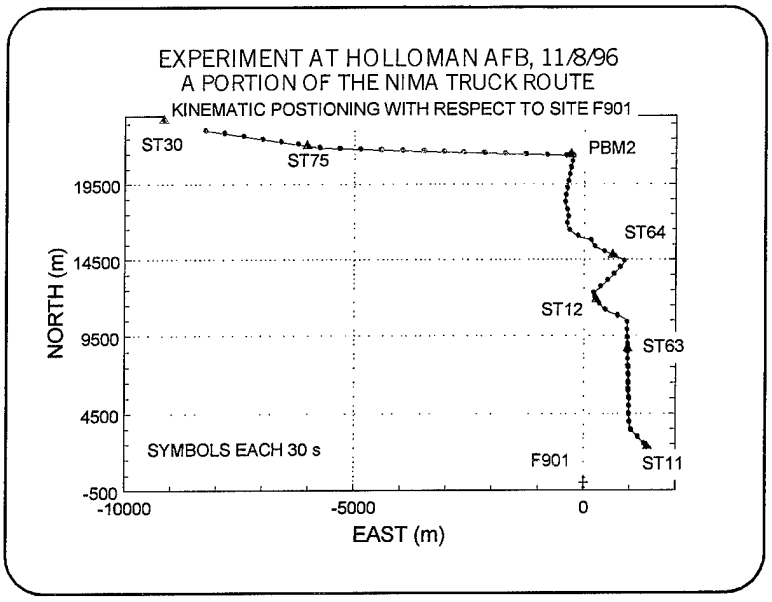

Figure 18—NIMA Vehicle Route

GDOP was three or smaller most of the time.

This data set provides an opportunity to compare results against independently established absolute positions. The markers indicated in Figure 18 have known coordinates. Two of these will be used to illustrate the accuracy and repeatability of the kinematic relative positioning technique. Of course, any error in the position of the reference site F901 will add to the apparent absolute error in the other site positions.

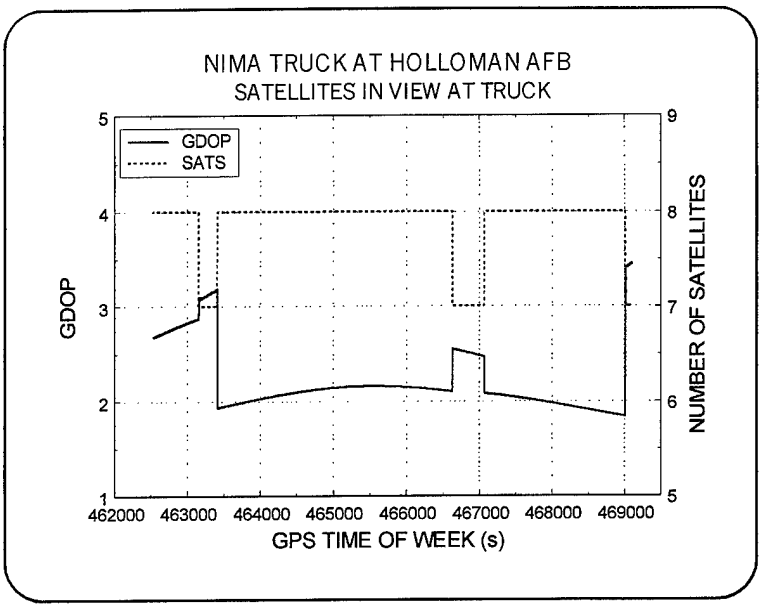

Figure 19—GDOP and the Number of Satellites in View at Site F901

The NIMA operation involved carrying a GPS antenna attached to the outside of the vehicle, so that data was collected continuously while in motion as well as when stopped at a marker. The antenna on its pole would be detached from the vehicle and walked to the marker. The point at the bottom of the pole would be placed on the monument center and the pole leveled. It would stay stationary there for several minutes. It would then be walked back to the vehicle and reattached. The vehicle would then proceed on to the next site, where the process would be repeated.

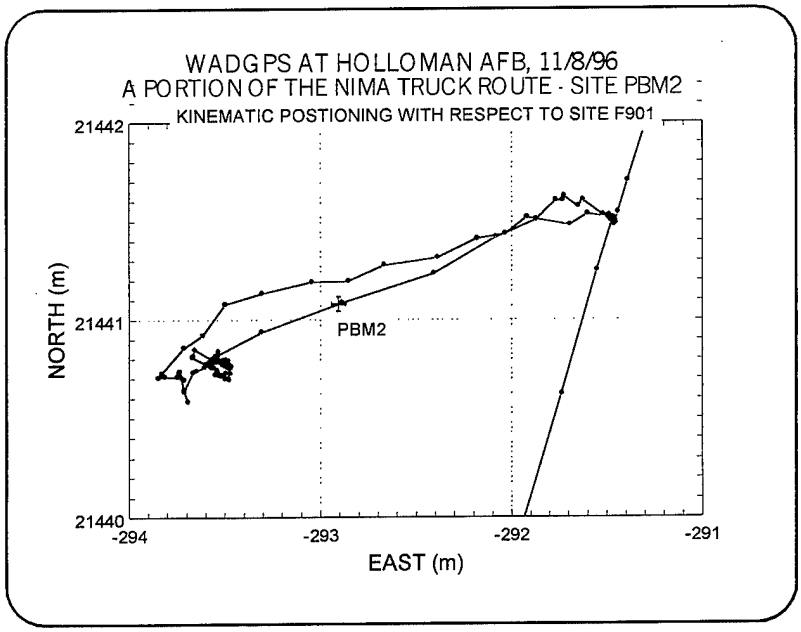

Figure 20—NIMA East-North Antenna Position in the Vicinity of Site PBM2

An example of the process described above is shown in Figure 20 at site PBM2. This plot shows the east and north components of the stop at PBM2 with respect to F901 in meters. The known location of the mark is indicated as a ✠ symbol in the plot. The kinematic relative position of the marker is at the cluster of dots about 0.6-m west and 0.3-m south of the cross. Absolute errors in the tabulated location of PBM2 and F901 probably account for the disagreement in position. Figure 21 shows the east and ellipsoid height components. Again, the PBM2 mark is indicated by the ✠ symbol and the antenna location (2.067 m above the mark) is indicated by the tri-

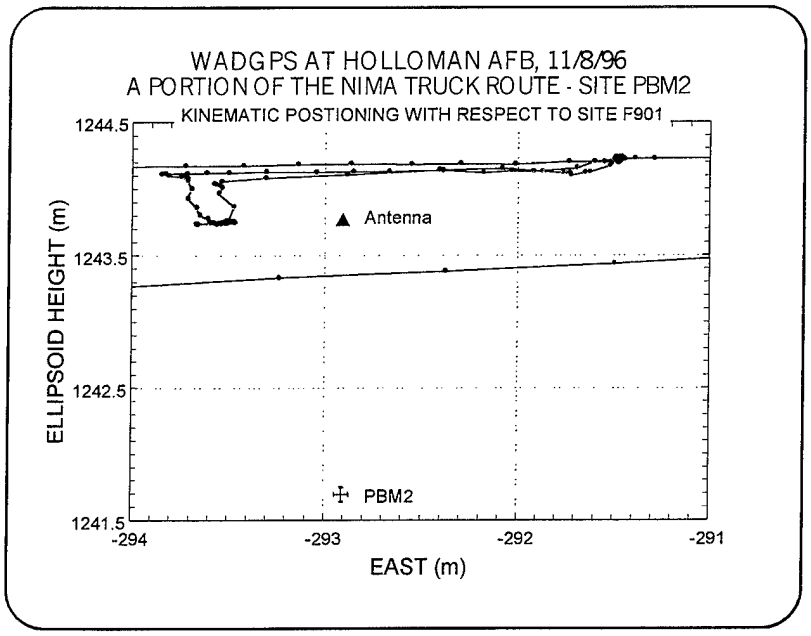

Figure 21—NIMA East-Height Antenna Position in the Vicinity of Site PBM2

angle. The agreement in height is very good. Figure 22 shows a high-resolution look at the scatter in the kinematic solution in the east and ellipsoid height components. A 1-cm diameter circle (plotted as an ellipse because of the different scales on the two axes) is included for reference. The repeatability of the kinematic (truth) solutions during the time the antenna was over the mark is at the centimeter level as claimed.

The stops at site ST63 will be displayed next. This is the only site during the 2 hours of F901 operation where two stops were made. Figure 23 shows the east-north activity in the vicinity of ST63, and Figure 24 shows the

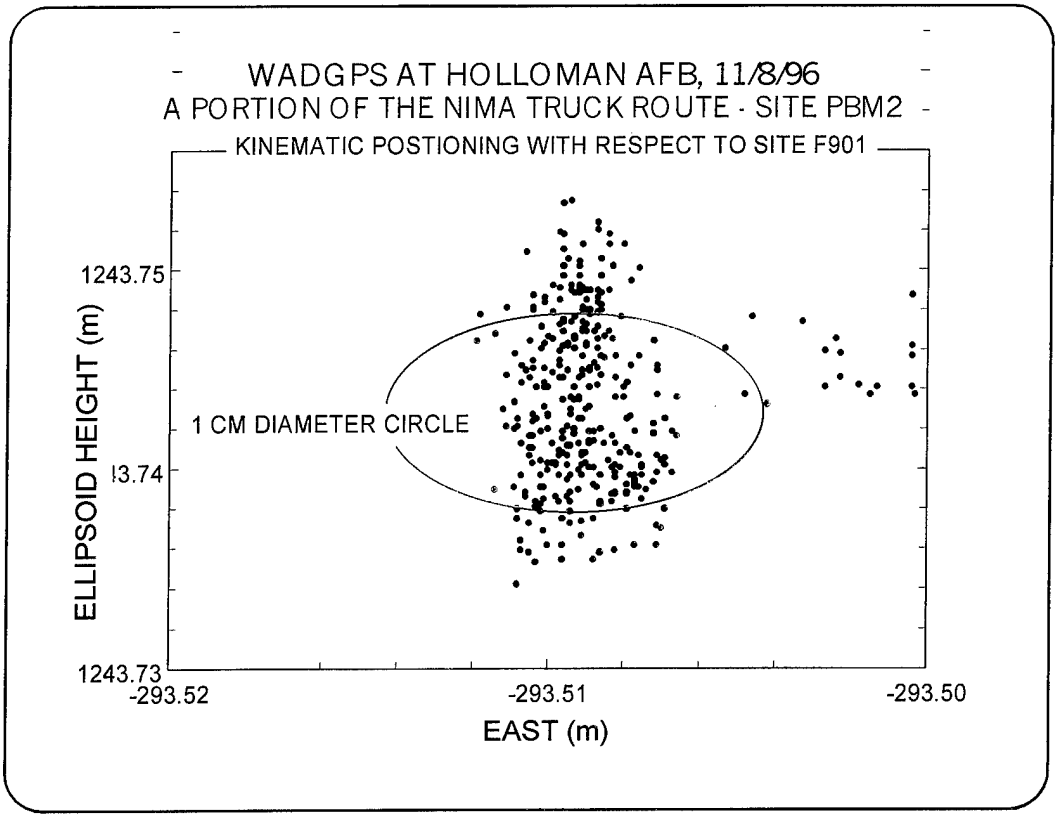

Figure 22—Scatter in the East-Height Position of PBM2 from Kinematic Positioning

north-ellipsoid height components. The first stop was in the southbound direction and the second was in the northbound direction. The accepted position for ST63 is indicated by the ⌖ symbol. The actual position of the mark appears to be near the horizontal blob in the center of Figure 23.

A closer look at the solutions while the antenna was at the mark is shown in Figures 25 and 26. The southbound solutions are shown as filled circles and the northbound solutions as open circles. A 3-cm diameter circle is included on each plot for reference. The filled symbols form a tighter cluster within the reference circle than the open symbols, but both sets are included within the circle. This shows that the kinematic truth solutions are repeatable at the 3-cm level after a period of time has passed, and the constellation of satellites have formed a different configuration.

The evidence just presented for sites PBM2 and ST63 shows that the kinematic truth is reliable, so it will be used to evaluate the positioning accuracy of the other four techniques during the 2-hr period. Figures 27 through 30 show the differences between the simulated PPS solutions, PAN, range corrected SPS, and smoothed pseudorange solutions, respectively; and the truth. These differences are smaller than those from the aircraft flight and all are plotted in ±5-m axes.

The solutions minus the truth from the three test data sets discussed in Section 2 are summarized in Tables 1 through 4. The standard deviation in each component from the three test cases is computed and listed in the *Average* σ row of each table. The Route 301 standard deviations are much greater than the others and dominate, but are consistent in relative magnitude with, the other two. If the Route 301 results are discarded, all four techniques have mean values smaller than 10 m from the truth and standard deviations smaller than 5 m. The PAN means are 1 m or smaller,

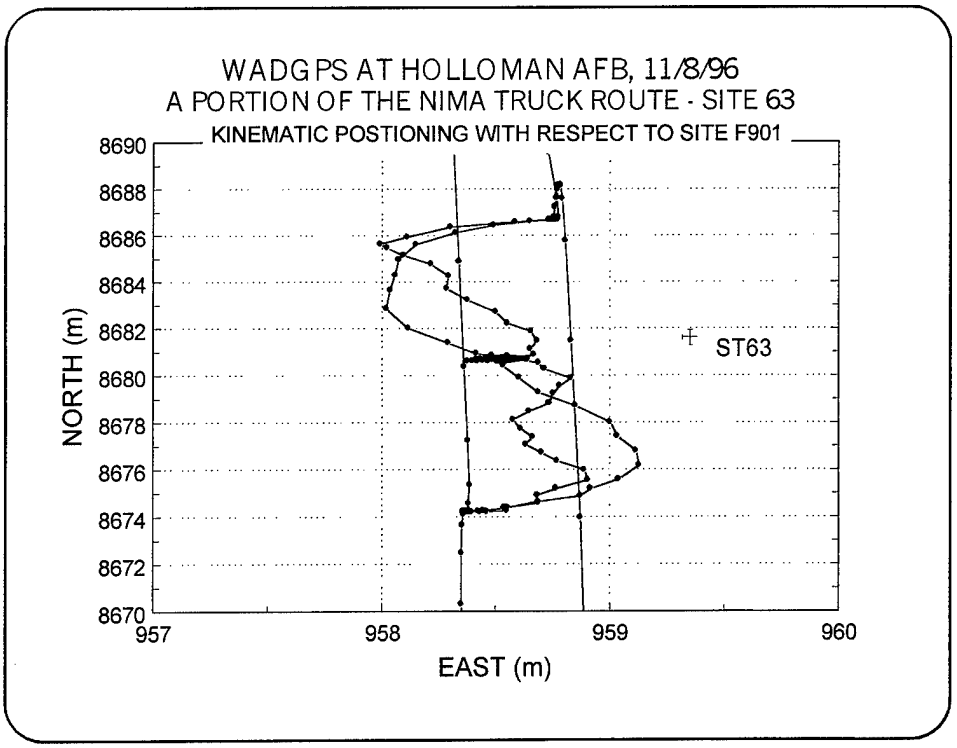

Figure 23—Kinematic Solutions in the Vicinity of ST63 in the East-North Components

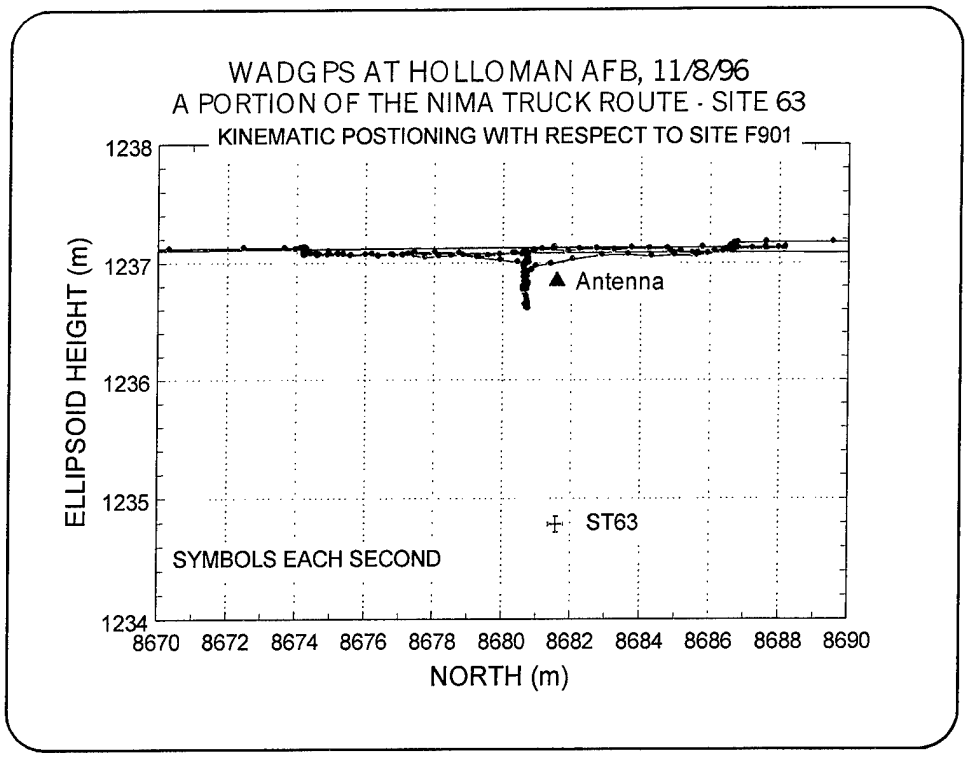

Figure 24—Kinematic Solutions in the Vicinity of ST63 in the East-Height Components

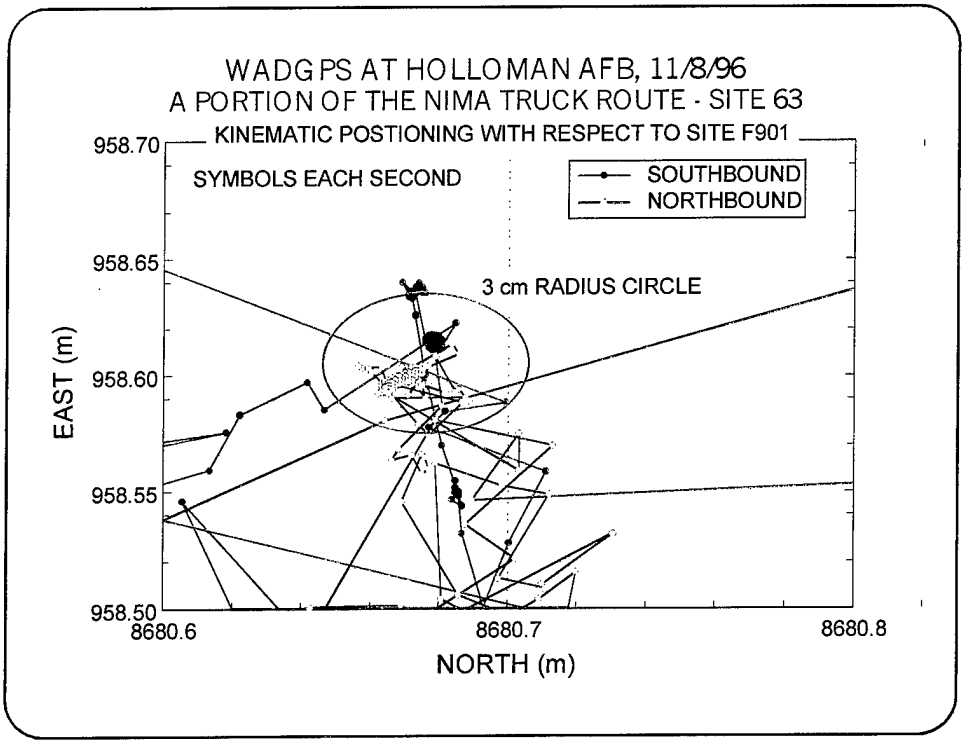

Figure 25—Scatter in the East-North Solutions at Site ST63

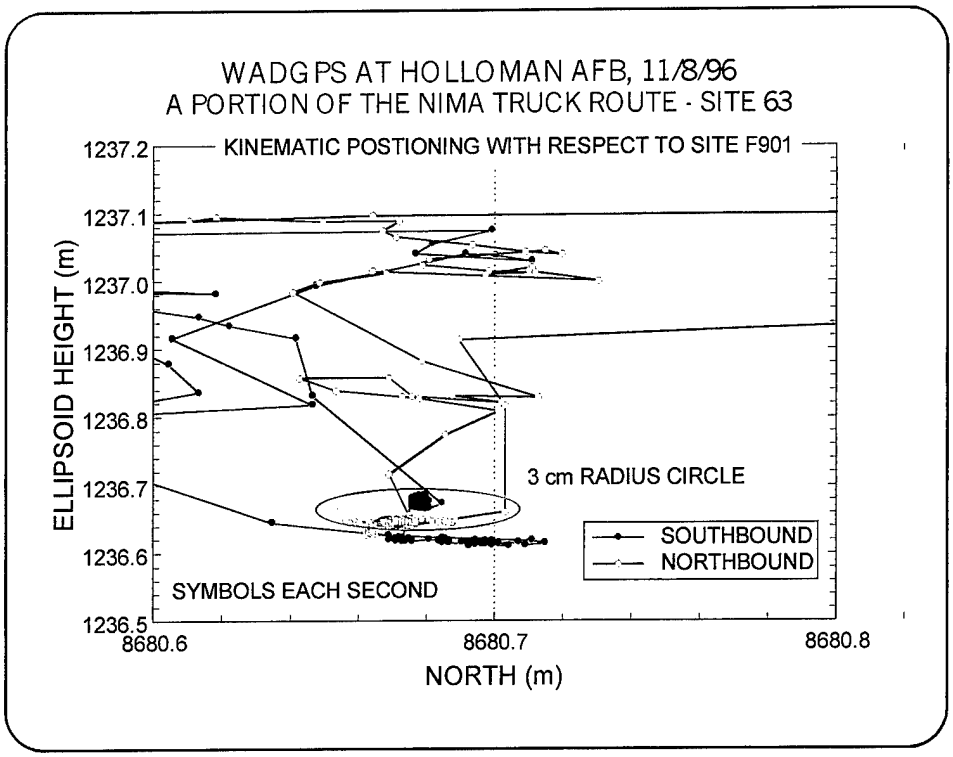

Figure 26—Scatter in the North-Height Solutions at Site ST63

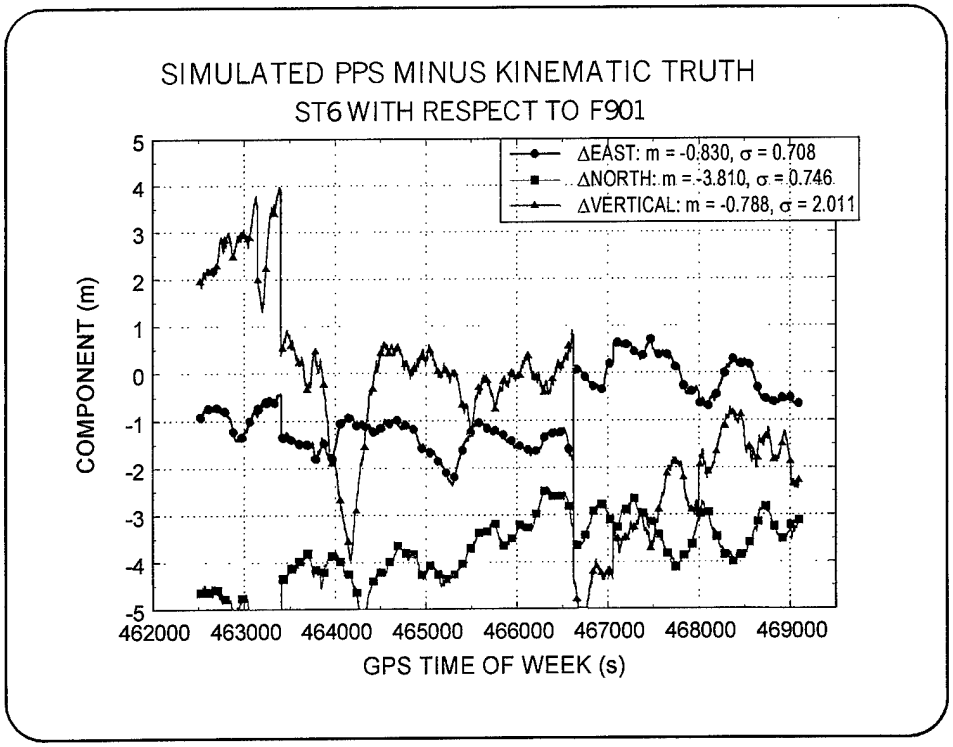

Figure 27—PPS Solutions for the NIMA Vehicle Minus Truth

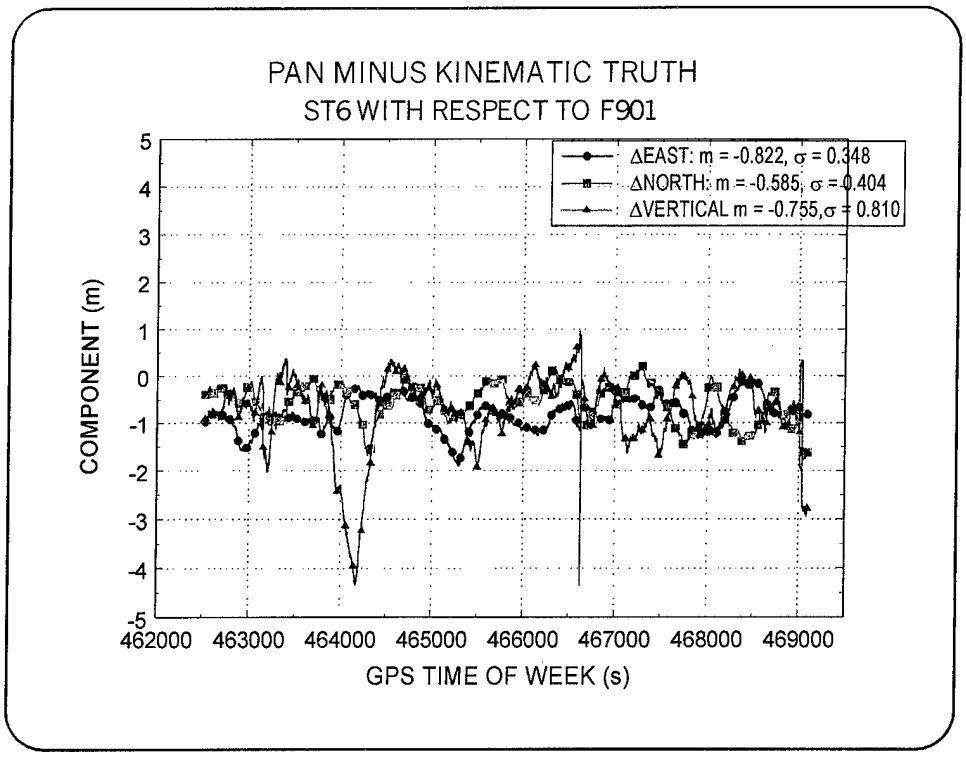

Figure 28—PAN Solutions for the NIMA Vehicle Minus Truth

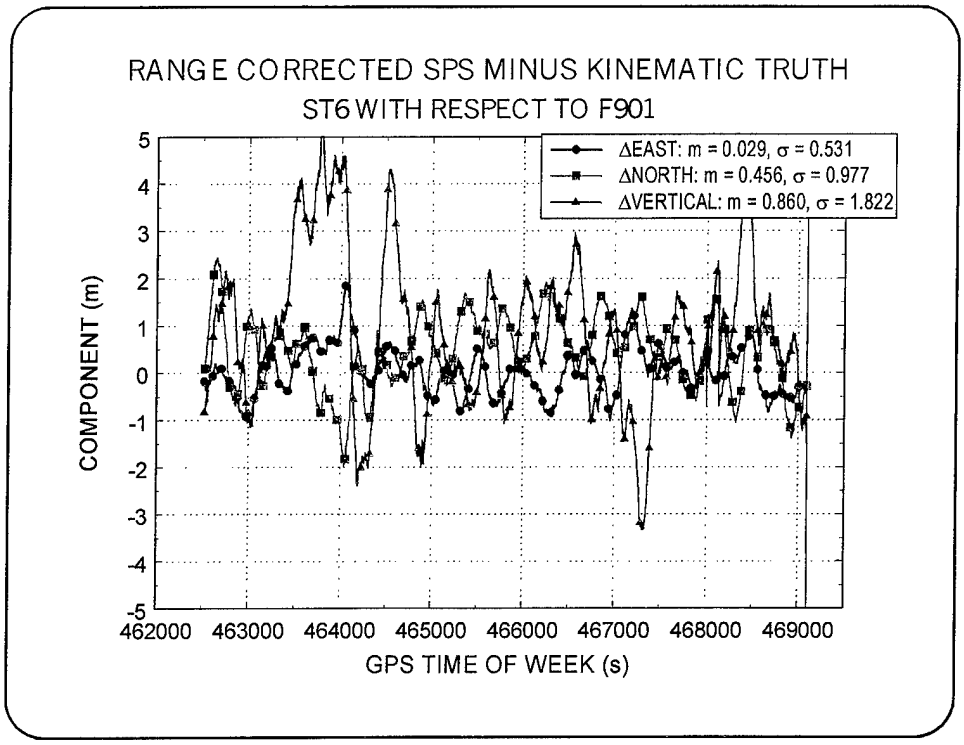

Figure 29—Range-Corrected SPS Solutions Minus Truth

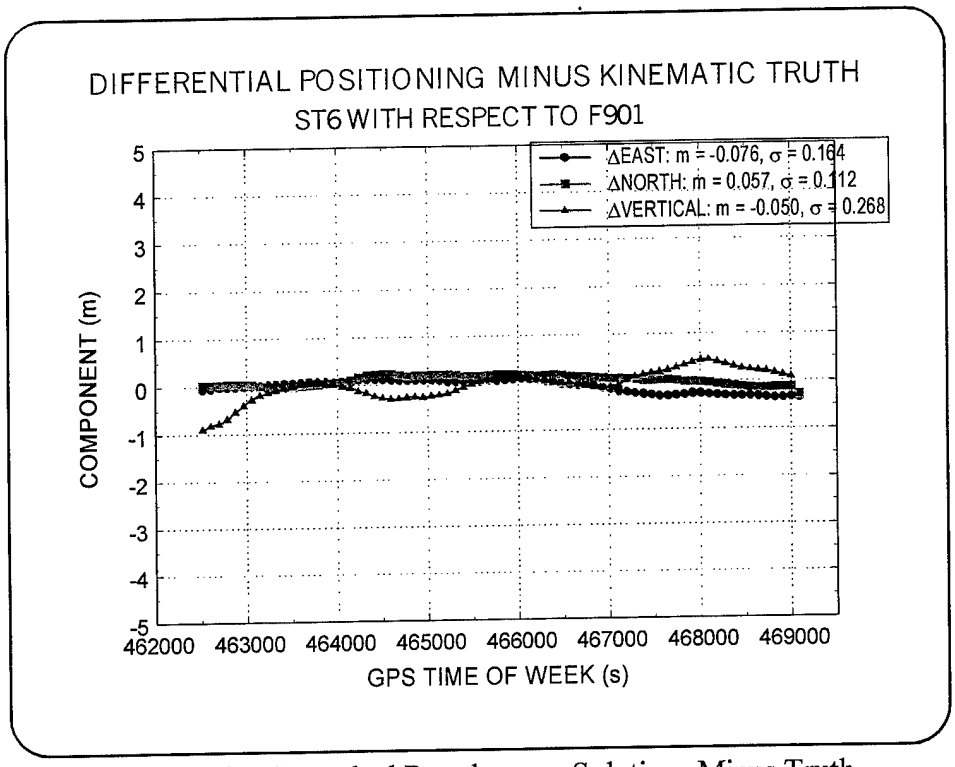

Figure 30—Smoothed Pseudorange Solutions Minus Truth

Table 1— Simulated PPS

Units = meters	EAST				NORTH				VERTICAL			
	MAX	MIN	MEAN	σ	MAX	MIN	MEAN	σ	MAX	MIN	MEAN	σ
PIPER	3.55	-1.02	0.99	1.48	-1.53	-11.81	-6.95	2.85	13.89	-1.62	9.57	2.90
RTE 301	108.08	-256.12	-1.71	6.68	261.63	-105.15	0.37	6.90	161.53	-115.68	-2.80	5.47
HOLLOMAN	0.72	-2.38	-0.83	0.71	-2.43	-5.94	-3.81	0.75	3.96	-5.40	-0.79	2.01
AVERAGE σ				2.95				3.50				3.46

Table 2—PAN Improvement

Units = meters	EAST				NORTH				VERTICAL			
	MAX	MIN	MEAN	σ	MAX	MIN	MEAN	σ	MAX	MIN	MEAN	σ
PIPER	0.90	-0.75	0.05	0.42	1.82	-0.40	0.54	0.52	2.89	-0.60	1.02	0.83
RTE 301	-257.99	108.15	-2.06	6.70	264.64	-104.35	1.42	6.87	158.51	-116.13	-3.19	5.06
HOLLOMAN	0.61	-2.01	-0.82	0.35	0.22	-1.78	-0.59	0.40	0.95	-4.35	-0.76	0.81
AVERAGE σ				2.49				2.60				2.23

Table 3— Range-Corrected SPS

Units = meters	EAST				NORTH				VERTICAL			
	MAX	MIN	MEAN	σ	MAX	MIN	MEAN	σ	MAX	MIN	MEAN	σ
PIPER	2.17	-0.58	0.48	0.52	0.64	-3.32	-1.19	0.65	5.81	-5.64	0.90	1.95
RTE 301	243.60	-255.40	-0.49	14.74	488.2	-249.3	1.46	24.17	189.7	-118.6	-0.03	17.57
HOLLOMAN	1.88	-14.00	0.03	0.53	49.83	-1.98	0.46	0.98	70.25	-3.35	0.86	1.82
AVERAGE σ				5.27				8.60				7.11

Table 4— Smoothed Pseudorange Relative Positioning

Units = meters	EAST				NORTH				VERTICAL			
	MAX	MIN	MEAN	σ	MAX	MIN	MEAN	σ	MAX	MIN	MEAN	σ
PIPER	0.35	-0.30	0.08	0.15	-0.52	-0.96	-0.79	0.06	0.99	-0.53	0.09	0.27
RTE 301	0.77	-4.05	-0.98	1.26	3.98	-1.00	0.95	1.11	3.45	-6.71	-1.94	1.23
HOLLOMAN	0.11	-0.40	-0.08	0.16	0.22	-0.30	0.06	0.11	0.44	-0.92	-0.05	0.27
AVERAGE σ				0.53				0.43				0.59

with standard deviations under a meter. However, the smoothed pseudorange relative positioning solutions are the best performers, with means smaller than 1 m and standard deviations under 0.5 m. This potential will be explored in the next section with reference sites at greater distances.

2.4 Other Reference Sites

PPS and PAN solutions are absolute; that is, they do not need to have a reference site collect data simultaneously. In effect, the reference sites for absolute positioning are those in the GPS Monitor Station Network. Since the satellite ephemerides are derived from observations obtained at the reference sites, the satellites carry the information about the monitor station locations and transfer it to the users through each satellite's predicted or fitted position. The users then use the satellite signals to complete the link back to the monitor stations.

The addition of simultaneous observations at a known static reference site can be used to remove some of the common mode errors that exist in the propagation of signals from orbit to the ground. The uncertainty of the satellite's positions can also be reduced, thus forming a stronger link to the monitor stations. During the data collection by the NIMA vehicle at Holloman, several other static sites, some at considerable distances, simultaneously collected data at 1-s epochs. Figure 31 is a time line showing the periods for which data were collected at seven other sites. The time segment coinciding with the 2-hr period for which the F901 provided kinematic truth was used to demonstrate high-quality relative positioning over extended distances. The sites and their approximate straight-line distances from Holloman AFB are listed in Table 5.

The ellipsoid heights of the NIMA vehicle were found relative to each of these sites and are plotted in the following figures. These illustrate that relative positioning can give acceptable results over continental distances. Figure 32 shows the truth ellipsoid height plotted with the PPS, PAN, and range-corrected SPS. For comparison, the truth is plotted on all of the following figures. Figure 33 shows the solutions with Austin or Monterey as reference sites. Figure 34 shows the solutions with Calgary or Dahlgren as reference sites. Figure 35 shows the solutions with Ottawa, Yellowknife, or St. John's as reference sites. The Canadian sites used Rogue receivers, while the other sites used Ashtech Z-XIIs. The St. John's site shows jumps that may indicate a receiver problem and might have something to do with the 10-m disagreement for a portion of the period considered.

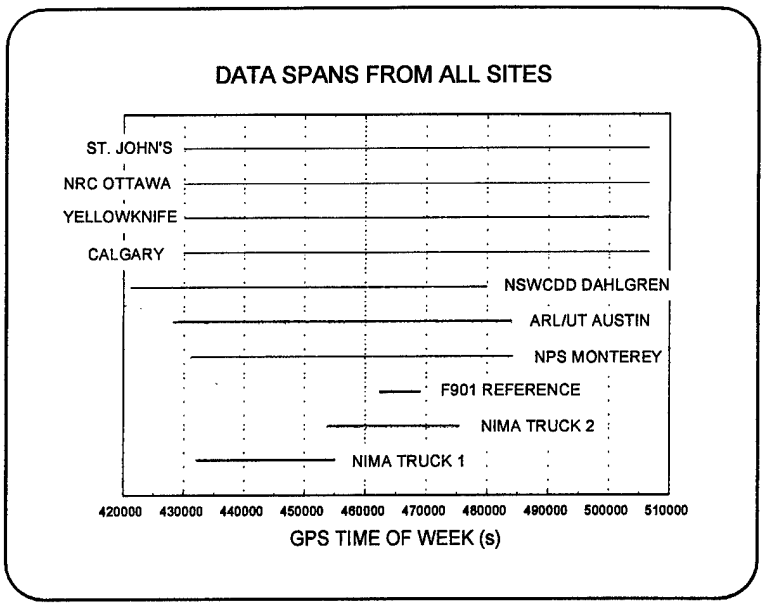

Figure 31—Observation Spans from Other Static Reference Sites

From the results of this analysis, it can be argued that the two-frequency pseudorange relative-positioning algorithm is the best all-around performer. It requires a reference site, but the reference site does not have to be close to the operational area; indeed, it can be thousands of kilometers distant and still provide good results. The benefits of relative positioning are that the PPS solutions are not needed, and consequently, all receivers can be operated unkeyed as long as they are capable of providing two frequency pseudorange observations. Dual-frequency observations are not required; a single-frequency pseudorange relative positioning algorithm developed by Dr. Remondi is used in Section 3.

Table 5—Distances of Remote Sites from Holloman AFB, New Mexico

RECEIVER SITE	DISTANCE (km)
Austin, Texas (ARL/UT)	**845**
Monterey, California (NPS)	**1476**
Calgary, Alberta, Canada (UC)	**2072**
Dahlgren, Virginia (NSWCDD)	**2675**
Ottawa, Ontario, Canada (NRC)	**2926**
Yellowknife, Northwest Territory, Canada	**3282**
St. John's, Newfoundland, Canada	**4622**

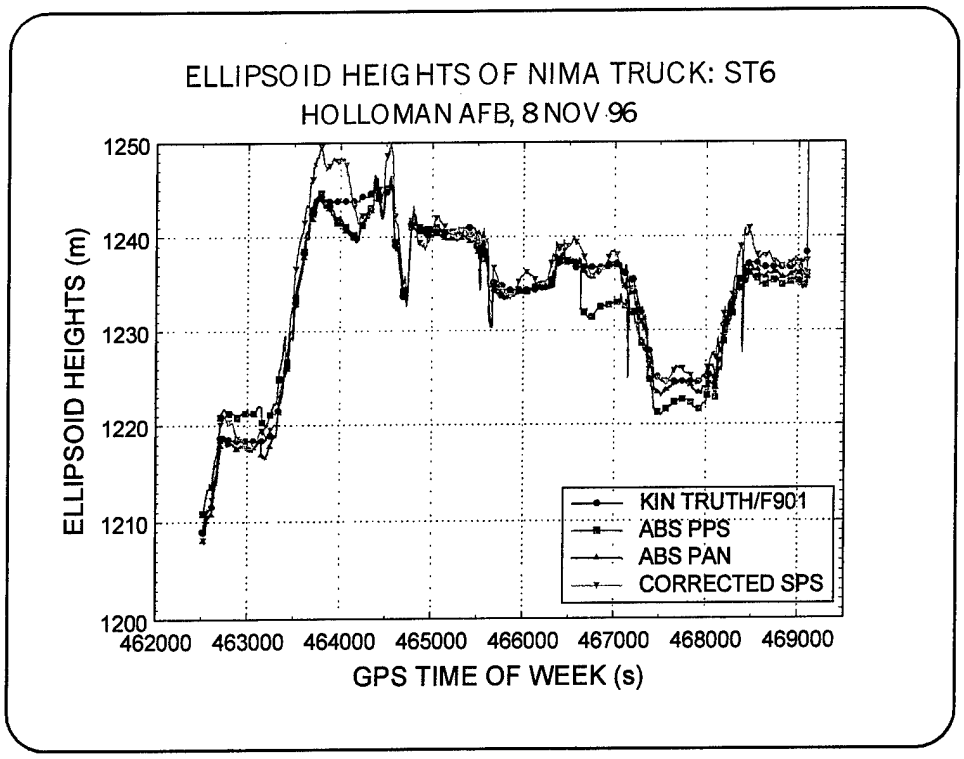

Figure 32—PPS, PAN, and Range-Corrected SPS

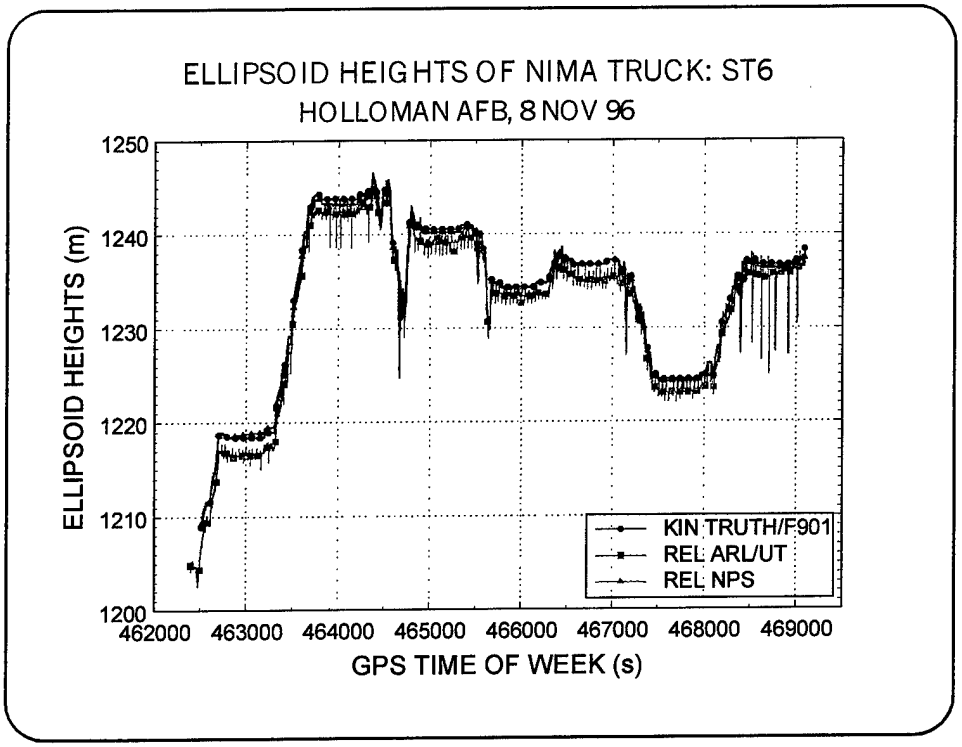

Figure 33—NIMA Vehicle Positioned From Austin and Monterey

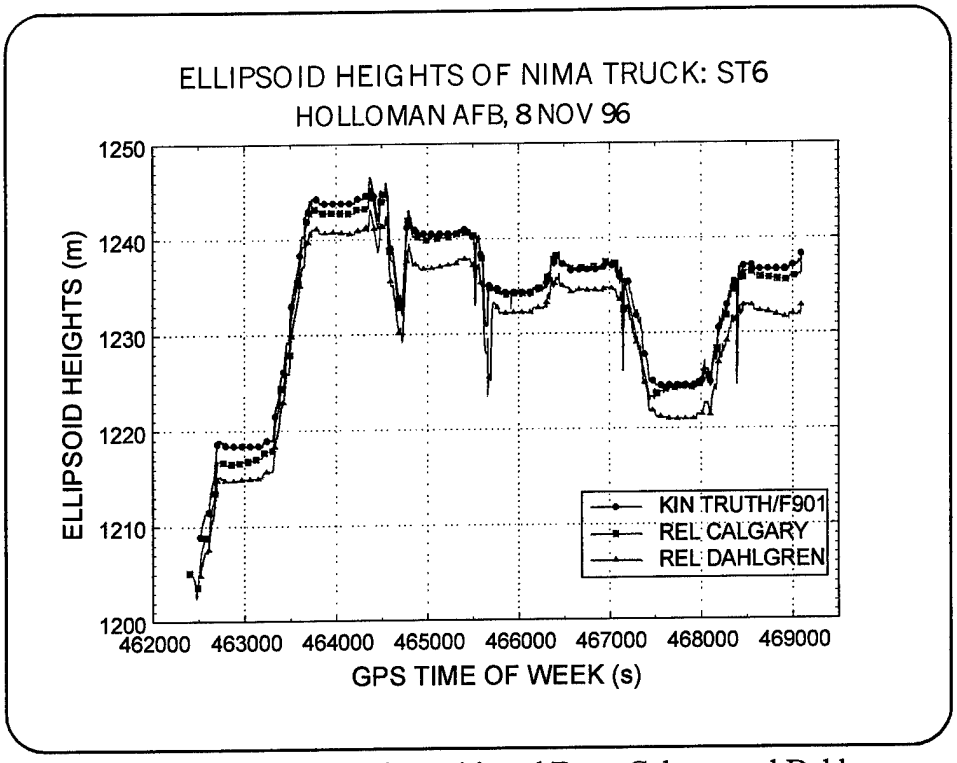

Figure 34—NIMA Vehicle Positioned From Calgary and Dahlgren

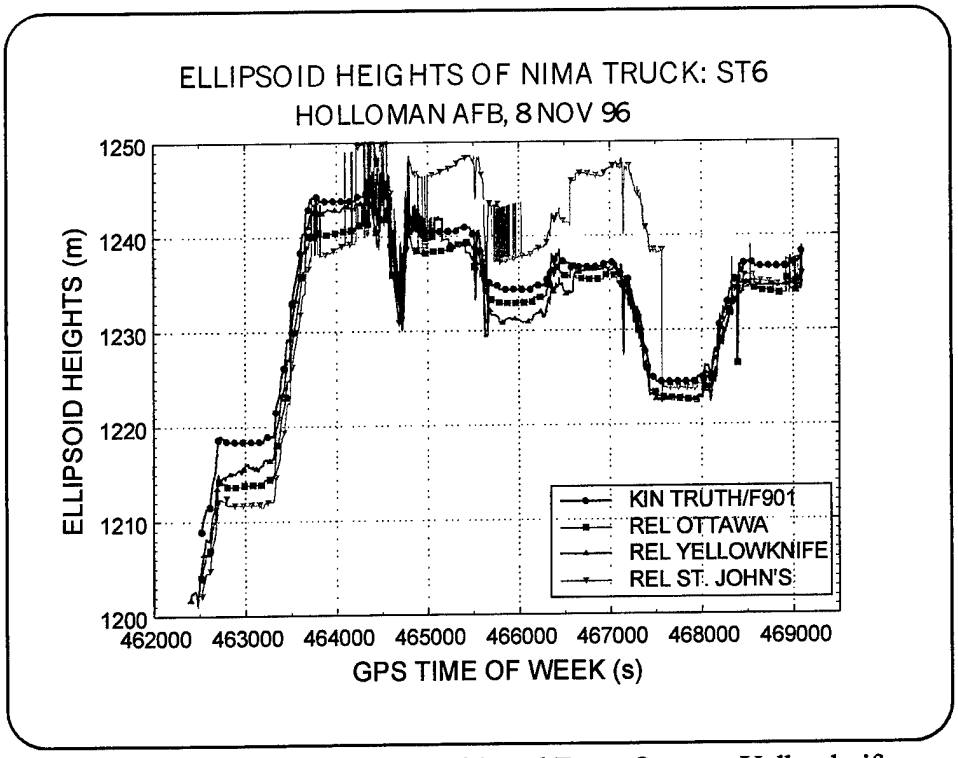

Figure 35—NIMA Vehicle Positioned From Ottawa, Yellowknife, and St. John's

3.0 NIMA ROAD TEST

During 1997 on days 190 through 193, a road test was conducted to collect an extensive GPS data set with multiple receivers. The goal of the 4-day excursion was to collect GPS data while traveling along interstate highways and, then, to evaluate the quality of the postprocessed height solutions. A NIMA van with three different receiver types and two antennas traveled from St. Louis, Missouri, to Toledo, Ohio, and back along I-55 and I-80. Two Ashtech receivers shared an antenna mounted on the van roof near the front of the vehicle, while a Trimble receiver operated from a single antenna mounted about a meter behind the first. Data was collected at 1-s intervals most of the time, except for the last day, when the interval was 2 s on all receivers. At several points along the route, transects were run on roads perpendicular to the interstate highways. NIMA operated no reference sites simultaneously with the 4-day trek, but some data were collected at NSWCDL and 30-s data has been downloaded from three NOAA CORS sites located near St. Louis, Milwaukee, and Detroit. These data were used for relative positioning solutions.

The road test data was characterized by many satellite dropouts and periods of poor signal strength that result in navigation solutions that are not as good as they could be under more stable conditions. The data quality is inferior to that from the ARL/UT aircraft flight and NIMA Holloman AFB truck experiments discussed in Section 2. In order to try and better understand the reason for the poor quality data seen in the NSWCDL Rte. 301 and NIMA road tests, an investigation of multipath was undertaken. The premise for this initiative was that increased multipath due to vehicle motion might be the cause of the low-quality navigation solutions. It was found however, contrary to the authors' expectations, that the average multipath from the NIMA road test data set did not exceed the average multipath computed from data collected at static sites. However, it can be seen from the plots that follow, that the character of the computed multipath indicator is qualitatively different between the static and dynamic data sets. In particular, the multipath indicator computed from the dynamic data is characterized by impulses, while the data from static sites is not.

3.1 Performance of the Receivers

Before proceeding with the multipath analysis, the performance of the receivers will be illustrated. Tables of the number of epochs tracked on each day and plots of the number of satellites tracked as a function of GPS time follow. A single day, 193, was chosen for the plots because the receiver performance on that day was generally the best of the four days. The two receivers that shared an antenna were an Ashtech MD-XII single-frequency receiver, whose performance is listed in Table 6, and a Z-XII dual-frequency receiver, listed in Table 7. The Trimble receiver, listed in Table 8, was a 4000MSGR dual-frequency receiver. As shown in Table 8, the Trimble—though dual-frequency capable—was usually set up to collect single-frequency observations. The data were downloaded when the receiver memory filled, so on some days, multiple files were collected. These

Table 6—Observation Epochs from the Ashtech MD-XII Receiver

DAY	BEGIN TOW	END TOW	NUMBER OF EPOCHS	EPOCHS WITH 4 SATS %	NUMBER OF OBSER-VATIONS	OBS OF L1 %	OBS OF L2 %	OBS OF C1 %	OBS OF P1 %	OBS OF P2 %
190A	325180	337627	12038	93.6	63400	98.7	98.7	100	0	0
191A	390661	401890	10955	97.1	65008	98.8	98.8	100	0	0
191B	402615	408700	6022	97.6	37390	99.0	99.0	100	0	0
191C	414526	424778	9933	92.6	47016	98.4	98.4	100	0	0
191D	424779	434138	8864	92.3	50130	98.5	98.5	100	0	0
192A	489011	486519	7319	91.0	40283	98.0	98.0	100	0	0
192B	486818	494766	3922	93.8	23811	96.0	96.0	100	0	0
192C	494768	509176	6740	87.6	35253	97.3	97.3	100	0	0
192D	509252	524244	7117	87.2	35739	96.6	96.6	100	0	0
193A	559712	582508	11136	95.5	64403	97.7	97.7	100	0	0

Table 7—Observation Epochs from the Ashtech Z-XII Receiver

DAY	BEGIN TOW	END TOW	NUMBER OF EPOCHS	EPOCHS WITH 4 SATS %	NUMBER OF OBSER-VATIONS	OBS OF L1 %	OBS OF L2 %	OBS OF C1 %	OBS OF P1 %	OBS OF P2 %
190A	325173	343291	18089	98.9	112732	97.9	90.1	100	90.2	90.1
191A	397075	412506	15433	99.9	114780	98.0	92.3	100	92.8	92.3
191B	414123	424783	10651	99.5	61788	96.9	83.1	100	83.6	83.1
191C	424785	435488	9445	100	60452	96.9	85.7	100	86.2	85.7
192A	419018	486661	7645	99.8	53926	96.6	78.6	100	79.7	78.6
192B	486764	497367	5303	99.9	39485	95.9	83.1	100	83.2	83.1
192C	499052	511359	6155	99.3	35561	94.8	80.5	100	81.0	80.5
192D	511598	519249	3827	99.7	26504	94.3	67.4	100	68.6	67.4
192E	519878	523479	1802	99.7	11627	97.5	88.6	100	88.9	88.6
193A	559740	582743	11489	99.9	80790	95.9	88.9	100	89.3	88.9

are indicated by the letters A, B, C, etc., following the day number in the left-hand column. The column headed "Epochs with Four Satellites" indicates the percentage of epochs where solutions were possible. The columns headed by percentages of observations for L1, L2, C1, P1, and P2 indicate the number of epochs where good data from at least one satellite was obtained for phase on L_1, for phase on L_2, for pseudorange on L_1 C/A code, for pseudorange on L_1 P code, and for pseudorange on L_2 P code.

Table 8—Observation Epochs from the Trimble Receiver

DAY	BEGIN TOW	END TOW	NUMBER OF EPOCHS	EPOCHS WITH 4 SATS %	NUMBER OF OBSER-VATIONS	OBS OF L1 %	OBS OF L2 %	OBS OF C1 %	OBS OF P1 %	OBS OF P2 %
190A	325062	343592	18498	96.0	92897	94.0	0.1	99.9	89.8	0
191A	390884	424394	33469	98.7	223331	94.5	0	99.9	90.1	0
191B	427145	437436	10288	97.6	66330	90.9	51.1	100	0	51.1
192A	478832	486376	7543	99.3	52780	92.0	43.4	100	0	43.4
192B	486830	511928	12547	98.9	82781	92.7	52.7	100	0	52.7
192C	511990	524252	6085	96.1	40443	92.1	49.0	100	0	49.0
193A	559922	582638	11357	99.4	79958	95.1	57.9	100	0	57.9

Plots of the satellites tracked on day 193 by each receiver are shown in Figures 36 through 38. The figures show the elevation angle for each satellite in view during the day. The vertical lines indicate where observations from a satellite were not recorded or were edited. Figure 36 shows the results from the MD-XII receiver, Figure 37 the results from the Z-XII, and Figure 38 the results from the Trimble. The Z-XII displays the fewest edited epochs while the MD-XII displays the most. These results are also typical for the other days of observations.

Another indication of the relative tracking performance of these receivers during the NIMA road test is given by the total number of satellites tracked at each epoch and the corresponding GDOP. Figures 39 through 41 show this information for day 193. The constant changes in the number of satellites tracked make it difficult for the receivers to provide high-quality observations. When the number of satellites in view is dependent upon the external environment, the geometric strength suffers, and the solutions may be poorly determined. The GDOP is an indicator of the solution quality due to geometry. Again it is clear, based upon the number of satellites tracked, that the Z-XII performs the best and the MD-XII the worst.

3.2 Multipath Indicator Model

The multipath indicator to be described is a way to quantitatively evaluate the difference between range difference observations obtained from pseudoranges and the equivalent observations obtained from phases. These differences are attributed to multipath, though any propagation phenomena that affects the two kinds of observations in a manner similar to multipath may be lumped into the indicator. The formulation that follows is attributed to Dr. Benjamin Remondi. In order to begin, two frequency pseudorange and phase observations are required. Therefore, use of the observations from the NIMA road test restricts the evaluation to the Ashtech Z-XII receiver, since the other two receivers did not record two frequency pseudoranges. Any multipath–like time delays that affect the pseudorange and phase observations in the same manner cannot be detected by this indicator. This means that it is possible to have rapid accelerations in the observations that may violate the tracking ability of the receiver tracking loops, causing satellite mistracking, without these accelerations being detected by the indicator.

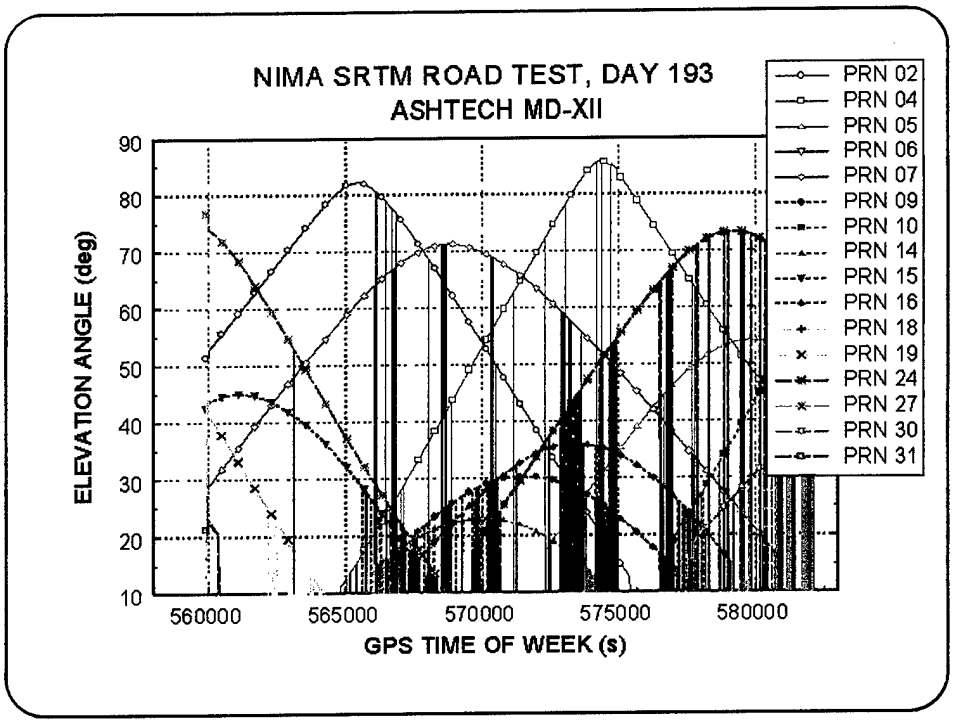

Figure 36—Satellites Tracked by the MD-XII Indicated by Their Elevation Angles

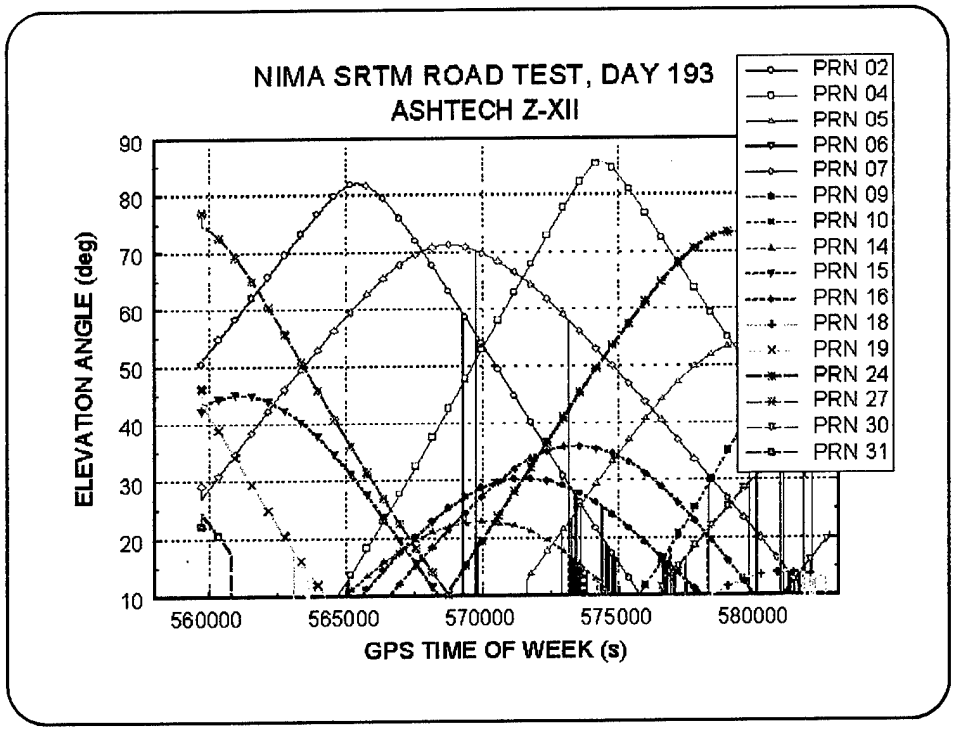

Figure 37—Satellites Tracked by the Z-XII Indicated by Their Elevation Angles

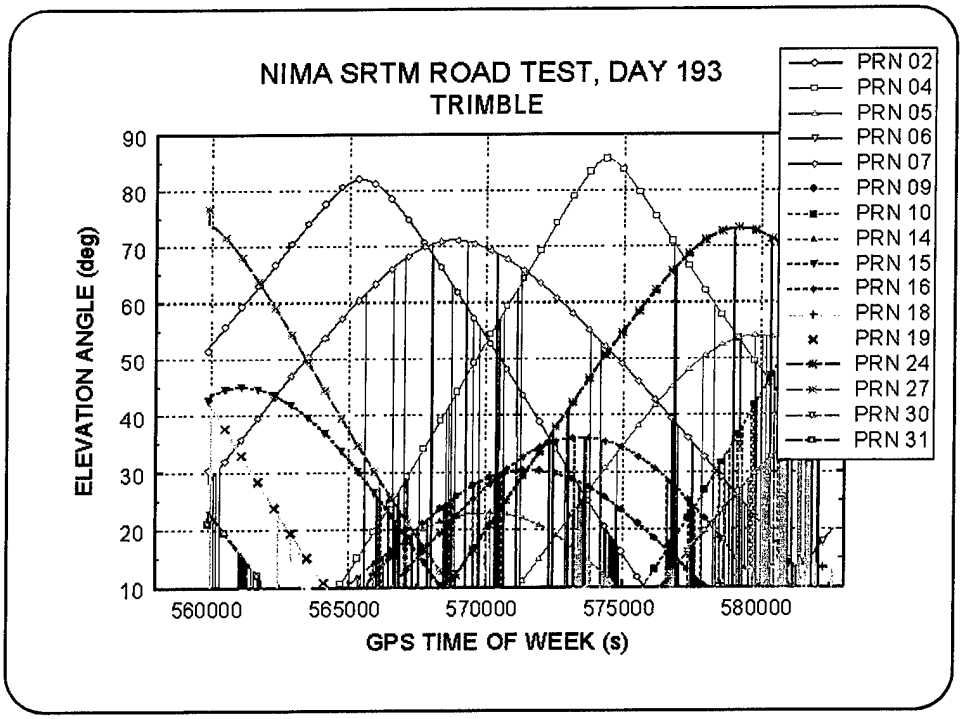

Figure 38—Satellites Tracked by the Trimble Indicated by Their Elevation Angles

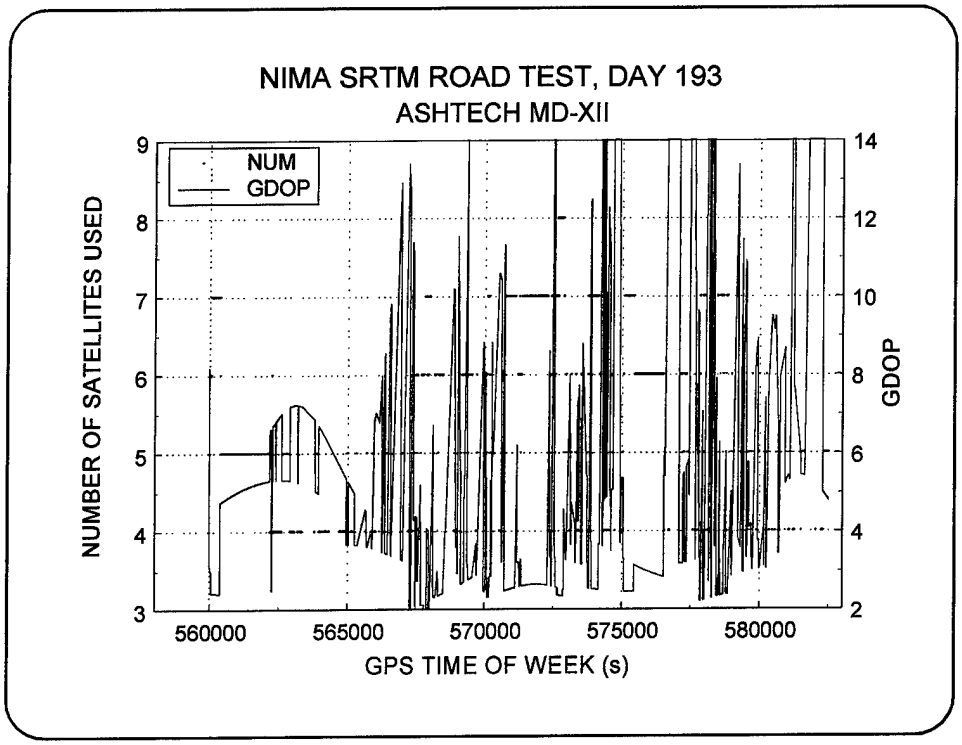

Figure 39—Number of Satellites Used by the MD-XII for Solutions and GDOP

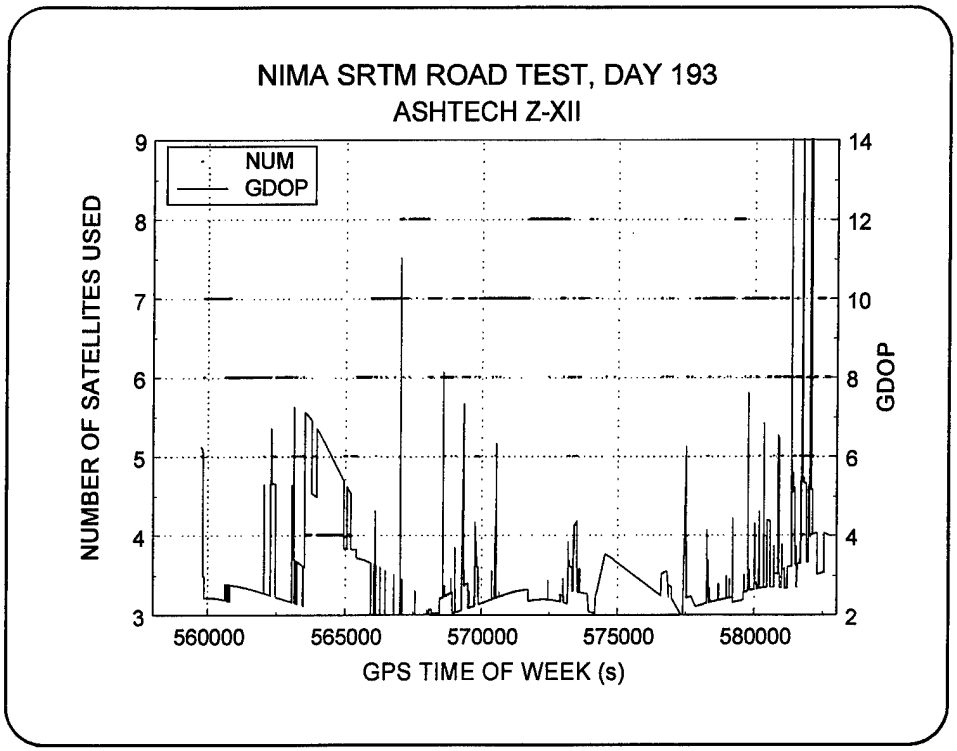

Figure 40—Number of Satellites Used by the Z-XII for Solutions and GDOP

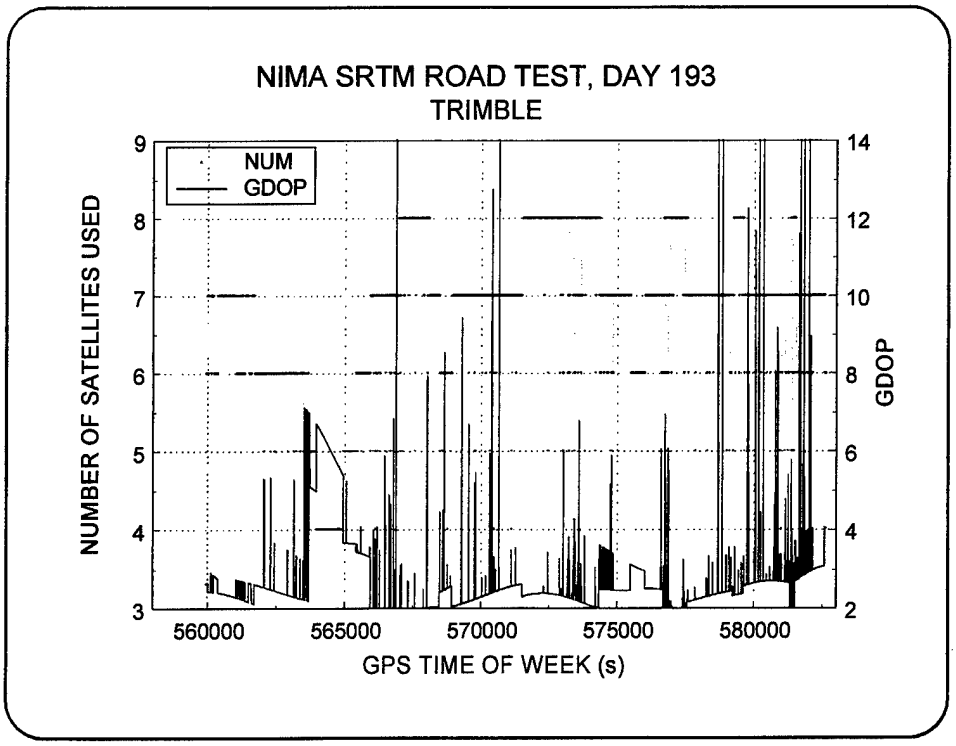

Figure 41—Number of Satellites Used by the Trimble for Solutions and GDOP

The L_1 and L_2 pseudorange observation equations are given by Equations (1) and (2) below.

$$\rho_{1ji} = r_{\cdot ji} + T_{\cdot ji} + \frac{c}{f_1^2} I_{\cdot ji} + c(\Delta t_{\cdot\cdot i} - \Delta t_{\cdot ji}) + M_{1ji} \tag{1}$$

$$\rho_{2ji} = r_{\cdot ji} + T_{\cdot ji} + \frac{c}{f_2^2} I_{\cdot ji} + c(\Delta t_{\cdot\cdot i} - \Delta t_{\cdot ji}) + M_{2ji} \tag{2}$$

The symbols are defined by the following:

ρ_{1ji} is the pseudorange observation on L_1 to satellite j at time t_i

$r_{\cdot ji}$ is the geometric range to satellite j at time t_i

$T_{\cdot ji}$ is the tropospheric refraction to satellite j at time t_i

$I_{\cdot ji}$ is the ionospheric refraction to satellite j at time t_i

$\Delta t_{\cdot\cdot i}$ is the receiver time offset at time t_i

$\Delta t_{\cdot ji}$ is the satellite j time offset at time t_i

M_{1ji} is the pseudorange multipath at L_1 to satellite j at time t_i

The difference between the two observations is written as Equation (3). All the geometric information is removed in the difference because both frequencies experience common delays due to the geometric propagation time. The receiver and satellite clock offsets are also common and are removed. What remains are the ionospheric effects and multipath.

$$\rho_{2ji} - \rho_{1ji} = c\, I_{\cdot ji}\left(\frac{1}{f_2^2} - \frac{1}{f_1^2}\right) + M_{2ji} - M_{1ji} \tag{3}$$

A similar set of equations can be written for the phase observations. These are written as Equations (4) and (5), where the integer cycle ambiguity has been omitted.

$$\lambda_1 \phi_{1ji} = r_{\cdot ji} + T_{\cdot ji} - \frac{c}{f_1^2} I_{\cdot ji} + c(\Delta t_{\cdot\cdot i} - \Delta t_{\cdot ji}) + m_{1ji} \tag{4}$$

$$\lambda_1 \phi_{2ji} = r_{\cdot ji} + T_{\cdot ji} - \frac{c}{f_2^2} I_{\cdot ji} + c(\Delta t_{\cdot\cdot i} - \Delta t_{\cdot ji}) + m_{2ji} \tag{5}$$

The symbols in these equations are defined by the following:

ϕ_{1ji} is the phase observation on L_1 to satellite j at time t_i

λ_1 is the L_1 wavelength in meters

$r_{\cdot ji}$ is the geometric range to satellite j at time t_i

$T_{\cdot ji}$ is the tropospheric refraction to satellite j at time t_i

$I_{\cdot ji}$ is the ionospheric refraction to satellite j at time t_i

$\Delta t_{\cdot\cdot i}$ is the receiver time offset at time t_i

$\Delta t_{\cdot ji}$ is the satellite j time offset at time t_i

m_{1ji} is the phase multipath at L_1 to satellite j at time t_i

The difference between the two observations is written as Equation (6). The same terms are removed as in the pseudorange equations above.

$$\lambda_2 \phi_{2ji} - \lambda_1 \phi_{1ji} = -c I_{\cdot ji}\left(\frac{1}{f_2^2} - \frac{1}{f_1^2}\right) + m_{2ji} - m_{1ji} \qquad (6)$$

Next, Equations (3) and (6) are added to remove the ionospheric term. What is left in Equation (7) is just the difference in multipath between frequencies, and between pseudorange and phase. Usually, it is assumed that the phase multipath terms are much smaller than those contaminating the pseudorange, so the indicator is taken to be the multipath difference between the two-frequency pseudorange. In practice, these values at each epoch are differenced from a reference epoch, so that at the first epoch the indicated value is zero. The deviations from zero are then accumulated at later epochs as long as phase lock is retained.

$$\rho_{2ji} - \rho_{1ji} + \lambda_2 \phi_{2ji} - \lambda_1 \phi_{1ji} = M_{2ji} - M_{1ji} + m_{2ji} - m_{1ji} \qquad (7)$$

3.3 Multipath Indicator Results

Two-frequency pseudorange and phase data are required to compute this multipath indicator; therefore only the results from the Ashtech Z-XII receiver can be reported. As described above, the two-frequency observations are necessary in order to remove the ionospheric contribution, and the pseudorange and phase are used together to eliminate the geometric effects. What remains are the ionosphere-free differences between pseudorange and phase. For comparison purposes, multipath profiles from several static sites unrelated to the NIMA data set are presented first. Figure 42 shows the multipath evaluated at a static site *Patrick* located near Frederick, Maryland, in May 1997. Several satellites are shown. Each curve starts at the left at an arbitrary value of zero. Ideally, the pseudorange and phase should track each other, the only differences being due to noise in the measurements. As time continues to the right, differences are accumulated between the pseudorange and phase that must be due to the different multipath characteristics seen by the pseudorange and

phase observations. Since it is generally agreed that the phase multipath error is much smaller than the pseudorange counterpart, the variations seen in Figure 42 must be primarily due to the difference between the two-frequency pseudorange multipath. Any multipath that is common to both data classes and both frequencies cannot be distinguished by this indicator.

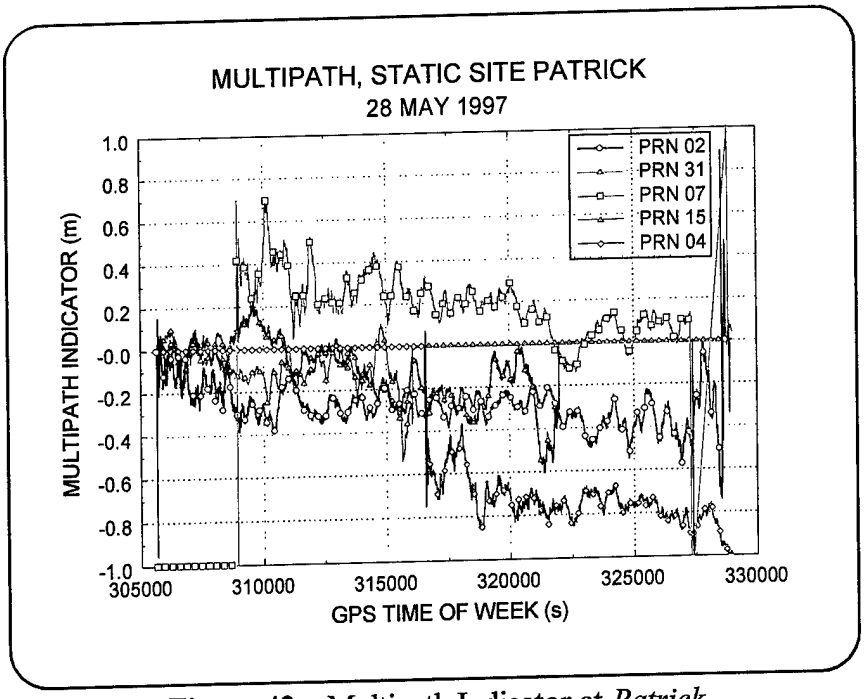

Figure 42—Multipath Indicator at *Patrick*

Observations of the same satellites at the same time from a different site should show a different signature. Figure 43 is the multipath indicator plot from a site called *Melsage*. Other sites were also operating at the same time as *Patrick* and *Melsage,* and all show different multipath characteristics.

The multipath plot shown in Figure 44 shows the signature from one satellite, PRN02, which was observed from several sites at the same time. The signatures are different at each site, as would be expected if the variations are due to multipath. But in all cases, the variations have a quasi-periodic nature around a slowly varying trend line. The signature observed from the NIMA van contains spikes or impulses that correspond to periods where the satellite tracking was interrupted. The cause of these impulses may be due to the receiver tracking loops trying to reacquire weak or rapidly varying signals. The loss of satellites is frequent in the NIMA van data, especially on L_2 since it is inherently weaker than the L_1 signal. Figure 45 illustrates the impulsive nature of the multipath indicator for day 190, with observations collected by the Z-XII receiver. On average, the standard deviations of the multipath indicators for the NIMA

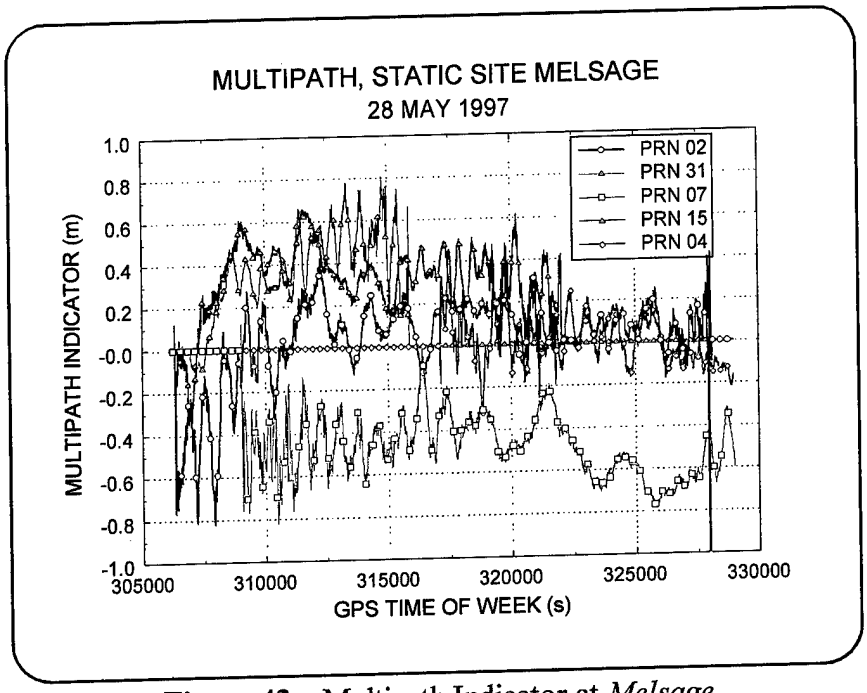

Figure 43—Multipath Indicator at *Melsage*

van with impulses are about the same as for the static cases. Table 9 lists these statistics.

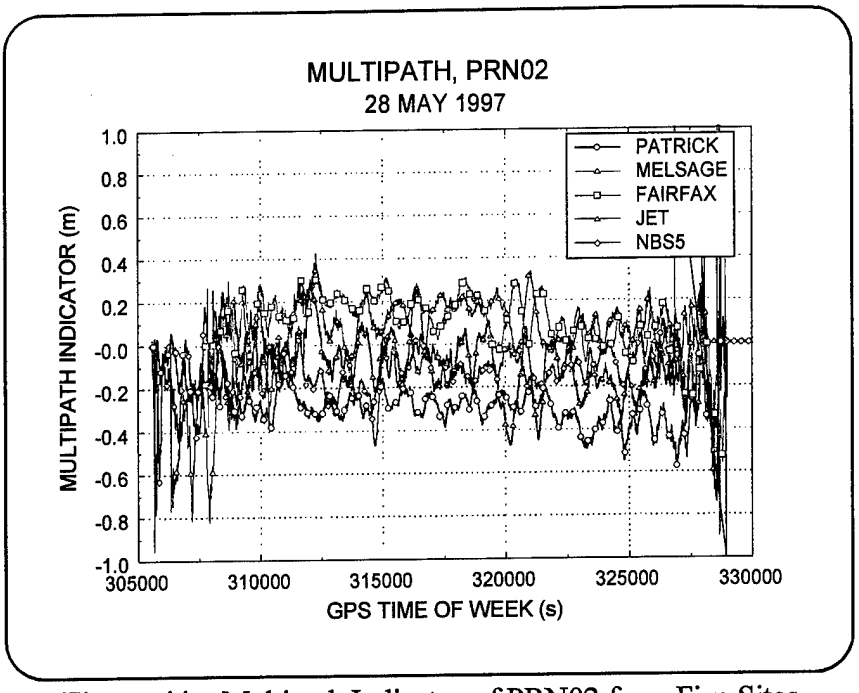

Figure 44—Multipath Indicator of PRN02 from Five Sites

Further evidence is available from the Route 301 observations collected near NSWCDL in April 1997, which were described in Section 2. In this case, an Ashtech Z-XII receiver with antenna on the roof of a car traveled along a four-lane divided highway collecting data at 1-s intervals. The multipath indicators for these observations are shown in Figure 46. Four of the five satellites were mostly continuously tracked, while PRN15 was not. The multipath indicator for the continuously tracked satellites (PRN 03, 18, 19, and 31) resembles the results for the static cases more than the NIMA van plots. But the result for PRN15 is more like the NIMA van results because of the occasional impulses, which coincide with periods when dropouts occurred.

The conclusion derived from these data sets is that multipath is not the primary cause of the dropouts since the multipath indicator is generally small for satellites that are continuously tracked, whether or not the site is static. When satellite tracking is interrupted and reacquisition is attempted, the receiver may produce a few observations that cause the multipath indicator to register an impulse. This may be especially true because of the lower signal level of L_2. The multipath indicator is sensitive to the differences between the two frequencies, or if the receiver treats these

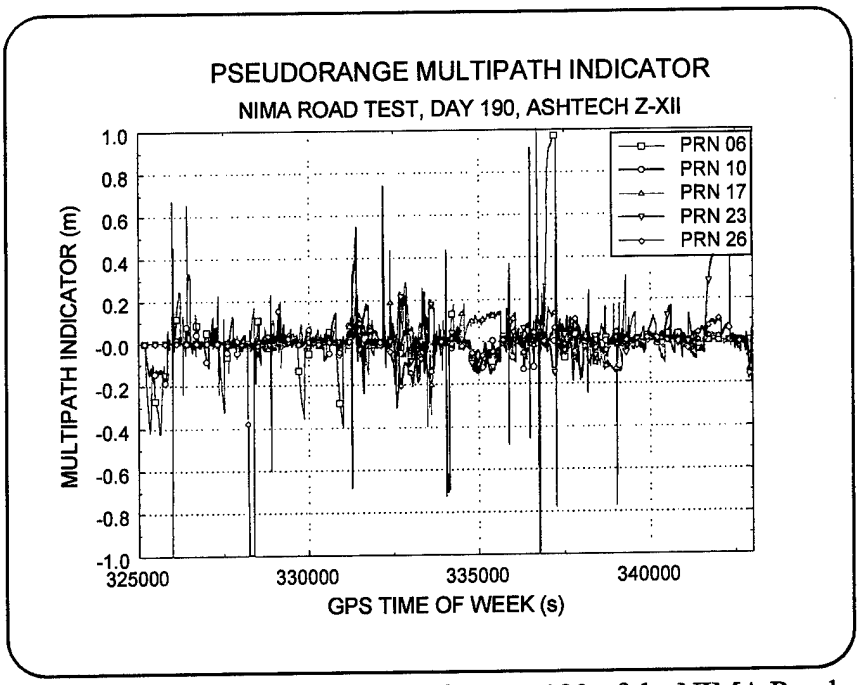

Figure 45—Multipath Indicator for Day 190 of the NIMA Road Test

Table 9—Multipath Indicators: Static and Dynamic Cases

STATIC SITES / PRN02		ROAD TEST DAY 190	
SITE	MULTIPATH	PRN	MULTIPATH
PATRICK	0.11	06	0.22
MELSAGE	0.19	10	0.06
FAIRFAX	0.14	17	0.06
JET	0.13	23	0.11
NBS5	0.11	26	0.17

signals differently because of the differing signal strength, the multipath indicator may be indicating a receiver instrumental effect rather than a propagation effect. In either case, this analysis cannot detect multipath that is common to both data classes, so no conclusions can be reached about common-mode multipath signals.

When there is solid tracking, the multipath indicator produces small numbers, which indicate little difference between the pseudoranges and phase observations and between frequencies. An example of this occurred on a stretch of I-55 near Lincoln, Illinois. Figure 47 shows the multipath indicator for this segment. Note that because the numbers are small, the scale has been expanded relative to Figures 41 through 46. These results indicate that the key to high-quality solutions depends upon a reduction in the number of satellite dropouts, so that satellite geometry remains good, and reacquisition attempts are minimized. A practical implementation of this may require special attention to detail in the selection of the GPS antenna and receiver. Maximization of the satellite signal on both frequencies implies that a low-noise, high-gain antenna preamplifier with superior out-of-band signal rejection be selected to eliminate interference. Spatial diversity through the use of several antennas may also be helpful.

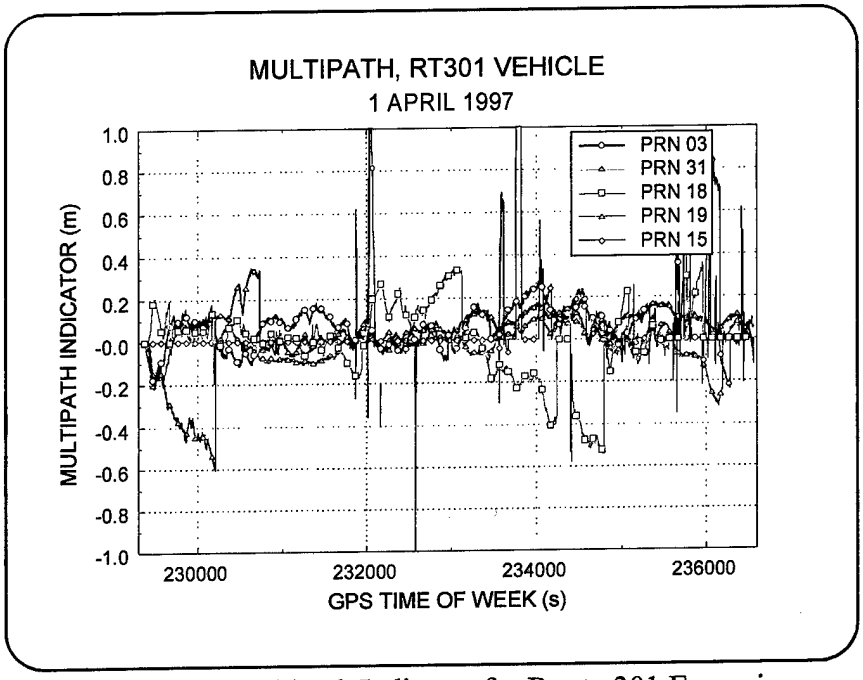

Figure 46—Multipath Indicator for Route 301 Excursion

3.4 Initial Point

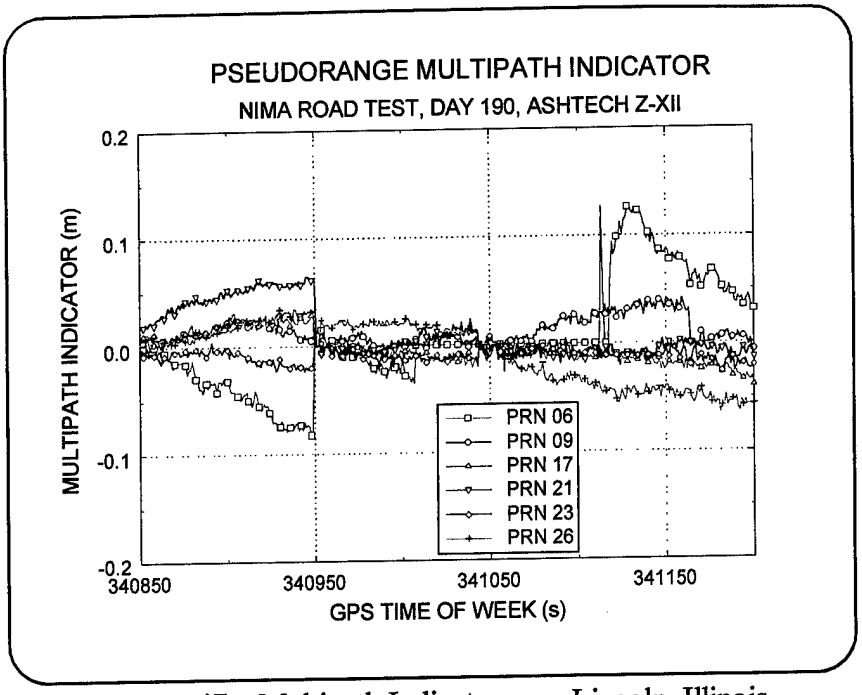

Figure 47—Multipath Indicator near Lincoln, Illinois

Before beginning the NIMA road test, the van collected data with the three receivers while static at the North Annex in St. Louis. This period of about ten minutes, before the van began its journey, provides an opportunity to view the relative scatter in the solutions among the three receivers. The Ashtech Z-XII navigation solutions are obtained from two-frequency ionospherically corrected pseudoranges. The solutions for the other two receivers are single-frequency solutions using the broadcast ionospheric model. The North Annex location was more than 40 km from the CORS site STL3—too far to be able to obtain On-The-Fly kinematic solutions for use as truth. Also, the CORS sites record data at 30-s intervals and, therefore, has the potential to provide only about 20 static truth solutions before movement begins. This is too few to allow a reliable kinematic solution with the current software.

The figures that follow show the consistency among navigation solutions obtained in different ways. Figure 48 shows the longitude and latitude of the simulated PPS solutions at North Annex for each of the receivers. Figure 49 shows the PPS ellipsoid height plotted against the GPS time of week. For reference, a 1-m square is included in the longitude-latitude plot. The corresponding PAN solutions are shown in Figures 50 and 51. Note that the Trimble solutions are separated from the Ashtech solutions by about a meter. This corresponds to the separation of the Ashtech and Trimble antennas. All three PAN solutions shown in Figure 50 are shifted to the west by about a meter compared to the PPS solutions seen in Figure 48. The heights are little changed as a result of the PAN improvement. Since there is no direct truth, the only comparison that can be made is through relative positioning with respect the NOAA CORS sites. The absolute position of CORS sites is known to be better than about 10 cm in all components.

Solutions using the data from each receiver, in turn referenced to a CORS site and data recorded at NSWCDL, are shown below for comparison to the PAN solutions. Figures 52 and 53 show the MD-XII solutions, Figures 54 and 55 the Z-XII solutions, and Figures 56 and 57 the Trimble solutions. These relative solutions use Dr. Benjamin Remondi's single-frequency pseudorange relative-positioning algorithm with the broadcast ionospheric model. The solutions are at 30-s intervals corresponding to the CORS observation interval. Figures 54 and 55 also include a range-corrected SPS solution. For this solution, the three CORS sites at St. Louis, Milwaukee, and Detroit were used as the weighted reference sites that generated the range corrections which were applied

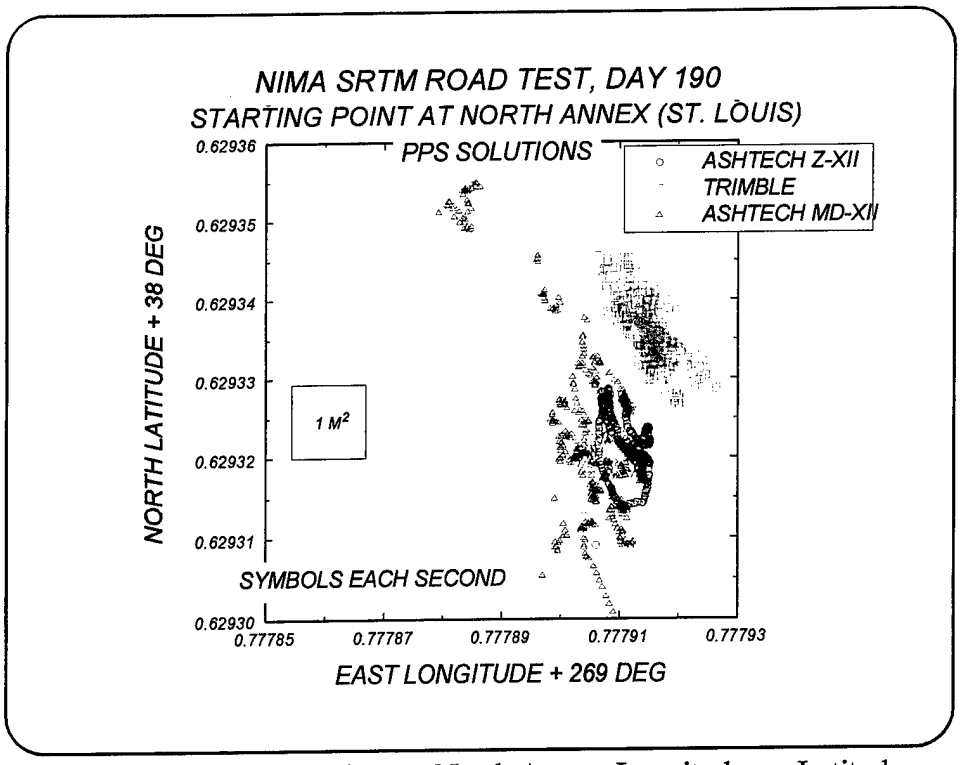

Figure 48—PPS Solutions at North Annex, Longitude vs. Latitude

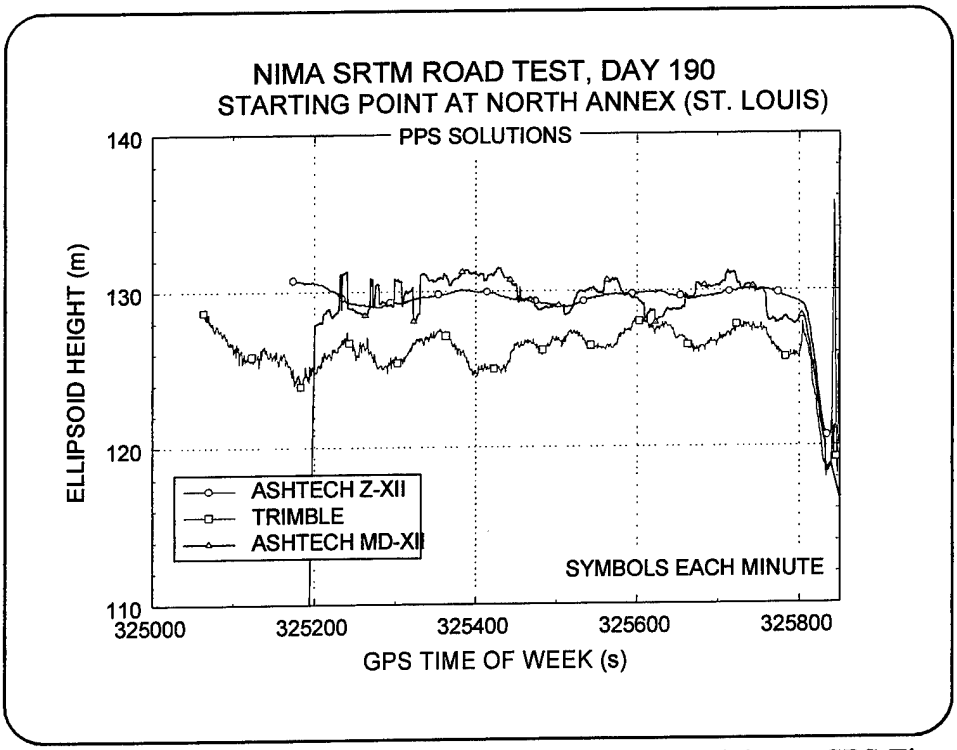

Figure 49—PPS Solutions at North Annex, Ellipsoid Height vs. GPS Time of Week

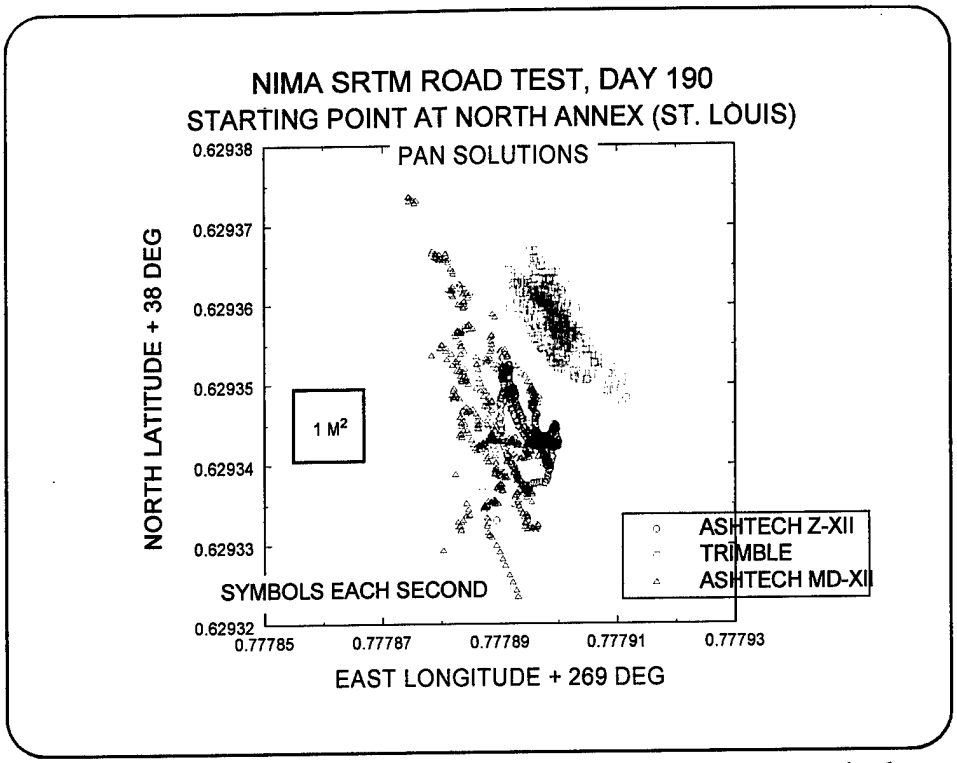

Figure 50—PAN Solutions at North Annex, Longitude vs. Latitude

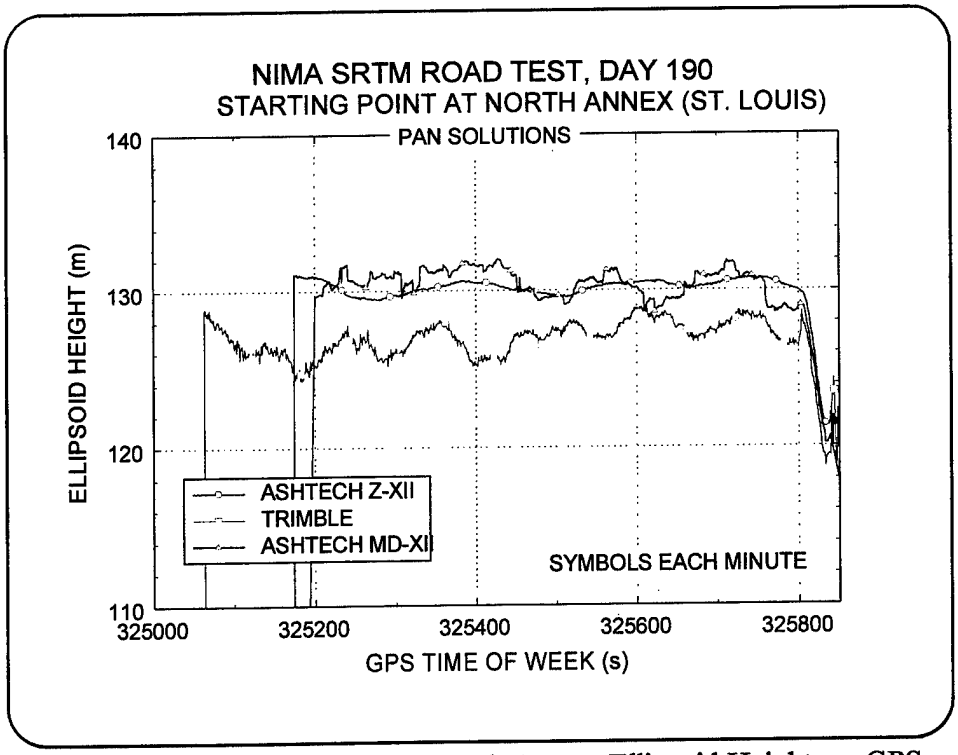

Figure 51—PAN Solutions at North Annex, Ellipsoid Height vs. GPS Time of Week

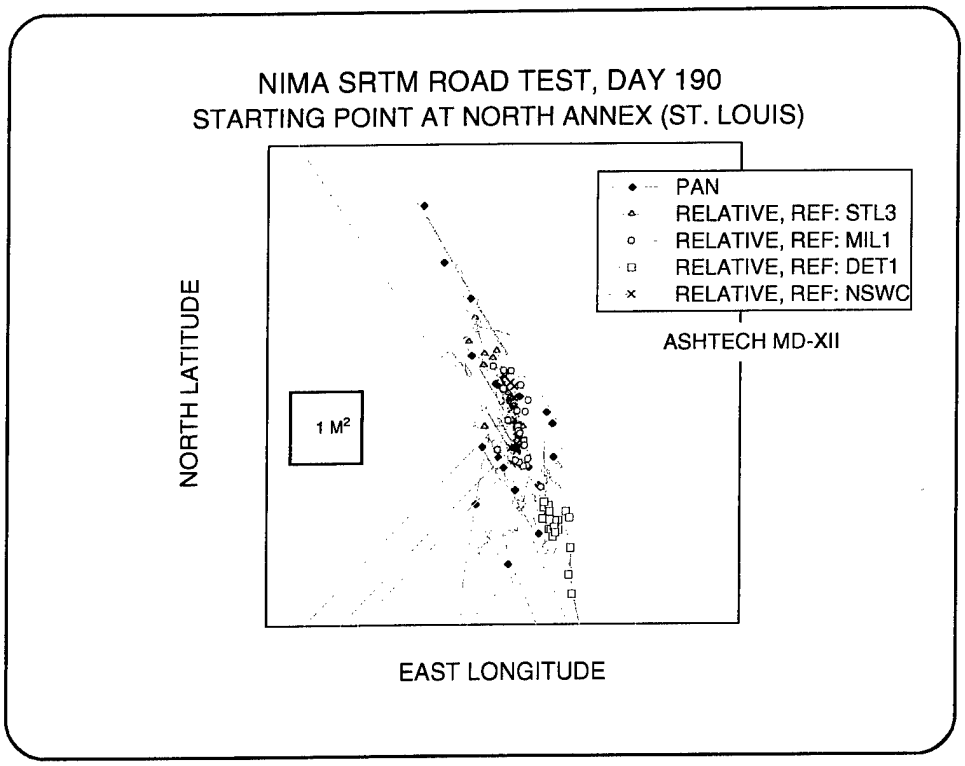

Figure 52—Relative Longitude vs. Latitude Solutions Compared to the PAN Solutions for the MD-XII Receiver

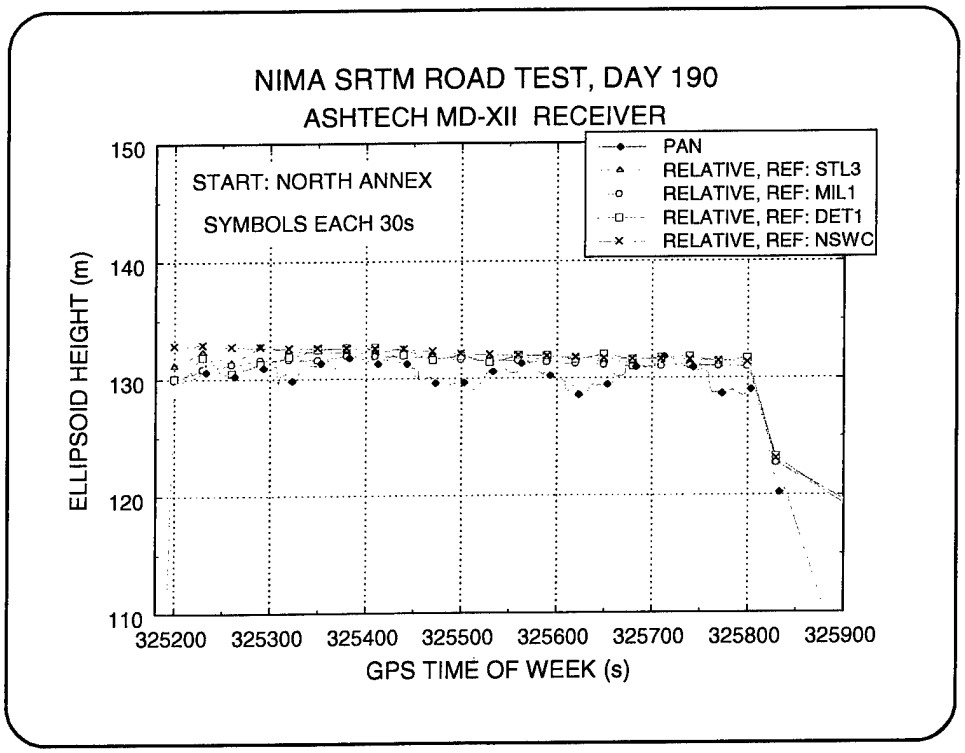

Figure 53—Relative Ellipsoid Height vs. GPS Time Solutions Compared to the PAN Solutions for the MD-XII Receiver

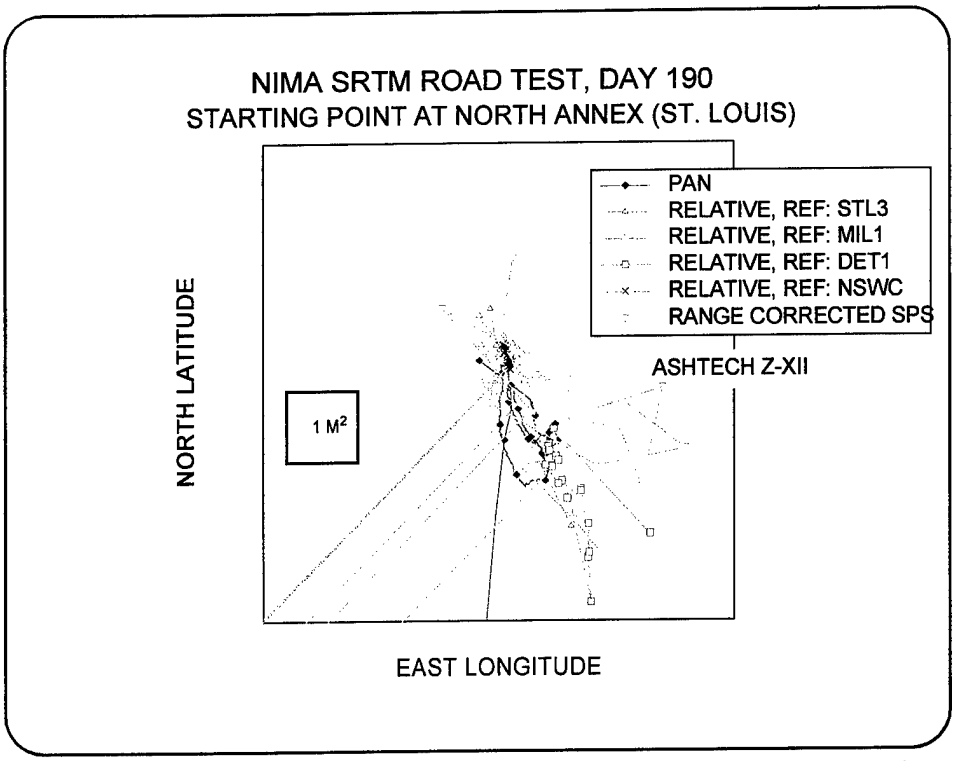

Figure 54—Relative Longitude vs. Latitude Solutions Compared to the PAN Solutions for the Z-XII Receiver

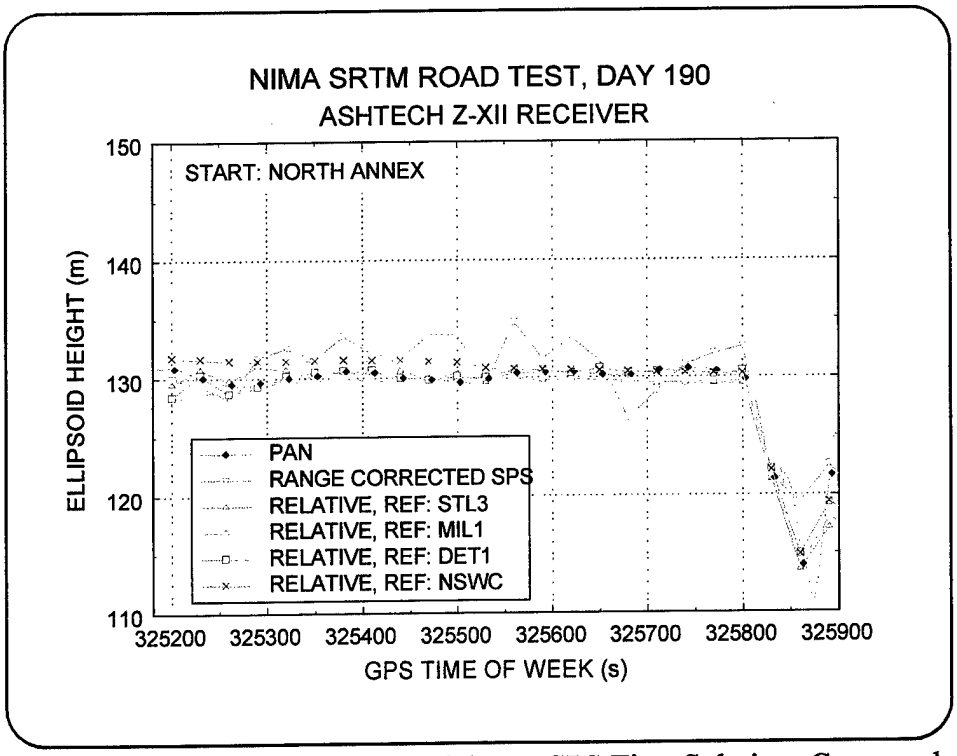

Figure 55—Relative Ellipsoid Height vs. GPS Time Solutions Compared to the PAN Solutions for the Z-XII Receiver

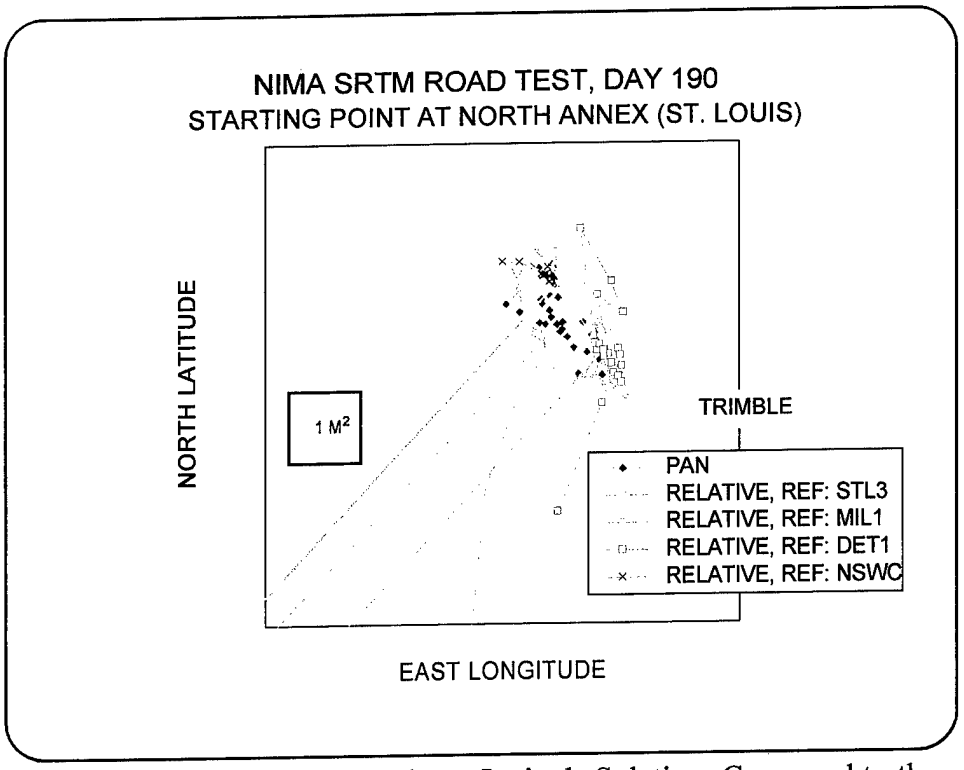

Figure 56—Relative Longitude vs. Latitude Solutions Compared to the PAN Solutions for the Trimble Receiver

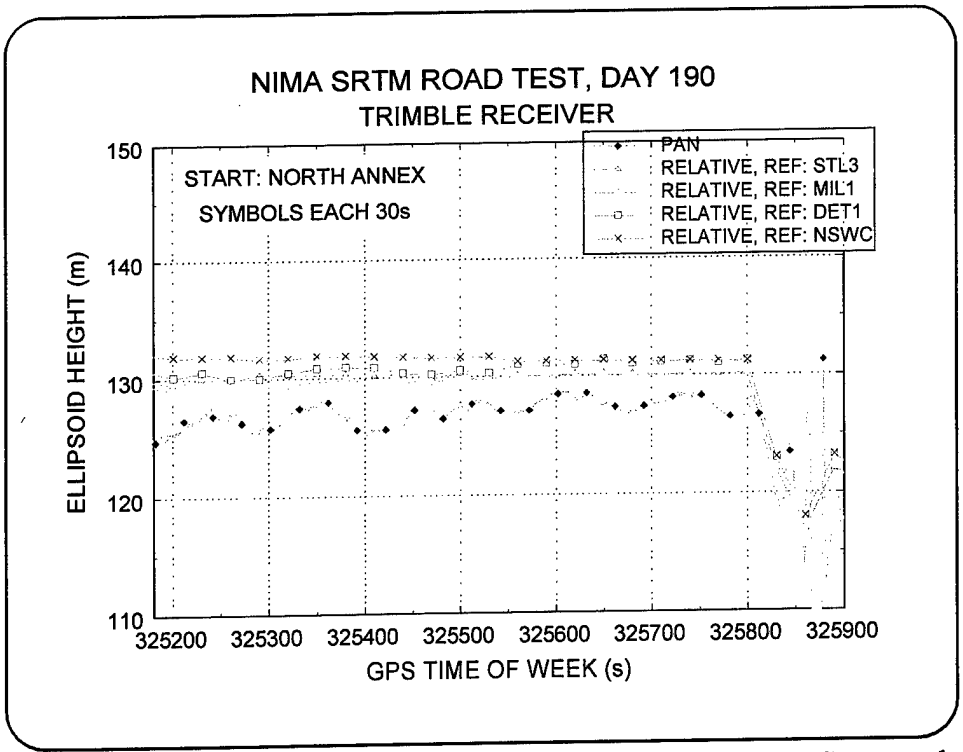

Figure 57—Relative Ellipsoid Height vs. GPS Time Solutions Compared to the PAN Solutions for the Trimble Receiver

to the Z-XII van observations at the North Annex. This technique is much noisier than the relative positioning results because no smoothing was applied to the corrections. Better results can be obtained with a more sophisticated algorithm.

In all cases, the longitude and latitude relative solutions agree well with the PAN solutions. The height solutions for all relative solutions are consistent, but the PAN height solutions indicate a few meters lower, especially in the case of the Trimble receiver. Six satellites were tracked on the three receivers, except for a period near the beginning where the MD-XII receiver alternated between five and six. This is apparent in the GDOP plot shown in Figure 58. Since, in this case, GDOP cannot be the explanation for the disagreement between the Trimble heights and the relative solutions or the Ashtech PAN solutions, the cause may be due to using the ionospheric model. This is unlikely, though, since Trimble and MD-XII solutions were single-frequency, and the same model was used for both.

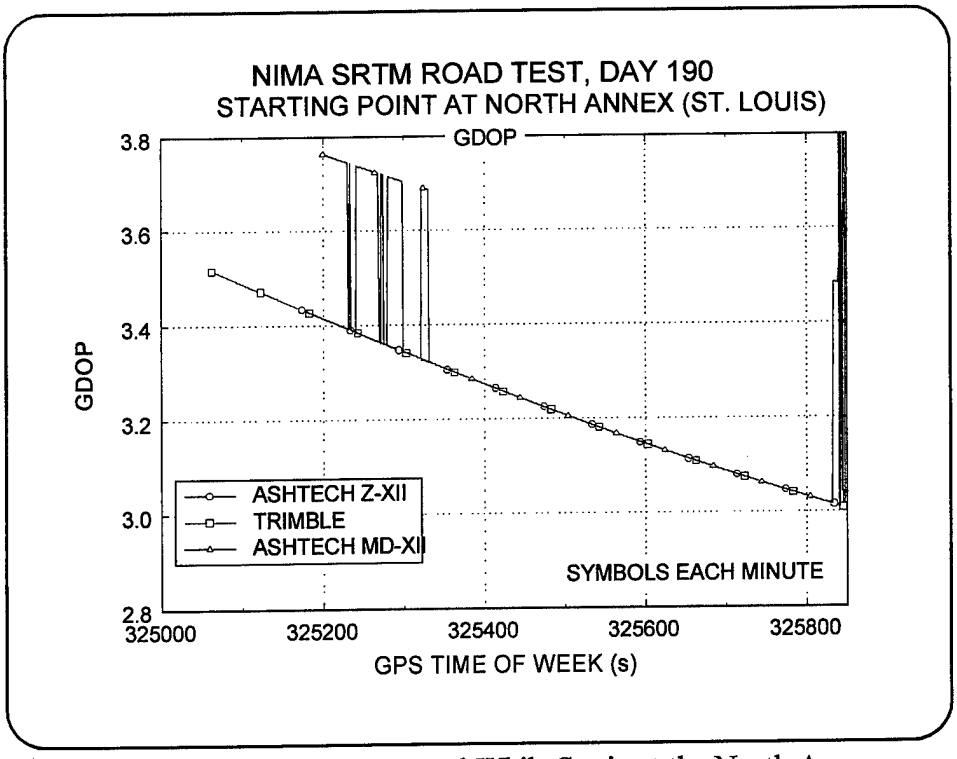

Figure 58—GDOP Computed While Static at the North Annex

3.5 Transect 1 Solutions

The location for Transect 1 was at the intersection of I-55 with I-72 near Springfield, Illinois, as in Figure 59. The solution tracks indicate the intersection to be a cloverleaf, with I-55 going under I-72. There were four passes made through this interchange. The first pass was on day 190 traveling north. The second was on day 191 traveling south. The third was also on day 191 traveling north. The last was on day 193 traveling south. The passes on day 191 were not transects—they were extra trips to meet a courier from St. Louis with a replacement download cable for the Z-XII receiver. The

Trimble receiver recorded all of the passes, the Z-XII missed the south pass on day 191, and the MD-XII missed day 190 and the south pass on day 191. The solutions from the MD-XII receiver were of poor quality and are not included in the following discussion. The solution tracks illustrated in the plots that follow give a qualitative feel for the accuracy of the PPS and PAN solutions obtained from the Z-XII and Trimble receivers.

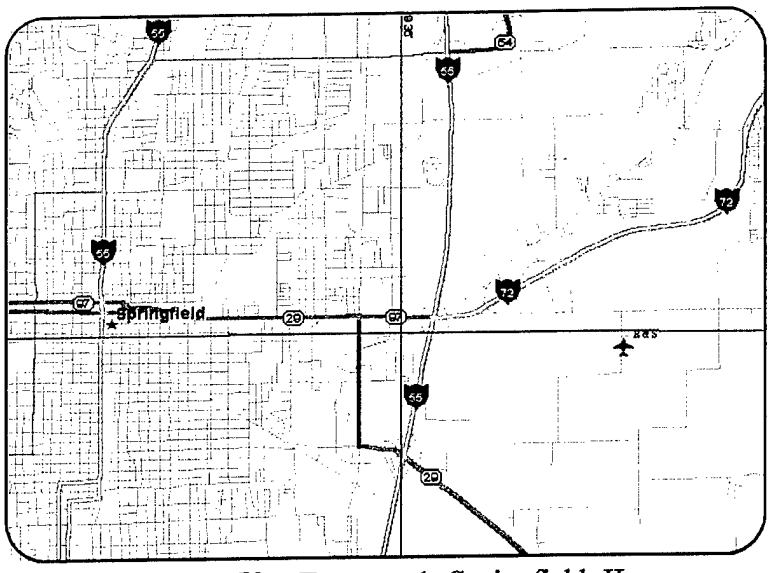

Figure 59—Transect 1, Springfield, IL

Figure 60 shows the Z-XII longitude and latitude solutions at this location, and Figure 61 shows the ellipsoid height vs. longitude. The same plots with PAN solutions from the Trimble receiver are shown in Figures 62 and 63. The height solutions have enough resolution to show that the east-west route on I-72 passes over the north-south route, though there is some height inconsistency between the solutions on days 190 and 193. Since a different satellite constellation was involved on the two days, the difference may be GDOP-related. In order to investigate this, GDOP plots are shown in Figures 64 and 65 in a format similar to the height solutions. They indicate that there was a lot of

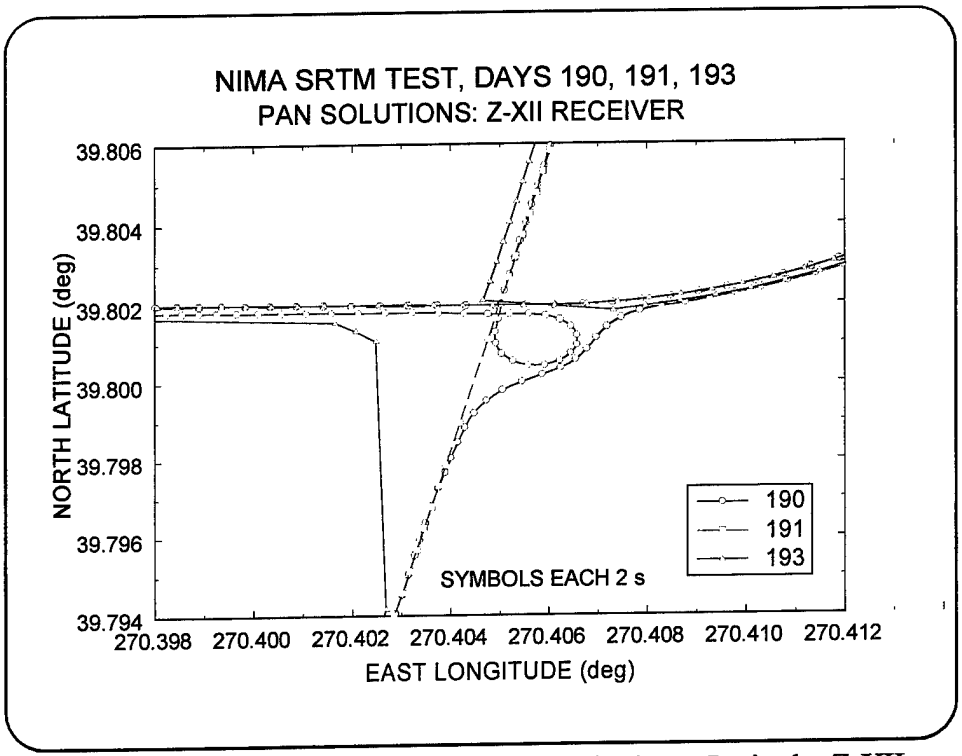

Figure 60—Transect 1 Interchange, Longitude vs. Latitude, Z-XII Receiver

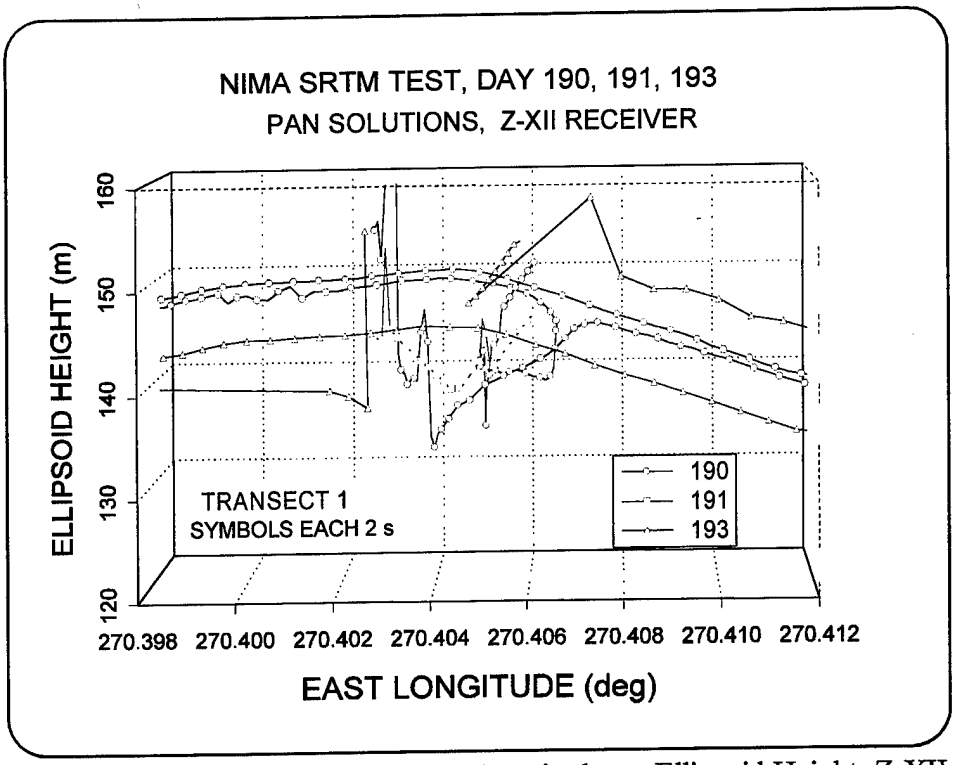

Figure 61—Transect 1 Interchange, Longitude vs. Ellipsoid Height, Z-XII Receiver

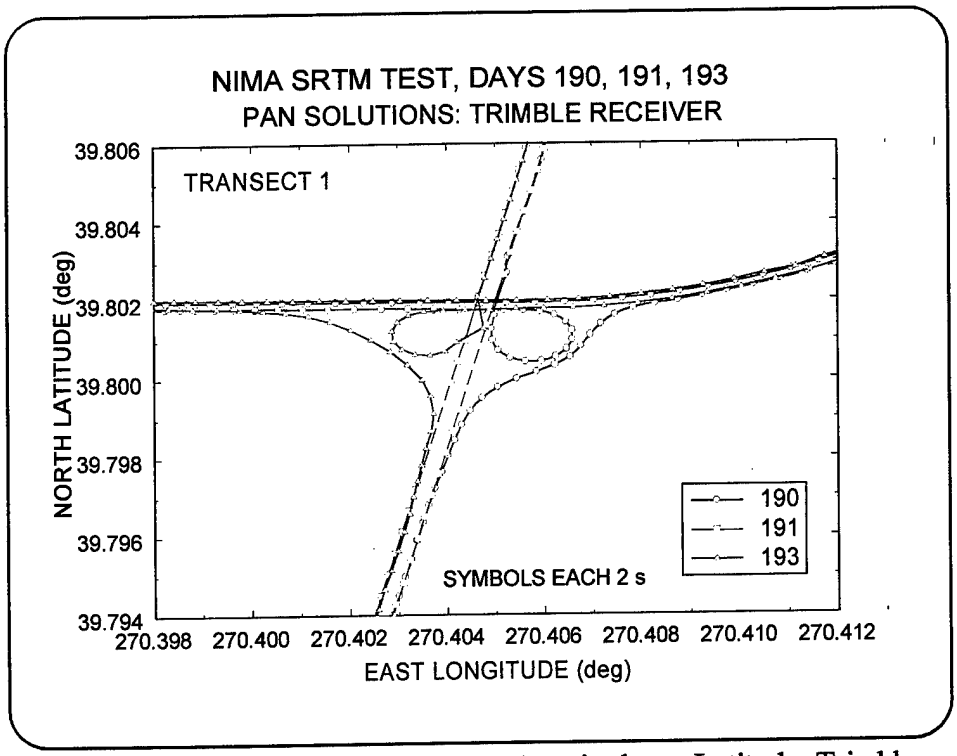

Figure 62—Transect 1 Interchange, Longitude vs. Latitude, Trimble Receiver

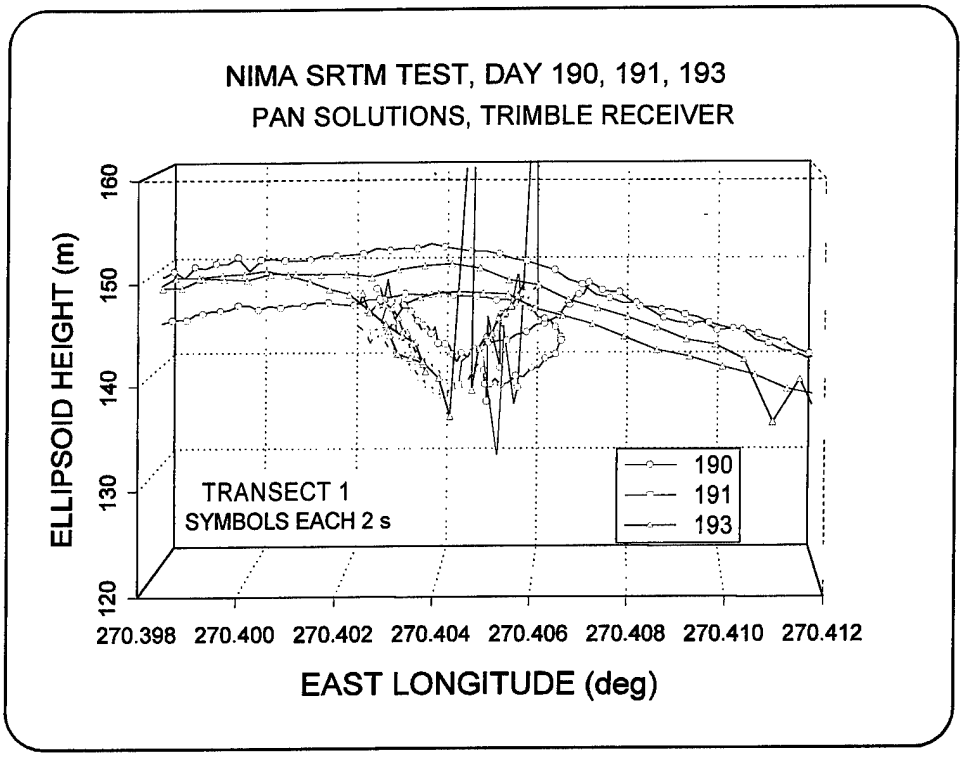

Figure 63—Transect 1 Interchange, Longitude vs. Ellipsoid Height, Trimble Receiver

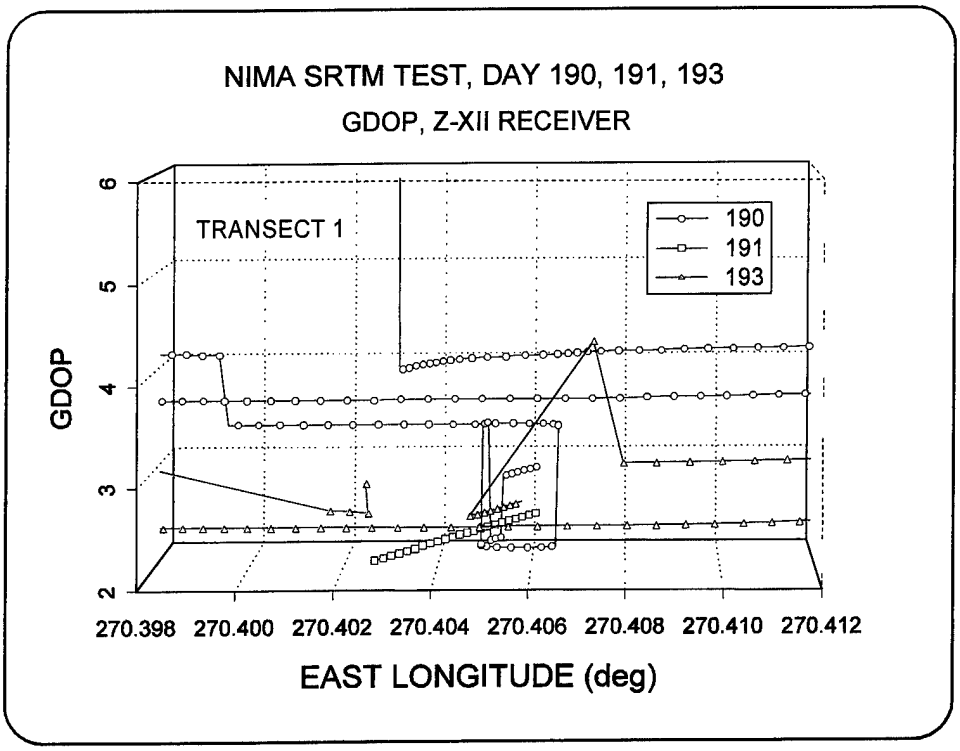

Figure 64—Transect 1 Interchange, Longitude vs. GDOP, Z-XII Receiver

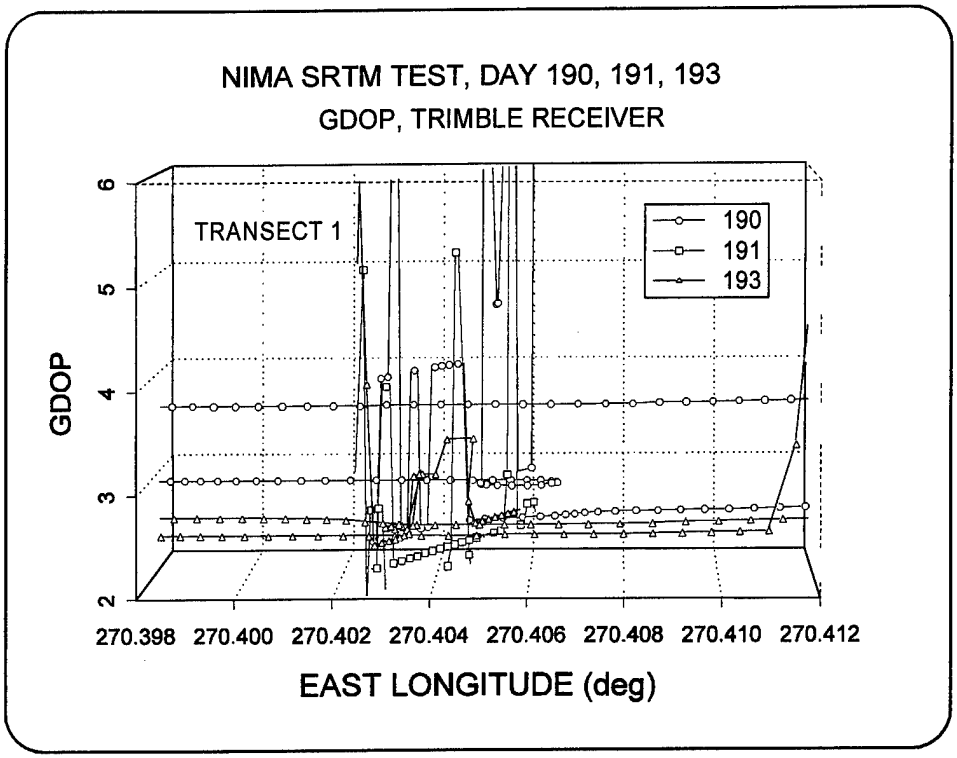

Figure 65—Transect 1 Interchange, Longitude vs. GDOP, Trimble Receiver

satellite dropout activity in the vicinity of the interchange overpass, with satellites being lost due to blockage. The Trimble seemed to perform better by being able to produce more solutions, but all Trimble solutions are single-frequency. The Z-XII solutions were two-frequency, and the software omits solutions when L_2 observations are lost, though L_1 may still have been tracking. Because of this there may be fewer satellites used in the Z-XII solutions; consequently, the Trimble GDOPs on days 190 and 193 generally are the same or better than the Z-XII solutions.

3.6 Lincoln, Illinois

A segment along I55 near Lincoln, Illinois, is include to show a region of good agreement between PAN solutions obtained on different days. A map of this area is included as Figure 66. Figures 67 and 68 are PAN longitude vs. latitude and longitude vs. ellipsoid height solutions from the Z-XII observations. This part of the interstate has some curves with hills or bridges that can be used to judge height repeatability. Since

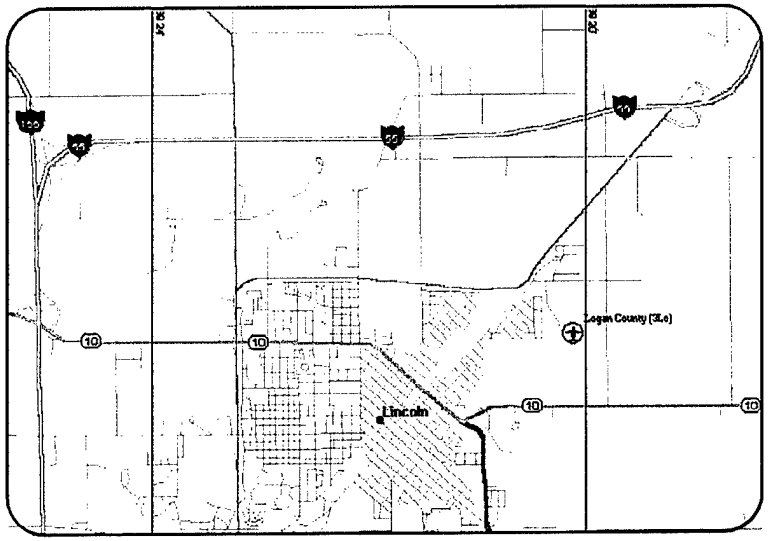

Figure 66—Lincoln, Illinois

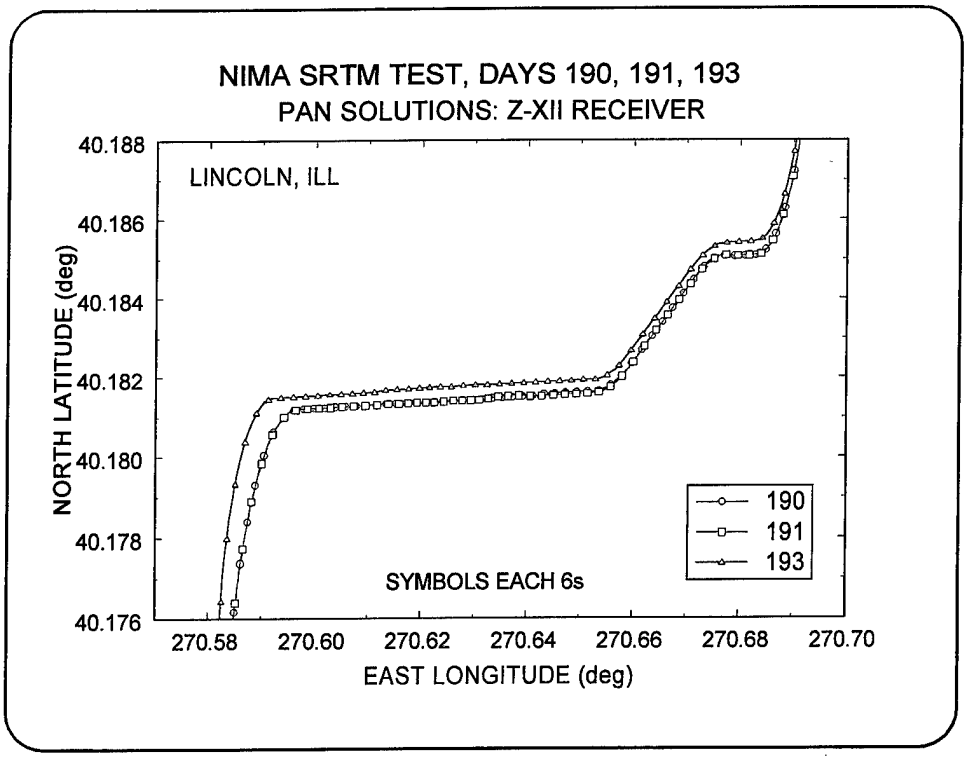

Figure 67—PAN Longitude vs. Latitude Solutions Near Lincoln, IL, from the Z-XII

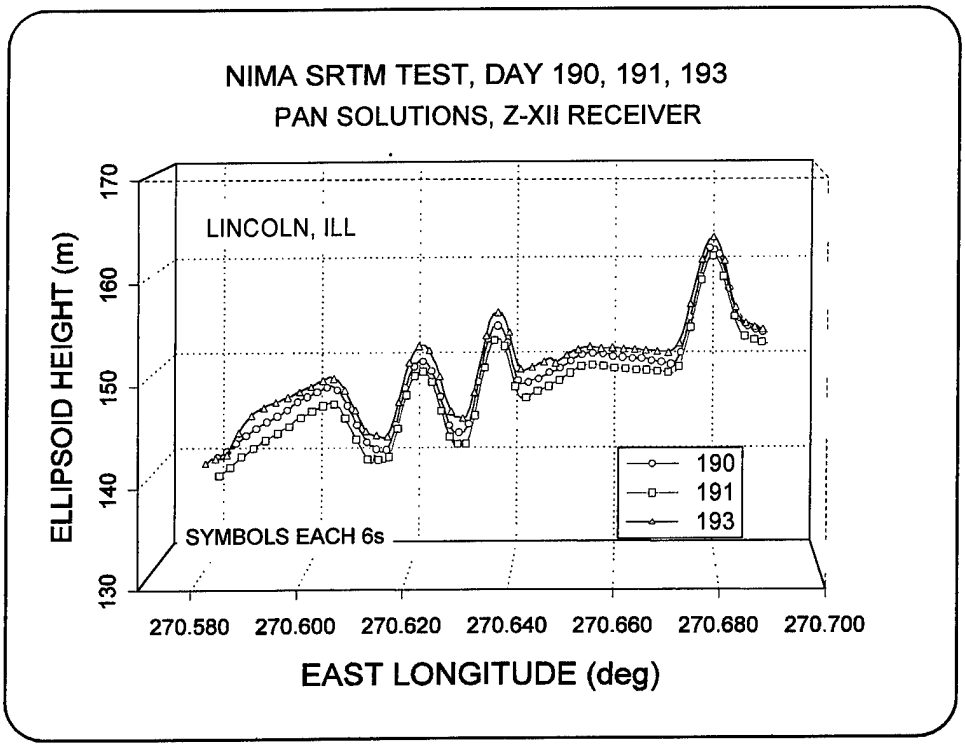

Figure 68—PAN Longitude vs. Height Solutions Near Lincoln, IL, from the Z-XII

tracking is good throughout, there must be few obstructions along the route. There are tracks from 3 days, as in the previous section, that can be used for comparison. Here, the ellipsoid height solutions show nice agreement among the tracks, with a variation of only a couple of meters. This same segment was used in Section 3.3 as an example to illustrate low-dynamic multipath.

Figures 69 and 70 show the Trimble PAN solutions and Figures 71 and 72 show the GDOP for this segment of interstate. These solutions are the showpieces of this analysis of the NIMA road test. They illustrate that under good conditions the ellipsoid heights can be estimated to within a couple of meters with PAN improvement.

The GDOP plots indicate that, for this segment, the Z-XII has fewer cases where spikes occur, but otherwise the GDOP curves are similar. The day 191 GDOP curve located between 3 and 4 in Figure 72 corresponds to the southbound track on that day; it was not observed by the Z-XII receiver and is not present in Figure 71. Since the results for this segment are quite good, the simulated PPS ellipsoid height results are also included in Figures 73 and 74 for comparison. These show a wider spread between the days, at times indicating a 10-m difference in height. These differences between PPS and PAN demonstrate that the precise ephemerides used in the PAN algorithm do produce a significant improvement over the PPS solutions.

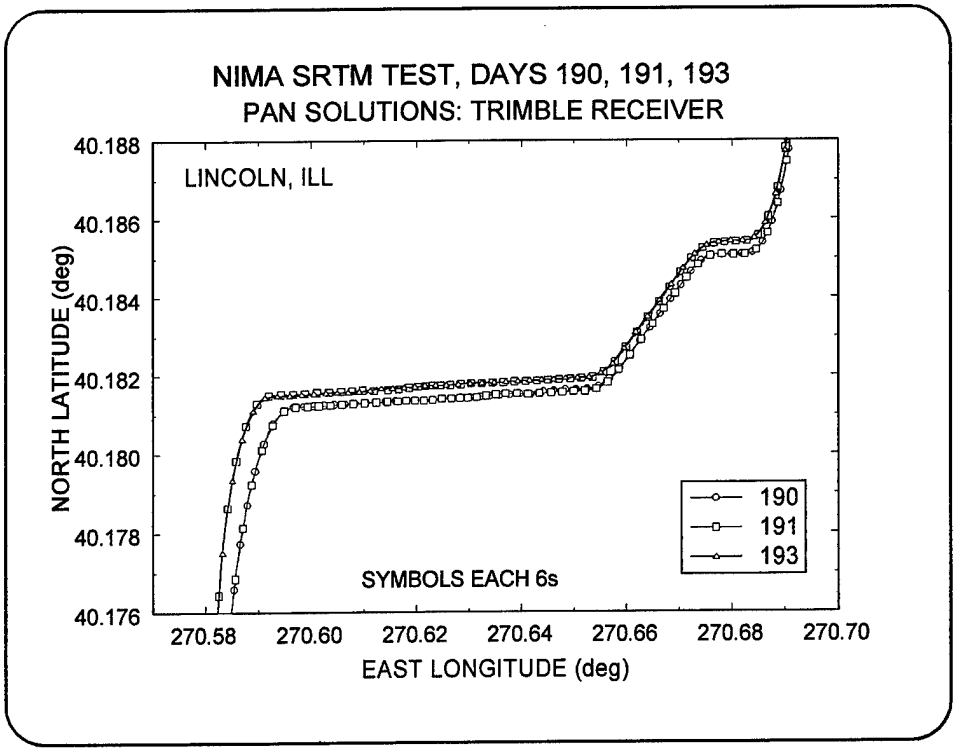

Figure 69—PAN Longitude vs. Latitude Solutions Near Lincoln, IL, from the Trimble

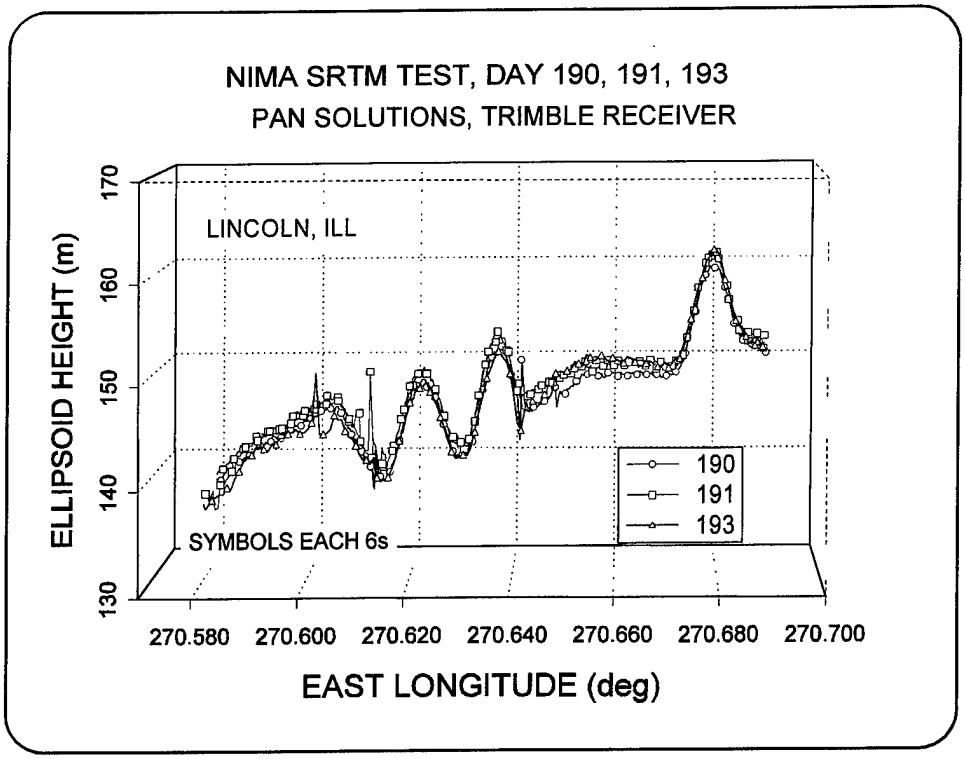

Figure 70—PAN Longitude vs. Height Solutions Near Lincoln, IL, from the Trimble

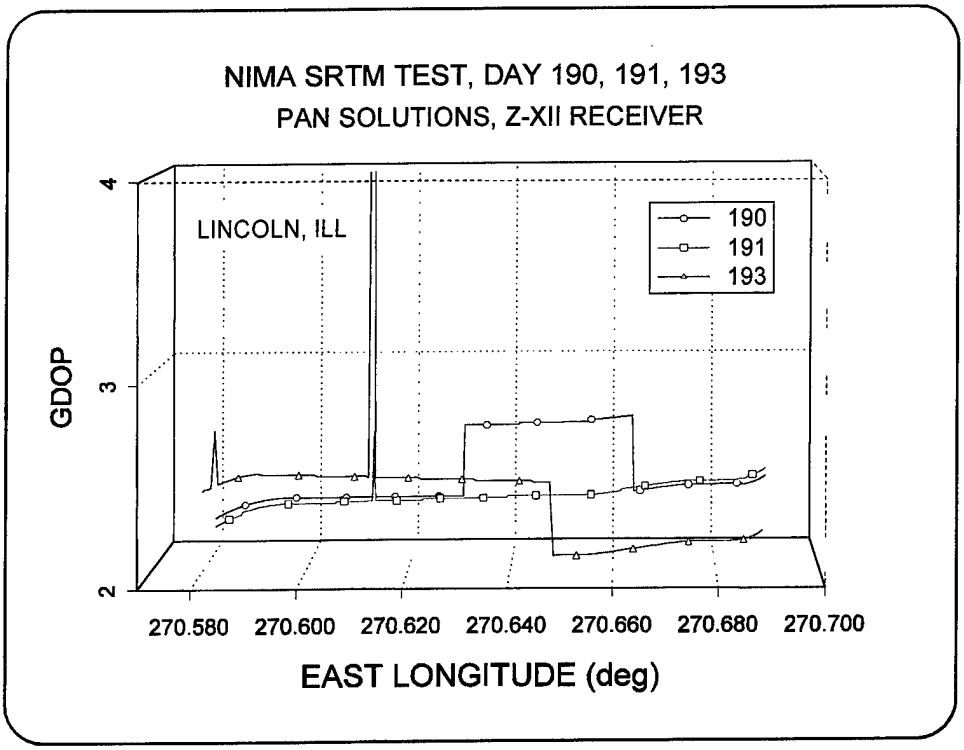

Figure 71—Longitude vs. GDOP Near Lincoln, IL, from the Z-XII

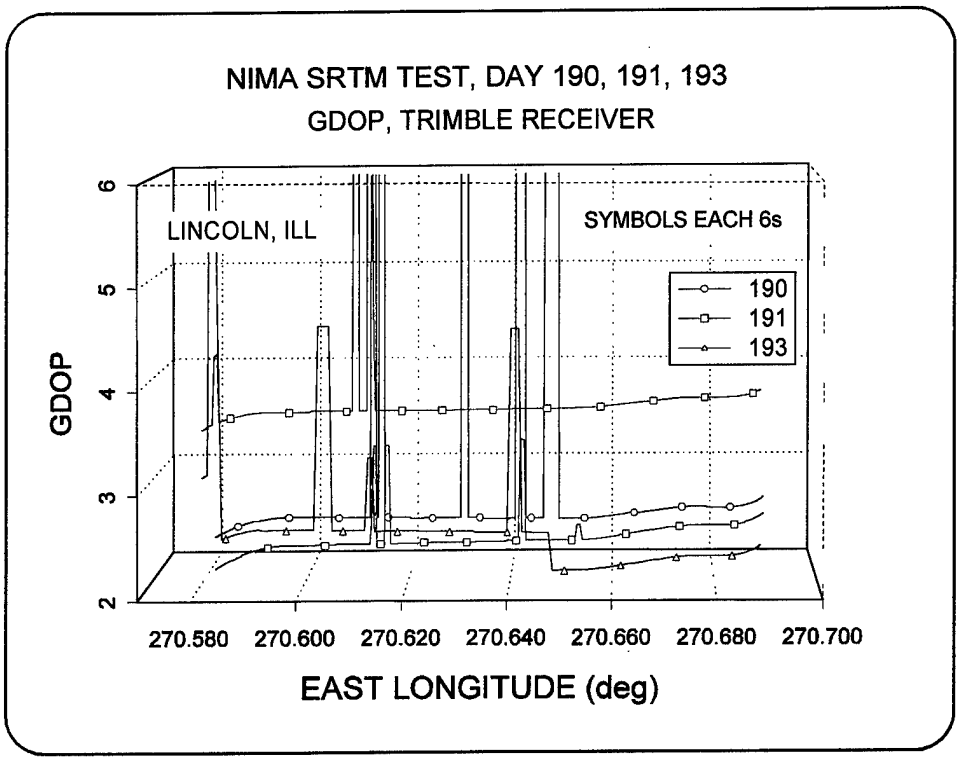

Figure 72—Longitude vs. GDOP Near Lincoln, IL, from the Trimble

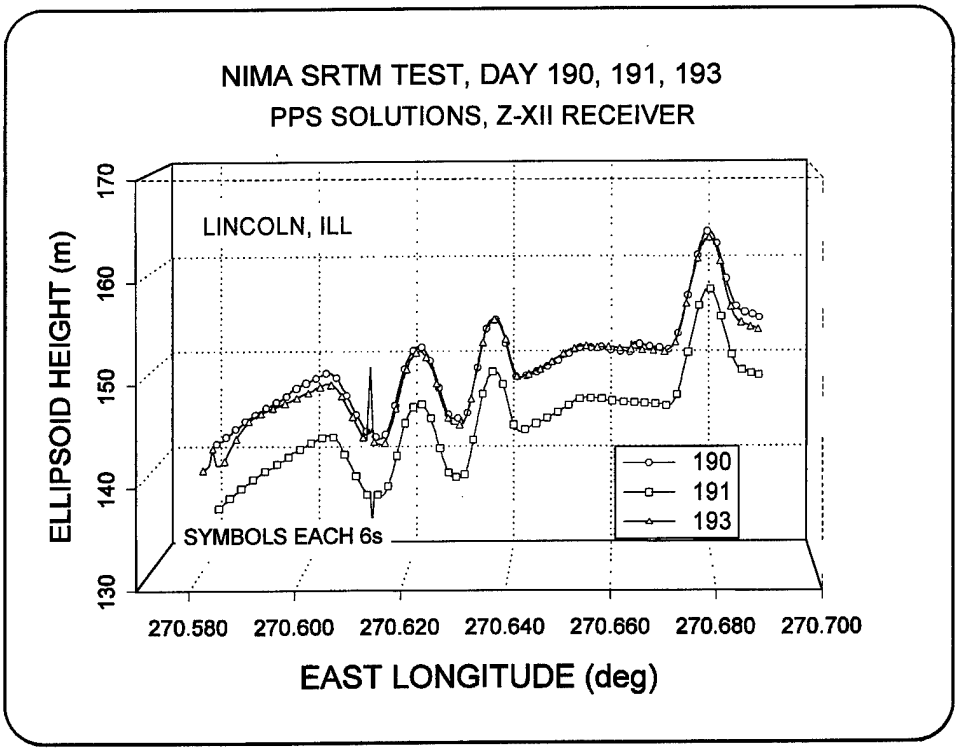

Figure 73—PPS Longitude vs. Ellipsoid Height Solutions Near Lincoln, IL, for the Z-XII

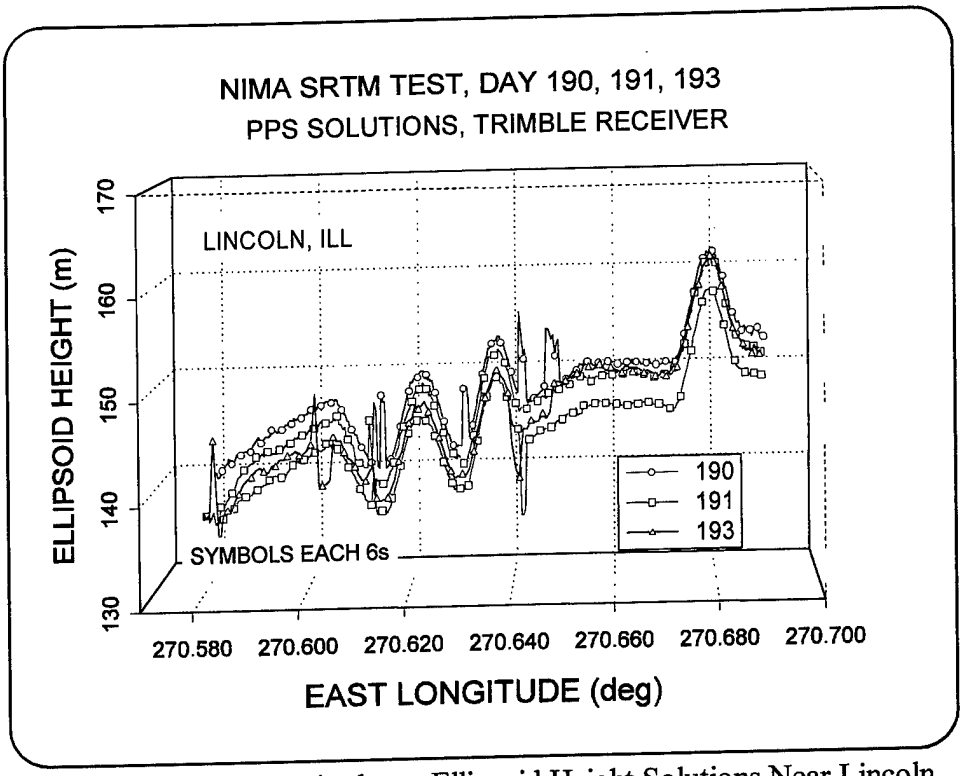

Figure 74—PPS Longitude vs. Ellipsoid Height Solutions Near Lincoln, IL, for the Trimble

3.7 I-80 in Indiana

The last segment of the NIMA road test to be discussed in this report is an east-west stretch along I-80 in Indiana (see Figure 75). On day 191 the NIMA van travelled east, and during the return trip on day 192, the van travelled west. For the approximate 25-min period covered, PPS, PAN, and single-frequency relative positioning solutions are presented. PAN solutions from the Z-XII receiver are illustrated in Figures 76 and 77. Figure 76 shows the longitude vs. latitude solutions, and Figure 77 shows the longitude vs. ellipsoid height solutions. The Trimble solutions using L_1 plus the ionospheric model are shown in Figures 78 and 79. The tracking of the Z-XII is better in this case because of fewer bad observations, which translate into solutions spikes. Also the Z-XII demonstrates better consistency in the ellipsoid height between the east and west tracks. The offset between days is on the order of only 2 to3 m, whereas the Trimble height offset exceeds 5 m during a significant portion of the segment. The GDOP computed for the two

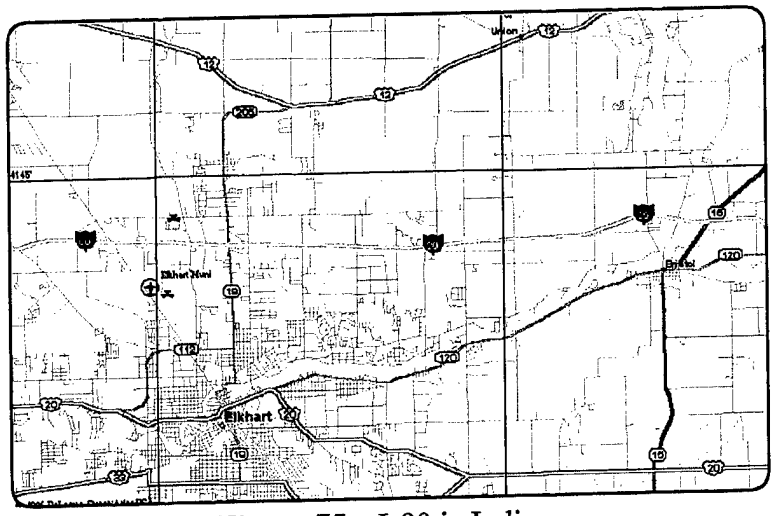

Figure 75—I-80 in Indiana

receivers is shown in Figures 80 and 81. The GDOP for both is at or below four for most of the segment, exceeding six only during short periods. Notice that the satellite losses, in the case of the Z-XII, may coincide with the "hills" in the ellipsoid height plot. These features must be due to overpasses where the interstate crosses over another road.

The PPS solutions for the Z-XII are included in Figures 82 and 83, and for the Trimble in Figure 84 and 85. These solutions, using the broadcast ephemerides, have a 10-m height offset in the Z-XII results and are considerable noisier, in the case of the Trimble, than the PAN solutions. It is questionable that height solutions with the degree of variation shown here would be useful for the proposed application. PAN improvement with the precise ephemerides seems to be the preferred processing method for the single user.

Single-frequency relative positioning solutions using Dr. Remondi's algorithm are presented next. These solutions are with respect to CORS reference sites at St. Louis, Milwaukee, Detroit, and Puerto Rico, as well as with respect to the data collected at NSWCDL. Figure 86 shows the ellipsoid heights on day 191 from Z-XII solutions compared to PAN, and Figure 87 shows the comparison with the Trimble solutions. Relative ellipsoid height solutions for day 192 are included as Figure 88 for the Z-XII and Figure 89 for the Trimble. The solutions obtained with respect to the three closest sites agree well for both receivers. The results from the most distant site—Puerto Rico—are acceptable on day 191 but are inconsistent on day 192. The solutions for the Z-XII receiver on day 192 are too low compared to the rest, but they are too high in the case of the solutions from the Trimble receiver. This discrepancy is not readily explainable.

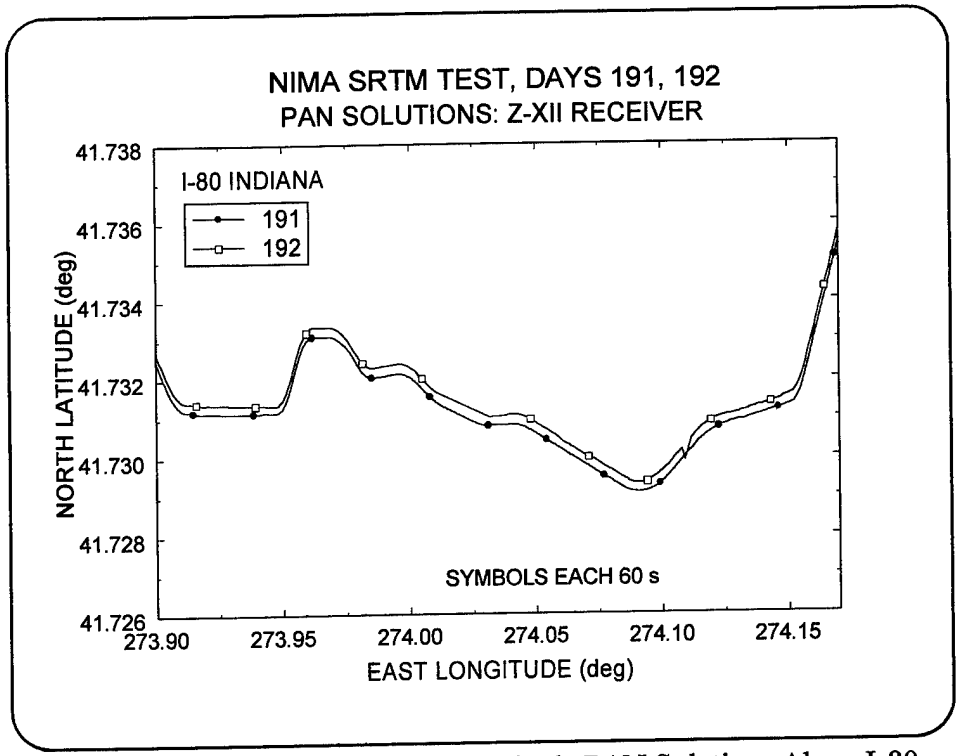

Figure 76—Z-XII Longitude vs. Latitude PAN Solutions Along I-80

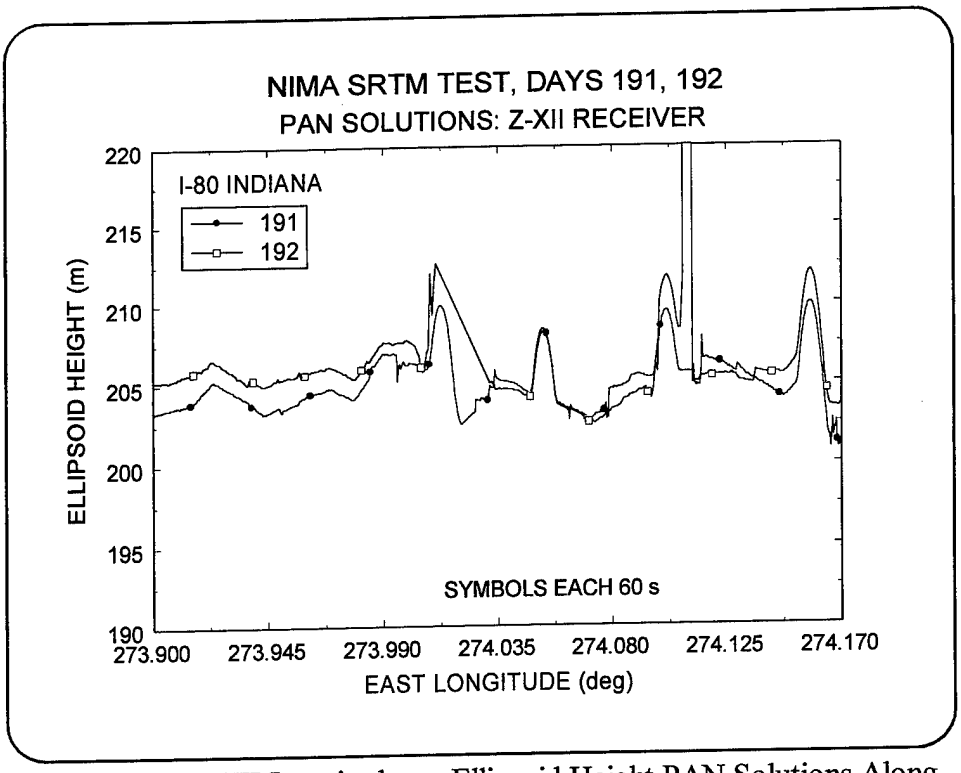

Figure 77—Z-XII Longitude vs. Ellipsoid Height PAN Solutions Along I-80

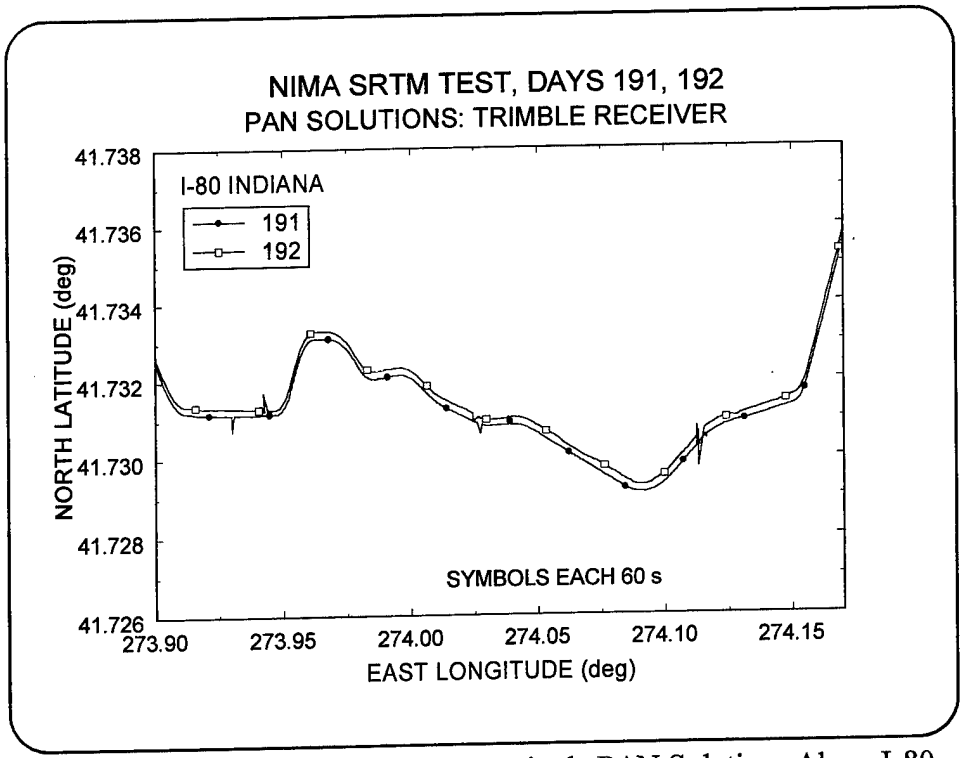

Figure 78—Trimble Longitude vs. Latitude PAN Solutions Along I-80

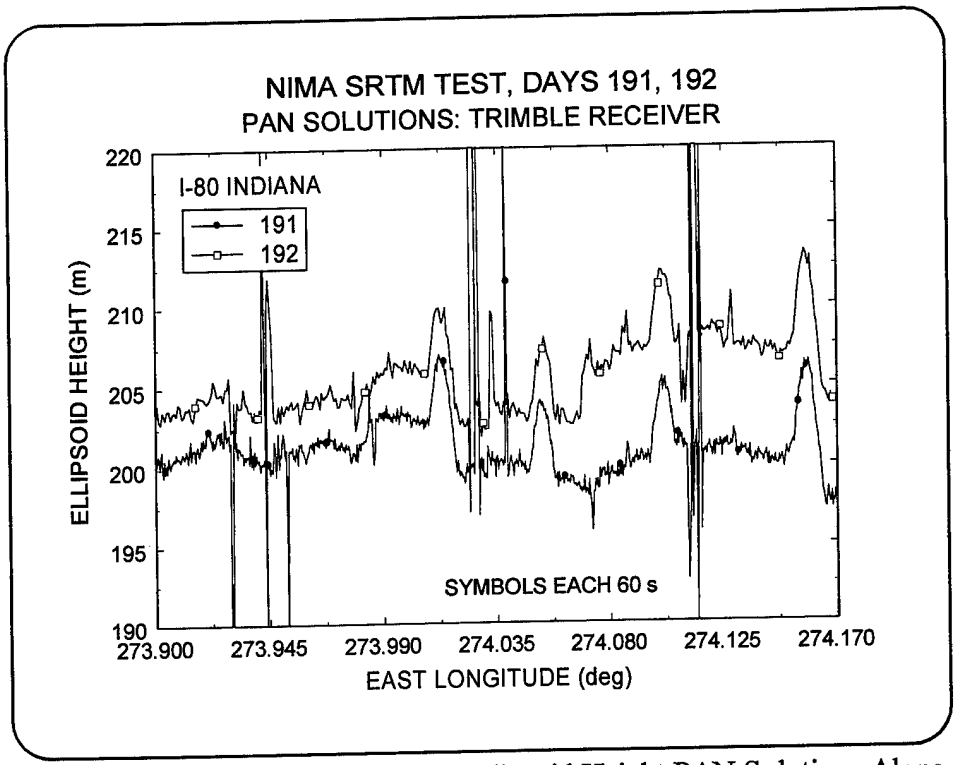

Figure 79—Trimble Longitude vs. Ellipsoid Height PAN Solutions Along I-80

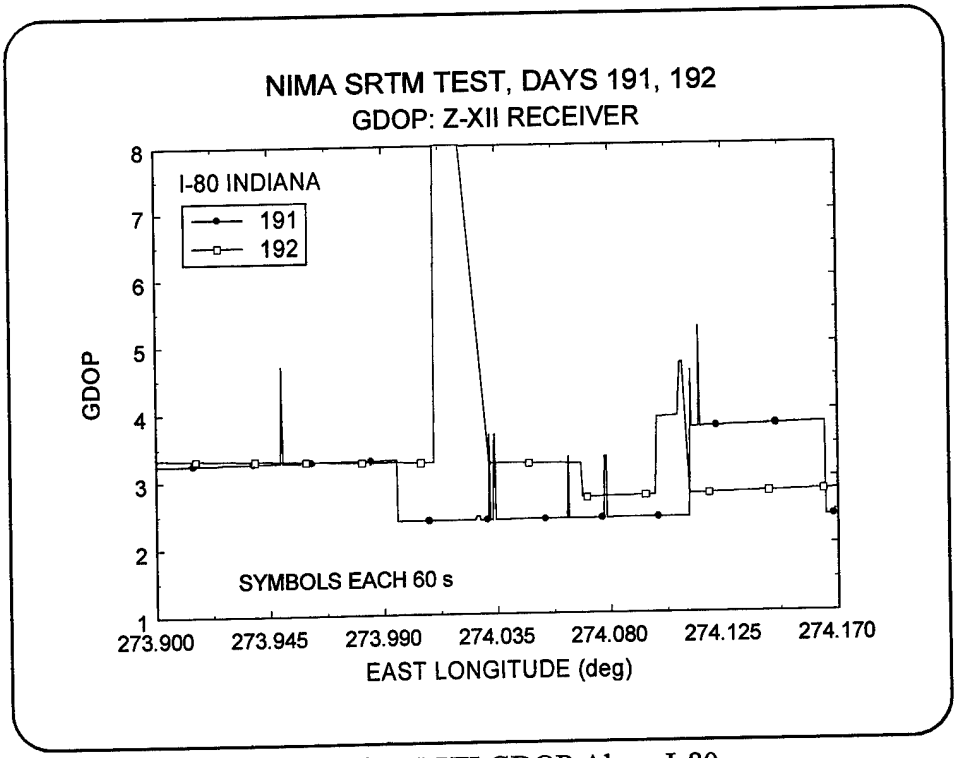

Figure 80—Z-XII GDOP Along I-80

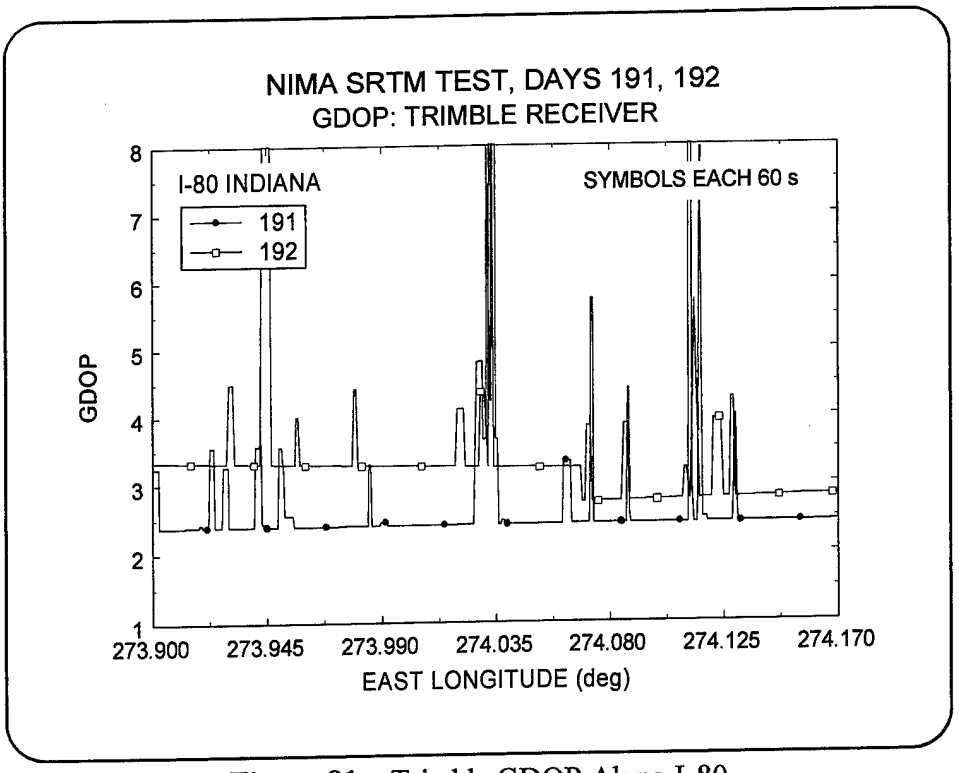

Figure 81—Trimble GDOP Along I-80

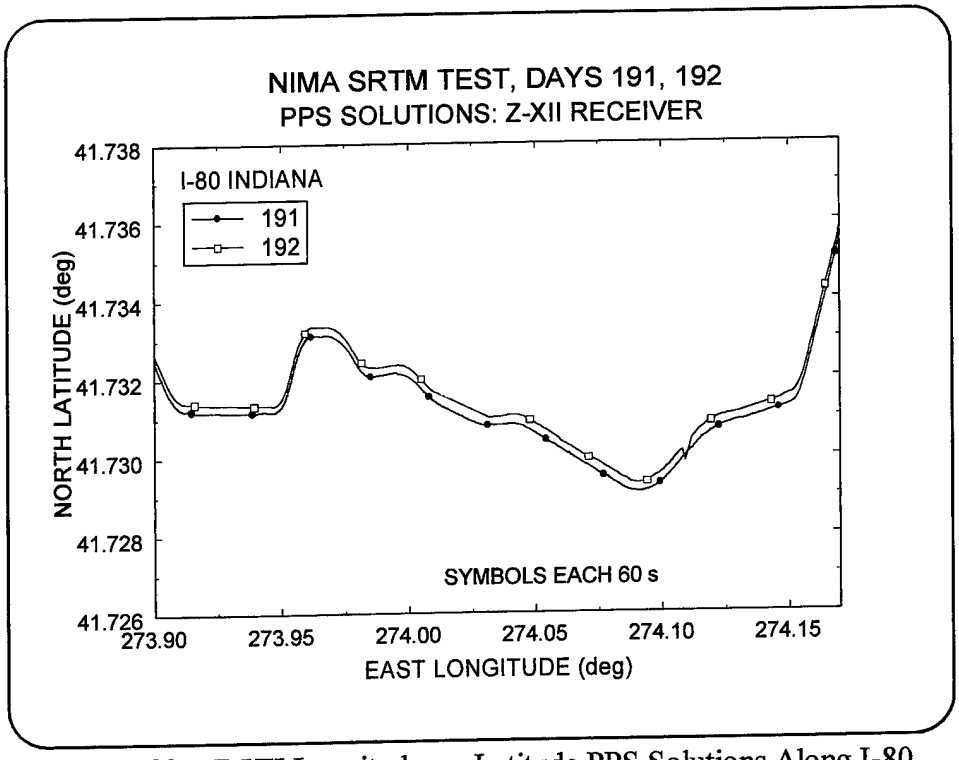

Figure 82—Z-XII Longitude vs. Latitude PPS Solutions Along I-80

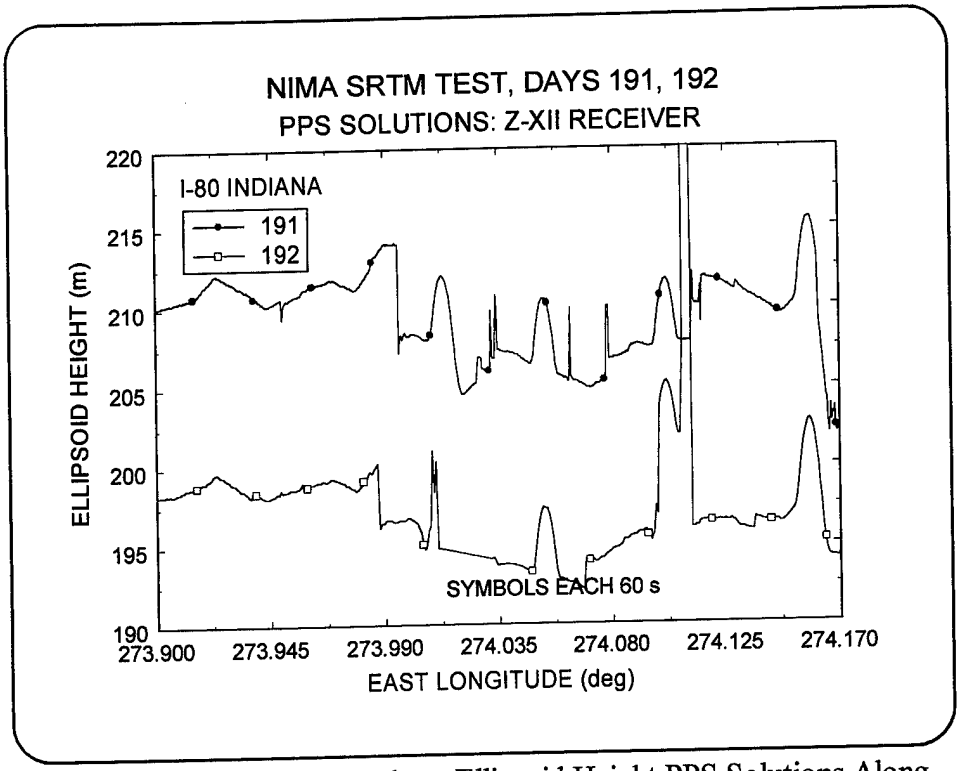

Figure 83—Z-XII Longitude vs Ellipsoid Height PPS Solutions Along I-80

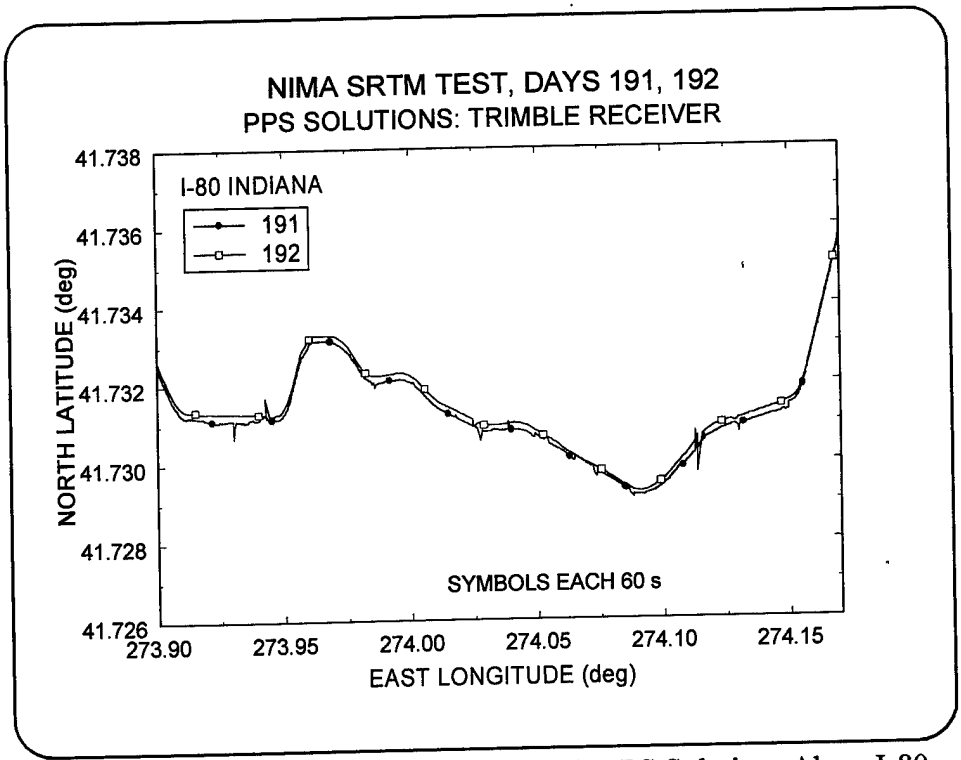

Figure 84—Trimble Longitude vs. Latitude PPS Solutions Along I-80

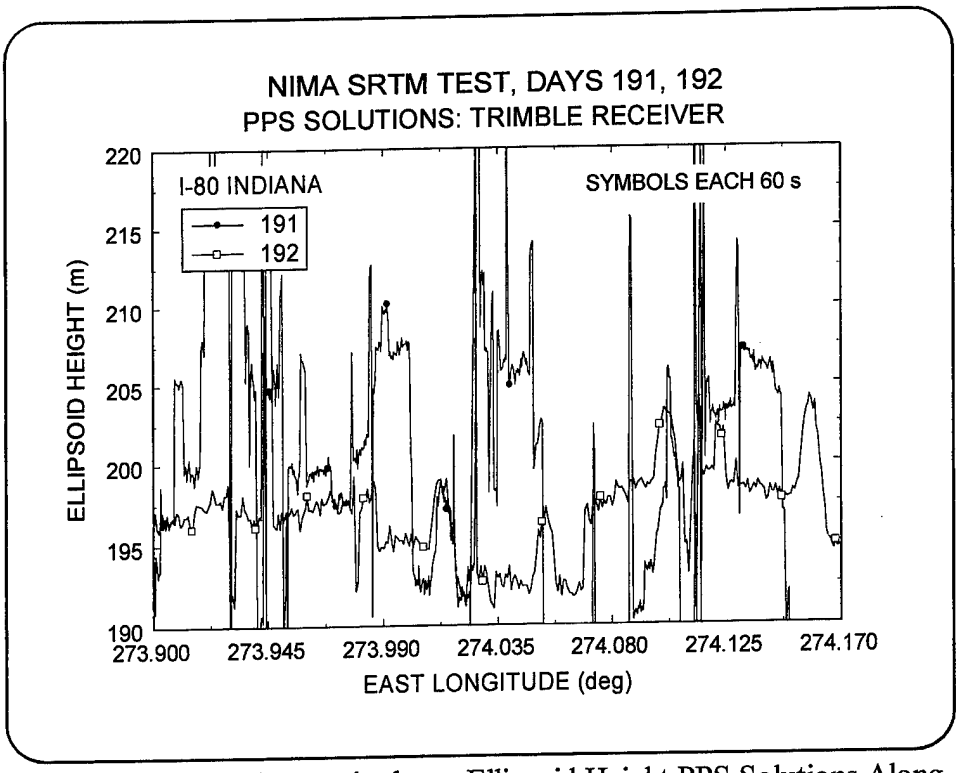

Figure 85—Trimble Longitude vs. Ellipsoid Height PPS Solutions Along I-80

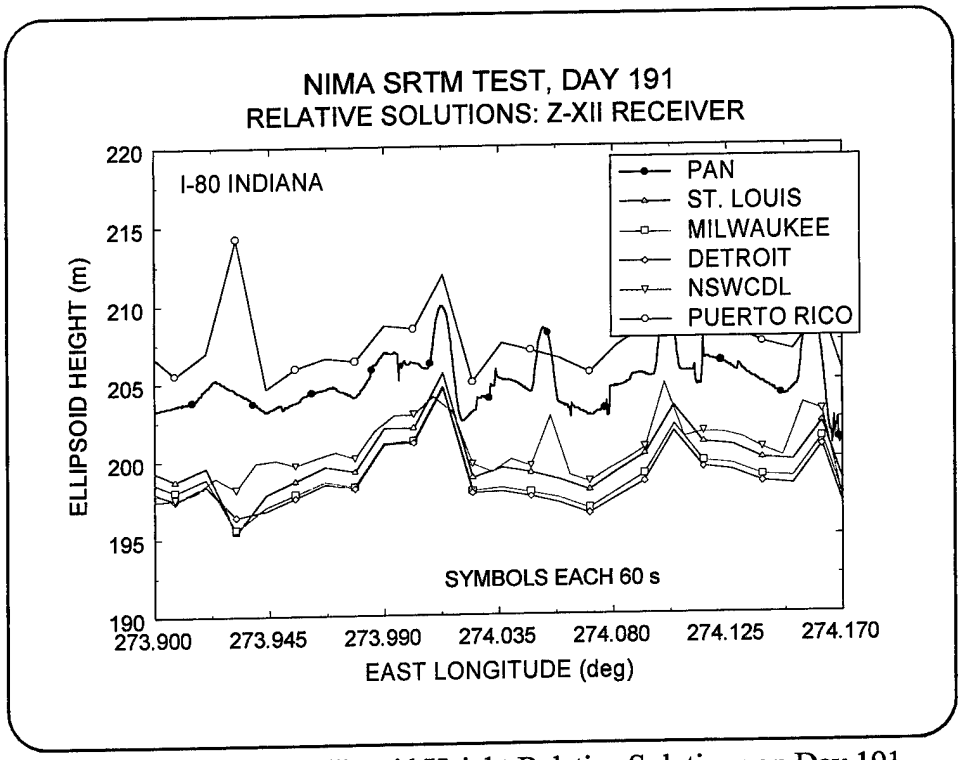

Figure 86—Z-XII Ellipsoid Height Relative Solutions on Day 191

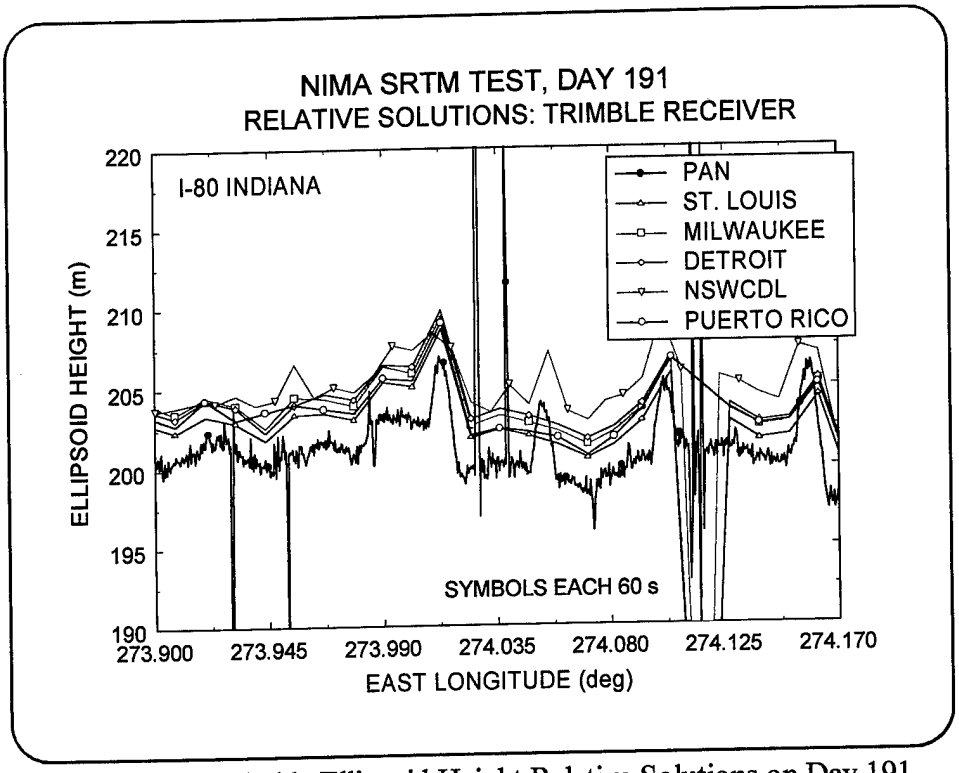

Figure 87—Trimble Ellipsoid Height Relative Solutions on Day 191

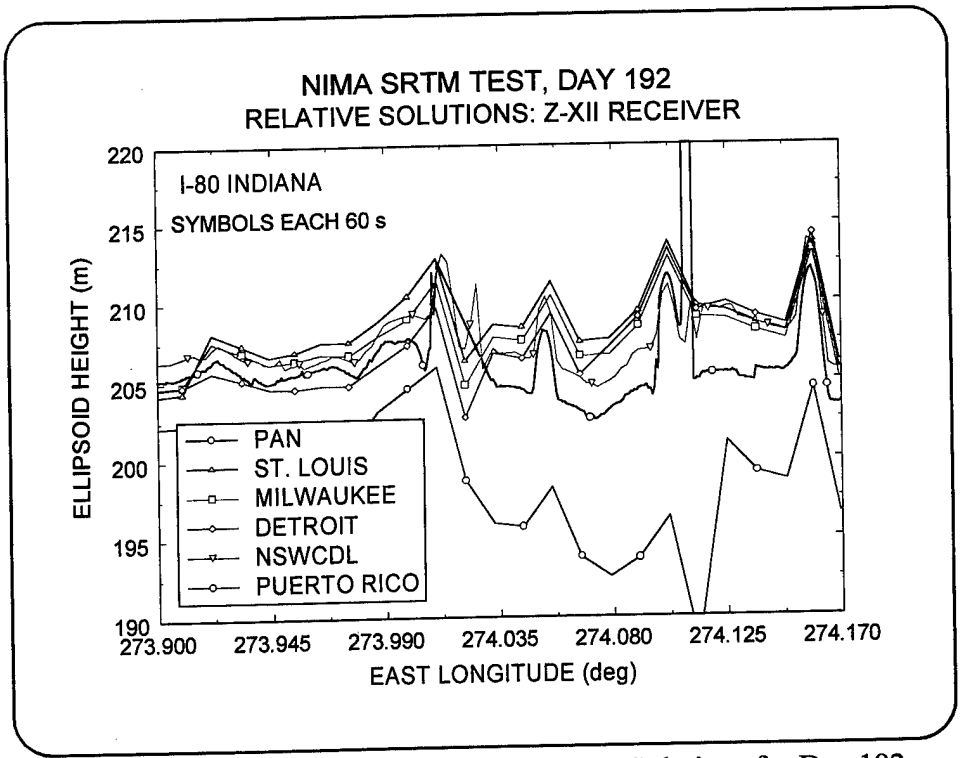

Figure 88—Z-XII Ellipsoid Height Relative Solutions for Day 192

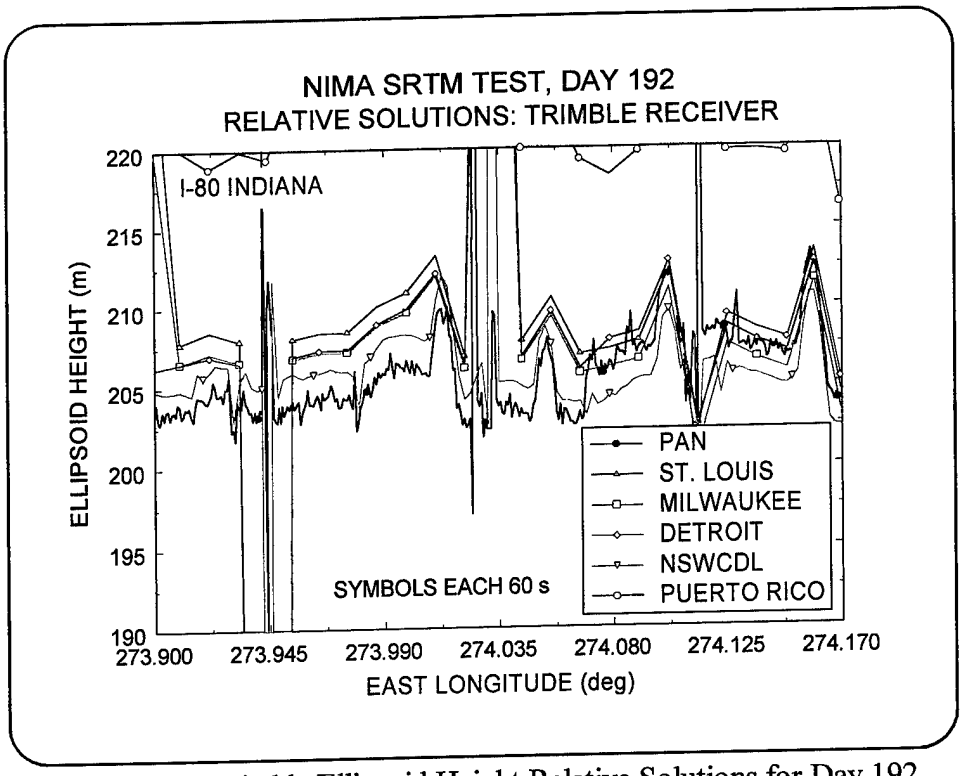

Figure 89—Trimble Ellipsoid Height Relative Solutions for Day 192

4.0 SUMMARY AND CONCLUSIONS

Requirements exist for instruments that can accurately determine terrain heights when operating from a distance. Proper evaluation of the accuracy obtained from these remote sensing devices requires a source of ground truth over wide areas. In order to support this ground truth requirement, the ability of current GPS receivers to rapidly acquire height solutions is of interest. This study investigated the quality of GPS absolute and relative positioning solutions that can be obtained from aircraft and ground vehicle platforms.

The results are very much dependent upon the platform and the local environment. Satellite dropouts due to line-of-sight blockage can be a problem in the case of ground vehicles. The aircraft solutions presented in Section 2.1 were virtually trouble free. For this test, the PAN solutions referenced to the kinematic truth had a mean vertical error of 1.02 m and a standard deviation of 0.83 m. The mean and standard deviations in the other two components were smaller. These should be compared to a mean of 9.57 m and standard deviation of 2.90 m for the simulated PPS.

The results presented in Section 2.3 from low dynamic vehicle motion over flat treeless terrain at Holloman AFB were also very good. For this test vehicle, the PAN solutions referenced to the kinematic truth had a mean vertical error of -0.76 m and a standard deviation of 0.81 m. The mean and standard deviations in the other two components again were smaller. These results should be compared to a mean of -0.79 m and standard deviation of 2.01 m for the simulated PPS.

Difficulties were experienced with data collected by receivers with antennas mounted on vehicle rooftops traveling along highways. These results were presented in Section 2.2 for data collected by NSWCDD near Dahlgren and in Section 3.0 for the extensive NIMA cross country road test. In these cases satellite dropouts were common and the quality of the solutions appeared to be dependent upon the receiver and antenna combination. For the Route 301 test, the PAN solutions referenced to the kinematic truth had a mean vertical error of -3.19 m and a standard deviation of 5.06 m. The mean and standard deviations in the other two components were on the same order. These should be compared to a mean of -2.80 m and standard deviation of 5.47 m for the simulated PPS. The fact that there is little difference between PAN and PPS solutions indicates that the major source of error was not the broadcast ephemerides, which can be improved by the PAN technique, but some other error source. The NIMA road test did not have a kinematic truth for comparison, but did exhibit many of the same problems as the Route 301 test. Day-to-day repeatability over the same terrain indicates that the PAN ellipsoid height solution errors for the road test were at the 2-5 meter level. The horizontal repeatability was somewhat better.

The solutions from these data sets do indicate that GPS can provide ellipsoid height solutions most of the time while traveling along interstate highways. The accuracy of the height solutions can be quoted only in a statistical sense because of the many variables that influence the result. Adequate preparation of the vehicle, receiver, and antenna are needed to insure the best performance. Testing of the system over a known course under various environmental conditions, and satellite availability should be done to establish the baseline performance statistics. Truth solutions from an independent source are also helpful to increase confidence in the baseline results.

5.0 REFERENCES

1. Hermann, Bruce R., "Five Years of Absolute Position at the Naval Surface Warfare Center," *Proceedings of the Sixth International Geodetic Symposium on Satellite Positioning*, The Ohio State University, March 1992.

2. Malys, Stephen; Bredthauer, Dennis; Hermann, Bruce; and Clynch, James, "Geodetic Point Positioning with GPS: A Comparative Evaluation of Methods and Results," *Proceedings of the Sixth International Geodetic Symposium on Satellite Positioning*, The Ohio State University, March 1992.

3. Lachapelle, G.; Klukas, R.; Roberts, D.; Qiu, W.; and McMillan, C., "One-Meter Level Kinematic Point Positioning Using Precise Orbits and Satellite Clock Corrections," *Proceedings of ION GPS-94*, Salt Lake City, Utah, September 1994.

4. Remondi, B. W., "Performing Centimeter-Level Surveys in Seconds with GPS Carrier Phase: Initial Results," *NAVIGATION*, Vol. 32, No. 4, 1985.

5. Hermann, B. R.; Evans, A. G.; Law, C. S.; and Remondi, B. W., "Kinematic On-The-Fly GPS Positioning Relative to a Moving Reference," *NAVIGATION*, Vol 42, No. 3, 1995.

6. Frodge, S.; DeLoach, S.; Remondi, B. W.; Lapucha, D.; and Barker, R., "Real-Time On-The-Fly Kinematic GPS System Results," *NAVIGATION*, Vol. 41, No. 2, 1994.

DISTRIBUTION

	Copies
DOD ACTIVITIES (CONUS)	
ATTN S MALYS NIMA/ TRB MAIL STOP P53 12300 SUNRISE VALLEY DR RESTON VA 20191-3448	5
ATTN R SMITH NIMA/ TR MAIL STOP P-53 12300 SUNRISE VALLEY DR RESTON VA 20191-3448	5
ATTN ANGUS JONES NIMA/GIMGD MS L-41 3200 S SECOND ST ST. LOUIS MO 63118	5
COMMANDING OFFICER CSSDD NSWC 6703 W HIGHWAY 98 PANAMA CITY FL 32407-7001	1
DEFENSE TECH INFORMATION CTR 8725 JOHN J KINGMAN RD SUITE 0944 FORT BELVOIR VA 22060-6218	2
NON-DOD ACTIVITIES (CONUS)	
THE CNA CORPORATION PO BOX 16268 ALEXANDRIA VA 22302-0268	1
ATTN MICHAEL ALBIN CHIEF ANGLO/AMERICAN ACQUISITIONS DIVISION LIBRARY OF CONGRESS 101 INDEPENDENCE AVENUE SE WASHINGTON DC 20540-4170	1

	Copies
INTERNAL	
B60	3
K43 SITZMAN	1
K43 MELKUN	1
T10	1
T12	2
T12 SWIFT	1
T12 CUNNINGHAM	1
T12 DURLING	1
T12 EVANS	1
T12 FUTCHER	1
T12 HERMANN	10
T12 O'TOOLE	1
T13	1